ARVAPALLI, DURGA MANJARI, Ph.D. Carbon Nanodots: Potential Applications in Biosensing, Drug Delivery and Free Radical Regulation. (2020)
Directed by Dr. Jianjun Wei. 120 pp.

Carbon nanodots (CNDs) outshined other traditional carbonaceous nanomaterials such as carbon nanotubes, fullerenes, etc., due to their unique properties, such as low toxicity, high biocompatibility, excellent photoluminescence, and ease of functionalization. Past few years, the research has been focused extensively on synthesis, and application of the CNDs in various bio-medical fields, yet the full potential in understanding the properties and mechanisms needs to be explored. The current research dissertation focusses on fundamentals and the applications of selected carbon nanodots in three different aspects: biosensing, drug delivery and free radical regulation. The first part of the research concentrates on the synthesis of high quantum yield CNDs and their use as fluorescence turn off sensor in the detection of iron ions with improved selectivity and sensitivity. Upon addition of iron ions, the fluorescence intensity of the CNDs decreases in concentration dependent manner, attributing to the charge transfer between CNDs and iron ions, which is further verified using electrochemical analysis. The second part of the research is focused on the loading of curcumin onto CNDs to enhance the bioavailability of the hydrophobic drug. Curcumin release studies show better release in an acidic environment (pH-5.0), conferring the chance of more drug release in tumor microenvironment compared to normal tissues. Curcumin loaded CNDs present increased cellular cytotoxicity in cancer cells even at low concentrations, proving the efficacy of the CNDs as drug delivery vehicles. The third part of the research investigates the concentration dependent pro-oxidant and antioxidant properties of photoluminescent

curcumin-derived nanoparticles (Curc-dots) synthesized from native curcumin. The synthesized Curc-dots retained some of the characteristic functional groups of the native curcumin with size less than 10 nm. The cell viability studies showed the antioxidant and prooxidant effects of the Curc-dots at low and high concentrations, respectively. The Curc-dots are taken up by cells with a bright blue fluorescence in cells and demonstrated chemo-protective nature when treated with H_2O_2, a free radical inducer. Overall, the findings from this dissertation research opens a wide platform in understanding the underlying mechanisms and unique properties of CNDs in various fields of medicine such as drug delivery, and bioimaging.

CARBON NANODOTS: POTENTIAL APPLICATIONS IN BIOSENSING, DRUG DELIVERY AND FREE RADICAL REGULATION

by

Durga Manjari Arvapalli

A Dissertation Submitted to
the Faculty of The Graduate School at
The University of North Carolina at Greensboro
in Partial Fulfillment
of the Requirements for the Degree
Doctor of Philosophy

Greensboro
2020

Approved by

_____
Committee Chair

APPROVAL PAGE

This dissertation written by Durga Manjari Arvapalli has been approved by the following committee of the Faculty of The Graduate School at The University of North Carolina at Greensboro.

Committee Chair_____
Jianjun Wei

Committee Members_____
Joseph M. Starobin

_____
Dennis R. LaJeunesse

_____
Shyam Aravamudhan

_____
Date of Acceptance by Committee

_____
Date of Final Oral Examination

ACKNOWLEDGEMENTS

I would like to thank my advisor Dr. Jianjun Wei for his valuable guidance throughout the journey I had at JSNN. His support, organizational skills, attitude towards the research work has inspired me to pursue my thesis work. His advice on writing scientific papers and response letters to editors would surely be helpful in my future research.

Besides my advisor, I would like to thank my committee members: Dr. Joseph Starobin, Dr. Dennis LaJeunesse and Dr. Shyam Arvamudhan for their insightful comments, support and encouragement over the years.

I thank all my lab members Dr. Zeng, Dr. Liu, Dr. Mabe, Dr. Wendi, Dr. Harish, Alex, Zuowei, Bhawna, Kokougan, Anitha, Ziyu, Frank, Mengxin and Mahsa for their continuous support and encouragement.

I would like to thank Jerri Price and Nancy Knight for the timely help with the administrative questions I had. And, I am grateful to JSNN for the continuous financial support though my research years.

I would express eternal gratitude to my parents Venkata Ramana Rao Arvapalli and Padmaja Arvapalli for their unconditional love, constant support, care and belief they had in me. I would attribute all the credit to my parents for who I am today. My brother, Vedavyas Arvapalli has been a constant support to me in every obstacle I have faced during my doctoral research. My husband Venkata Ravi Kumar Gangineni has been supportive of my research. My sister Durgesh Alapati, and brother in law Kalyan Alapati

has been so helpful during the initial struggle in the United States. My nephews Samay and Sanjay helped me to cope with the thesis stress. Blessings from my grandmother, Sunitha Devi Movva, family support and friend's encouragement kept me going through the research and not letting me give up.

TABLE OF CONTENTS

Page

LIST OF TABLES

Page

LIST OF FIGURES

Page

CHAPTER I

INTRODUCTION

With old societal issues being tackled, new problems are being brought to the surface. During the past decade, nanoscience revolutionizes the society with advancements in information technology, medicine, transport, energy, defense, food safety, and environmental science industry.[1] The nanoparticles provide unique properties that differ from the traditional bulk solids.[2] Nanoparticles (NPs) are clusters of atoms in the size range of 1-100 nm and depending on the size, morphology, physical and chemical characteristics, are categorized into metal NPs, ceramic NPs, polymeric NPs lipid based NPs, and carbon based NPs.[3] Carbon based nanoparticles attracted lots of attention due to their high mechanical strength, electrical and thermal conductivity, and optical properties and can be classified into 0D, 1D, 2D or 3D depending on the overall shape and electron movement.[4]

Carbon nanodots (CNDs), a relatively new class of carbon based nanomaterials, have been attracting a lot of attention due to their unique properties such as stable photoluminescence, good biocompatibility and aqueous solubility, and low toxicity.[5-6] Carbon dots were first obtained during the purification of single-walled carbon nanotubes in 2004.[7] Physical methods such as arc discharge, laser ablation/passivation, plasma treatment and chemical methods like ultrasonic/microwave, thermal or hydrothermal

oxidation, electrochemical synthesis can be used to synthesize CNDs.[6] CNDs are carbonaceous nanomaterials with sizes less than 10 nm and have potential applications in biosensing, drug delivery, and bioimaging.[8-10] CNDs biosensing application: Transition metal ions such as iron, copper, zinc, manganese, cobalt and nickel are an integral part in cellular processes such as respiration, gene transcription, proliferation and immune function.[11] Iron, an essential micronutrient is a part of hemoglobin that transports oxygenated blood.[12] Iron deficiency leads to sepsis in pregnant women and iron overload causes neurological disorders such as Parkinson's and Alzheimer's.[13] Iron homeostasis is crucial for survival of living organisms and therefore the levels need to be monitored. Various fluorescent materials such as quantum dots, and organic fluorescent dyes are being currently used for detection of iron,[14-15] but the irreversible photobleaching, toxicity and material instability renders their usage.[16-17] Therefore, the research has been shifted to CNDs which offer stable photoluminescence, low toxicity, short response time and resistance to photobleaching. Few reports demonstrated good sensitivity with detection confined only to micromolar range.[18-20] Despite the recent research, there is still a need for selective and sensitive detection of iron in nanomolar range with better understanding of the underlying detection mechanism. High quantum yield CNDs were synthesized in a cost-effective manner for the sensitive and selective detection of iron using microwave synthesizer. The underlying detection mechanism was investigated using an electrochemical technique, cyclic voltammetry. The two synthesized CNDs (E-CNDs and U-CNDs) were well characterized using AFM, TEM for size and morphology, whereas XPS, and FTIR were used for surface functional groups. E-CNDs showed a high

quantum yield of 64% incorporating high amounts (~12%) of nitrogen. Upon addition of Fe (III) ions, CNDs fluorescence intensity decreased in a concentration dependent manner with a fast response time of 1 minute which was evaluated using Stern-Volmer equation. The synthesized nanoprobes were successfully internalized inside endothelial cells and upon addition of Fe (III) ions, demonstrated quenching. The CNDs were able to detect iron in real samples such as tap water and human serum which was validated by ICP analysis. The underlying quenching reaction, of CNDs by Fe (III), is due to the charge transfer between the CNDs and Fe (III) by formation of CND-$(Fe\ (III))_n$ complex. The current work demonstrates high quantum yield CNDs as a fluorescence turn off sensor in the detection of Fe (III) with improved selectivity, fast response time, and better limit of detection than traditional methods.

CNDs in drug delivery: Curcumin, a natural polyphenolic spice obtained from *Curcuma Longa* is a dietary supplement with anti-microbial, anti-inflammatory, anti-cancer and antioxidant/pro-oxidant properties.[21-23] Regardless of its potential benefits, curcumin usage as a chemotherapeutic entity is limited by its poor bioavailability, low aqueous solubility, rapid metabolism and elimination.[24-26] Various nanoparticle-based drug delivery systems such as liposomes, polymeric nanoparticles, and hydrogels were formulated for enhancement of curcumin bioavailability and delivery to target site, but their usage is limited by low drug entrapment, instability and initial burst release. Presence of large number of surface functional groups on CNDs offer high surface for drug loading. Loading of curcumin onto CNDs enhances its bioavailability and overall drug tolerance with minimal side effects. In the second part of the research, CNDs were

used to load curcumin using physical adsorption. The characterized Curcumin loaded CNDs (Curc-CNDs) showed characteristic functional groups of curcumin, clearly indicating the successful conjugation of curcumin with CNDs. Curcumin release kinetics performed at two different physiological pH 7.4 and 5.0, showed controlled drug release, which was investigated using Korsmeyer-Peppas equation. The Curc-CNDs showed more release of curcumin at pH-5.0, due to weaker interactions of Curc-CNDs in acidic environment favoring the release in the tumor microenvironment and elicits its therapeutic effects at the target site. Curc-CNDs showed no significant anti-proliferative effects on normal cells, while the cancer cells showed notable decrease in the cell viability in a concentration dependent manner, which can be attributed to the more release of curcumin as observed from the release profile. Intracellular uptake studies showed the localization of Curc-CNDs both in the cytoplasm and nucleus with blue fluorescence, which might induce dose dependent DNA damage to nuclear as well as mitochondrial genome with increase of ROS levels and lipid peroxidation. The biocompatible CNDs based drug delivery system can provide loading of hydrophobic drugs and transport them to the target site without altering their chemical stability.

Curcumin nanoparticles: Reactive oxygen species (ROS) such as superoxide anions, peroxides and hydroxyl radicals are by-products of cell mediated signaling pathways.[27] The ROS levels alter during oxidative stress and the inbuilt antioxidant mechanisms cope up with the detrimental effects of ROS in high amounts.[28] But the pathological conditions, such as cancer, neurological disorders, atherosclerosis and hypertension[29] elevates the ROS levels beyond the control of cell's antioxidant

mechanisms, thereby causing irreparable damage to cellular structures such as nucleic acids, proteins and lipids.[30-31] Commercially available antibiotics such as butylated hydroxyanisole (BHA), butylated hydroxytoluene (BHT) are toxic and causes liver damage and carcinogenesis.[32] The need for natural anti-oxidants turns the light on curcumin, which has both antioxidant and pro-oxidant properties in cells. But the poor bioavailability, rapid metabolism and stability confounds the therapeutic effects.[26] Various delivery systems have been formulated to enhance the bioavailability of curcumin[33], but the stability still remians a question. Limited light is shed on the synthesis of curcumin nanoparticles. In this study, we used microwave synthesizer for the one pot synthesis of curcumin nanoparticles (Curc dots) from native curcumin. The use of ethylene diamine (EDA) as one of the precursor molecules incorporated nitrogen, making the Curc dots fluorescent and provides applications in bioimaging. The as-synthesized Curc dots are well dispersed in water and demonstrated size less than 10 nm, retaining some of the characteristic functional groups of curcumin. The antioxidant effects of Curc dots were evalauted using DPPH assay and confirmed using cyclic voltammetry. The antioxidation activity was found to be highest even at a low concentration of Curc dots (0.05 mg/mL). Curc dots acts as a proton donor to free radical DPPH*, stabilizing it to a neutral DPPH molecule. With increase in Curc dots concentration, the DPPH* availabity is decreased at the elcetrode surface, thereby reducing the redox peaks. The low concentration (0.01-0.08 mg/mL) of Curc dots have no cytotoxic effects on both normal and cancer cells, whereas the high concentrations (0.1-1.6 mg/mL) showed significant cytotoxicity on the cells. The concentration dependent antioxidant and pro-oxidant effects

of Curc dots were further verified using DCFH-DA assay. At low concentrations, less ROS is produced and at high concentrations more ROS is generated. The antioxidant or pro-oxidant activity depends on structure modification, curcumin concentration, presence of metal ions at free radical generation. The decrease in ROS generation can be attributed to the transfer of O-methoxy phenolic rings of Curc dots to free radicals, . The nano synthesis of curcumin enhances the anti-proliferative effects even at low concentrations compared to native curcumin, thereby offering potential in therapy to regulate ROS levels in tumor cells.

References

1. Nasrollahzadeh, M.; Sajadi, S. M.; Sajjadi, M.; Issaabadi, Z., Chapter 4 - Applications of Nanotechnology in Daily Life. In *Interface Science and Technology*, Nasrollahzadeh, M.; Sajadi, S. M.; Sajjadi, M.; Issaabadi, Z.; Atarod, M., Eds. Elsevier: 2019; Vol. 28, pp 113-143.

2. Kang, H.; Wang, L.; O'Donoghue, M.; Cao, Y. C.; Tan, W., Chapter 15 - NANOPARTICLES FOR BIOSENSORS. In *Optical Biosensors (Second Edition)*, Ligler, F. S.; Taitt, C. R., Eds. Elsevier: Amsterdam, 2008; pp 583-621.

3. Khan, I.; Saeed, K.; Khan, I., Nanoparticles: Properties, applications and toxicities. *Arabian Journal of Chemistry* **2019,** *12* (7), 908-931.

4. Tiwari, J. N.; Tiwari, R. N.; Kim, K. S., Zero-dimensional, one-dimensional, two-dimensional and three-dimensional nanostructured materials for advanced electrochemical energy devices. *Progress in Materials Science* **2012,** *57* (4), 724-803.

5. Kang, Z.; Liu, Y.; Lee, S.-T., Carbon Dots for Bioimaging and Biosensing Applications. In *Carbon-Based Nanosensor Technology*, Kranz, C., Ed. Springer International Publishing: Cham, 2019; pp 201-231.

6. Li, H.; Kang, Z.; Liu, Y.; Lee, S.-T., Carbon nanodots: synthesis, properties and applications. *Journal of Materials Chemistry* **2012,** *22* (46), 24230-24253.

7. Xu, X.; Ray, R.; Gu, Y.; Ploehn, H. J.; Gearheart, L.; Raker, K.; Scrivens, W. A., Electrophoretic Analysis and Purification of Fluorescent Single-Walled Carbon Nanotube Fragments. *Journal of the American Chemical Society* **2004,** *126* (40), 12736-12737.

8. Cao, L.; Wang, X.; Meziani, M. J.; Lu, F.; Wang, H.; Luo, P. G.; Lin, Y.; Harruff, B. A.; Veca, L. M.; Murray, D.; Xie, S.-Y.; Sun, Y.-P., Carbon Dots for Multiphoton Bioimaging. *Journal of the American Chemical Society* **2007,** *129* (37), 11318-11319.

9. Esteves da Silva, J. C. G.; Gonçalves, H. M. R., Analytical and bioanalytical applications of carbon dots. *TrAC Trends in Analytical Chemistry* **2011,** *30* (8), 1327-1336.

10. Yang, S.-T.; Cao, L.; Luo, P. G.; Lu, F.; Wang, X.; Wang, H.; Meziani, M. J.; Liu, Y.; Qi, G.; Sun, Y.-P., Carbon Dots for Optical Imaging in Vivo. *Journal of the American Chemical Society* **2009,** *131* (32), 11308-11309.

11. Dean, K. M.; Qin, Y.; Palmer, A. E., Visualizing metal ions in cells: An overview of analytical techniques, approaches, and probes. *Biochimica et Biophysica Acta (BBA) - Molecular Cell Research* **2012,** *1823* (9), 1406-1415.

12. Chifman, J.; Laubenbacher, R.; Torti, S., A Systems Biology Approach to Iron Metabolism. *Adv Exp Med Biol* **2014,** *844*, 201-225.

13. Silvestri, L.; Camaschella, C., Apotential pathogenetic role of iron in Alzeimer's Disease. *Journal of cellular and molecular medicine* **2008,** *12*, 1548-50.

14. Resch-Genger, U.; Grabolle, M.; Cavaliere-Jaricot, S.; Nitschke, R.; Nann, T., Quantum dots versus organic dyes as fluorescent labels. *Nature Methods* **2008,** *5* (9), 763-775.

15. Lesiak, A.; Drzozga, K.; Cabaj, J.; Banski, M.; Malecha, K.; Podhorodecki, A., Optical Sensors Based on II-VI Quantum Dots. *Nanomaterials (Basel, Switzerland)* **2019,** *9* (2).

16. Hardman, R., A toxicologic review of quantum dots: toxicity depends on physicochemical and environmental factors. *Environmental health perspectives* **2006,** *114* (2), 165-72.

17. Valizadeh, A.; Mikaeili, H.; Samiei, M.; mussa farkhani, S.; Zarghami, N.; Kouhi, M.; Akbarzadeh, A.; Davaran, S., Quantum dots: Synthesis, bioapplications, and toxicity. *Nanoscale research letters* **2012,** *7*, 480.

18. Li, C.; Wang, Y.; Zhang, X.; Guo, X.; Kang, X.; Du, L.; Liu, Y., Red fluorescent carbon dots with phenylboronic acid tags for quick detection of Fe(III) in PC12 cells. *Journal of colloid and interface science* **2018,** *526*, 487-496.

19. Zhang, J.; Yan, J.; Wang, Y.; Zhang, Y., One-Step Hydrothermal Approach to Synthesis Carbon Dots from D-Sorbitol for Detection of Iron(III) and Cell Imaging. *Journal of nanoscience and nanotechnology* **2018,** *18* (7), 4457-4463.

20. Shi, B.; Su, Y.; Zhang, L.; Huang, M.; Liu, R.; Zhao, S., Nitrogen and Phosphorus Co-Doped Carbon Nanodots as a Novel Fluorescent Probe for Highly Sensitive Detection of Fe3+ in Human Serum and Living Cells. *ACS Applied Materials & Interfaces* **2016,** *8* (17), 10717-10725.

21. Shishodia, S.; Sethi, G.; Aggarwal, B. B., Curcumin: getting back to the roots. *Annals of the New York Academy of Sciences* **2005,** *1056*, 206-17.

22. Wilken, R.; Veena, M. S.; Wang, M. B.; Srivatsan, E. S., Curcumin: A review of anti-cancer properties and therapeutic activity in head and neck squamous cell carcinoma. *Mol Cancer* **2011,** *10*, 12-12.

23. Rao, C. V.; Rivenson, A.; Simi, B.; Reddy, B. S., Chemoprevention of colon carcinogenesis by dietary curcumin, a naturally occurring plant phenolic compound. *Cancer research* **1995,** *55* (2), 259-66.

24. Panda, A. K.; Chakraborty, D.; Sarkar, I.; Khan, T.; Sa, G., New insights into therapeutic activity and anticancer properties of curcumin. *J Exp Pharmacol* **2017,** *9*, 31-45.

25. Kundu, M.; Sadhukhan, P.; Ghosh, N.; Chatterjee, S.; Manna, P.; Das, J.; Sil, P. C., pH-responsive and targeted delivery of curcumin via phenylboronic acid-functionalized ZnO nanoparticles for breast cancer therapy. *Journal of Advanced Research* **2019,** *18*, 161-172.

26. Anand, P.; Kunnumakkara, A. B.; Newman, R. A.; Aggarwal, B. B., Bioavailability of curcumin: problems and promises. *Molecular pharmaceutics* **2007,** *4* (6), 807-18.

27. Droge, W., Free radicals in the physiological control of cell function. *Physiological reviews* **2002,** *82* (1), 47-95.

28. Birben, E.; Sahiner, U.; Sackesen, C.; Erzurum, S.; Kalayci, O., Oxidative Stress and Antioxidant Defense. *World Allergy Organization Journal* **2012,** *5*, 9-19.

29. Kerr, S.; Brosnan, M. J.; McIntyre, M.; Reid, J. L.; Dominiczak, A. F.; Hamilton, C. A., Superoxide anion production is increased in a model of genetic hypertension: role of the endothelium. *Hypertension (Dallas, Tex. : 1979)* **1999,** *33* (6), 1353-8.

30. Girotti, A. W., Mechanisms of lipid peroxidation. *Journal of free radicals in biology & medicine* **1985,** *1* (2), 87-95.

31. Kelly, F. J.; Mudway, I. S., Protein oxidation at the air-lung interface. *Amino acids* **2003,** *25* (3-4), 375-96.

32. Witschi, H. P., Enhanced tumour development by butylated hydroxytoluene (BHT) in the liver, lung and gastro-intestinal tract. *Food and chemical toxicology : an international journal published for the British Industrial Biological Research Association* **1986,** *24* (10-11), 1127-30.

33. Li, X.; Chen, T.; Xu, L.; Zhang, Z.; Li, L.; Chen, H., Preparation of curcumin micelles and the in vitro and in vivo evaluation for cancer therapy. *Journal of biomedical nanotechnology* **2014,** *10* (8), 1458-68.

CHAPTER II

HIGH QUANTUM YIELD FLUORESCENT CARBON NANODOTS FOR DETECTION OF FE (III) IONS AND ELECTROCHEMICAL STUDY OF QUENCHING MECHANISM

This chapter has been published as: Arvapalli, D. M.; Sheardy, A. T.; Alapati, K. C.; Wei, J., High Quantum Yield Fluorescent Carbon Nanodots for detection of Fe (III) Ions and Electrochemical Study of Quenching Mechanism. Talanta 2019, 120538.

Overview

Carbon nanodots (CNDs) offer potential applications in photocatalysis, optoelectronics, bio-imaging, and sensing due to their excellent photoluminescence (PL) properties, biocompatibility, aqueous solubility, and easy functionalization. Recent emphasis on CNDs in the selective detection of metal ions is due to the growing concern for human and environmental safety. In this work, two types of fluorescent carbon nanodots (CNDs) are synthesized economically from ethylene diamine (E-CNDs) or urea (U-CNDs) in a single step microwave process. The as-prepared CNDs exhibit excellent PL at an excitation wavelength of 350 nm with a quantum yield of 64% for E-CNDs and 8.4% for U-CNDs with reference to quinine sulfate. Both E-CNDs and U-CNDs demonstrate high selectivity towards Fe (III) ions among different metal ions, by fluorescence quenching in a dose dependent manner. The limit of detection of E-CNDs

and U-CNDs is observed to be 18 nM and 30 nM, respectively, in the linear response range of 0-2000 µM with a short response time (seconds). The CNDs detect Fe (III) ions in tap water and serum sample with no spiking and the recovery was ~100% with the Fe (III) samples. Cellular internalization studies confirm the localization of the CNDs and the optical imaging sensing of Fe (III) ions inside living cells. A charge transfer fluorescence quenching mechanism, specifically between the CNDs and Fe (III), is proposed and examined using cyclic voltammetry. The overall characteristics of the E-CNDs provides a potential sensing platform in highly sensitive and selective detection of Fe (III) ions.

Introduction

Metal ions are an integral part in various biological and biochemical processes.[1] Iron is an essential micronutrient for the human body and most biological electron transfer processes rely on iron proteins.[2] Fe^{3+} is a major component of hemoglobin that facilitates oxygen transport in blood.[3] Iron deficiency in pregnant women have increased risk of anemia and sepsis associated with high mortality and morbidity rates.[4] Moreover, iron plays an important role in brain development of newborn babies,[5] body temperature regulation,[6] and muscle function.[7] Also, overload of iron may lead to neurological diseases such as Parkinson's and Alzheimer's.[8] Current detection techniques such as atomic absorption spectrometry and ion chromatography rely on the use of complicated sample preparation and instrumentation.[9] Therefore, monitoring of iron levels is challenging and detection with high sensitivity and selectivity is of great importance.

Use of fluorescent materials in the sensitive detection of biologically important metal ions has tremendous potential in the field of biomedicine.[1] Quantum dots and organic fluorescent dyes, due to their high quantum yield, are used widely as contrast agents for detection.[11] However, irreversible photobleaching and low optical absorption cross-section renders the limitation of the organic dyes in detection. Quantum nanoparticles have replaced the usage of organic dyes due to their broad absorption spectra[12] and quantum confinement effect,[11] but their instability[13] and the presence of toxic heavy metals limits their applications for detection in living cells.[14-15] Moreover, despite all the recent advancements in the field of biosensing, development of sensitive and selective fluorescence detection of Fe (III) ions is still a challenge. With this regard, effort has been taken in search of small nanoparticles[16-17] with better defined PL,[18] higher quantum yield,[19] and good biocompatibility for the detection of biologically significant metal ions.[20] Fluorescent carbon nanodots (CNDs), in the nanocarbon family, offer superior aqueous solubility,[18] robust chemical inertness, promising PL properties[21] and better biocompatibility than heavy metal quantum dots.[22-23] Moreover, polarized carbon atoms[24] and oxygen containing functional groups such as hydroxyl and carboxyl groups in the CNDs contribute to the overall hydrophilicity providing a better platform for easy functionalization of various organic, inorganic, and biological entities.[25-28] High sensitivity, short response time, stable PL, and low toxicity[29] of the CNDs provides a suitable platform for biosensing.[30]

In recent years, several reports have been focused on detection of iron using CNDs. These studies have shown that nitrogen-doping can effectively enhance

fluorescence quantum yield, resulting in high sensitivity and rapid response.[31-37] Various CNDs exhibited sensitivity towards iron with limits of detection confined to ppm levels,[38-39] however increasing the quantum yield could result in even more sensitive detection. Few reports demonstrated limit of detection (LOD) in nanomolar range using CNDs of a good quantum yield.[40-42] Moreover, multiple researchers have synthesized biocompatible CNDs that enable cell imaging along with iron sensing.[40,43-47] Despite all the recent advancements, there is still a need for the economical synthesis of an appropriate nanoprobe that offers high quantum yield, and improved sensitivity and selectivity. Additionally, the underlying detection mechanism is less studied and needs to be explored.

Hydrothermal method or microwave-assisted CNDs synthesis has been well established to doping different elements thus tuning the quantum yield.[48-53] Herein we use a facile, cost effective, one-step microwave synthesis of highly fluorescent, small, water-soluble CNDs using two different precursor molecules, ethylene diamine (EDA) for E-CNDs and urea for U-CNDs as a comparison study. The CNDs are well characterized and then used in the Fe (III) detection studies. The as synthesized E-CNDs showed the LOD of 18 nM with a quantum yield of 64% by incorporating a high amount of nitrogen (11-12%), comparable to previously nitrogen doped CNDs-based sensing probes for iron detection.[32, 36-37, 54] Upon addition of Fe (III) ions, the fluorescence intensity of the CNDs was quenched with a fast response time within 1 minute. The quenching of the CNDs upon addition of Fe (III) was evaluated using the Stern-Volmer equation. Iron (III) detection in real samples such as tap water and human serum was performed as an

application demonstration. Moreover, optical imaging of human endothelial (EA. Hy926) cells with Fe (III) incubation shows potential of using CNDs for iron sensing in living cells. The current work demonstrates high quantum yield CNDs as a fluorescence turn off sensor in the detection of Fe (III) with improved selectivity, fast response time, and better limit of detection than traditional methods. Moreover, to further understand the quenching reaction, of CNDs by Fe (III), which is inadequately studied, an electrochemical technique, cyclic voltammetry, was used to investigate the charge transfer between the CNDs and Fe (III) by changing the concentration of CNDs in the Fe (III) solutions.

Methods and Materials

Citric acid (ACROS Organics), Urea (Aldrich, 99% ACS reagent), Ethylenediamine (EDA, Fisher Scientific), quinine sulfate dihydrate, KCl (ACROS Organics), $CoCl_2$, $FeCl_2$ (Alfa Aesar), $FeCl_3$, $CrCl_3$, $AgNO_3$, $CuCl_2$, $CaCl_2$, $MgCl_2$, gold electrode, Ag/AgCl reference electrode, platinum electrode (Fisher Scientific), DMEM media, EA. hy926 cell line (ATCC), pen/strep solution, fetal bovine serum (Sigma Aldrich), CCK-8 assay kit (Sigma Aldrich), human serum. These materials were used in the present work without any further purification.

Fluorescent CNDs (E-CNDS & U-CNDs) were synthesized through a microwave-assisted procedure. Briefly, 960 mg of citric acid (ACROS Organics) was mixed with 1 ml EDA and 1 ml of DI water, and pyrolyzed in microwave synthesizer (CEM Corp 908005 Microwave Reactor) for 18 min at temperature below 150 ºC and 300 W power to synthesize E-CNDs. The brown foamy solution was dissolved in 5 ml of DI water and

dialyzed through MWCO 1000 membrane (Scientific Fisher) for 24 hrs. Similarly, U-CNDs were synthesized by mixing 1 g of urea with 1 g of citric acid and 1 ml of DI water and pyrolyzed in 150 W microwave for 12 min at 110^{o}c. The cooled reactant mixture was centrifuged at 3500 rpm for 20 min to remove large and aggregated particles. The two CNDs solutions were freeze dried for 24 hours using a freeze drier (Labconco Free Zone 6 Freeze Dryer).

The synthesized CNDs were characterized using Transmission Electron Microscopy (TEM, Carl Zeiss Libra 120 Plus). The CNDs samples were dropped onto carbon coated copper grids for analysis. The size was further characterized using Atomic Force Microscopy (AFM, Agilent 5600LS AFM) in tapping mode. AFM samples were prepared by dropping CNDs solutions onto a freshly cleaved mica surfaces and vacuum dried. Fourier transform infrared (FTIR) spectroscopy (Agilent FTIR) was used to investigate surface functional groups. XPS (Thermo Scientific ESCALAB Xi^{+}) and EDX (Bruker Nano XFlash Detector 5030) were used to determine elemental composition and atomic weight % of the as prepared CNDs. Zeta potential of the CNDs (0.05 mg mL^{-1}) was measured using Malvern Zetasizer ZEN3600. The optical properties of the CNDs were measured using UV-Visible spectroscopy (Varian Cary 6000i) and fluorescence spectroscopy (Horiba FluoroMax-4). Excitation-dependent behavior of the as prepared E-CNDs (0.01 mg mL^{-1}) and U-CNDs (0.1 mg mL^{-1}) was determined using a fluorescence spectrophotometer at different excitation wavelengths ranging from 330-450 nm.

The fluorescence quantum yield of the as synthesized CNDs was measured with Quinine Sulfate (QS) in 0.1M H_2SO_4 as a standard (QY: 54%) using the following equation:[53, 55-56]

$$\Phi_C = \Phi_{QS} \times \frac{Grad_C}{Grad_{QS}} \times \frac{{\eta_C}^2}{{\eta_{QS}}^2} \quad (2.1)$$

where, Φ represent the quantum yield, Grad is the gradient from the plot of integrated fluorescence intensity vs absorbance and η, refractive index (aqueous solution 1.33); the plots of E-CNDs and U-CNDs as a comparison to the standard QS are shown in Figure A.S1, respectively. The subscript QS and C denoted quinine sulfate and CNDs respectively.

The decrease in the fluorescence intensity of the CNDs with addition of Fe (III) ions was carried out for different time intervals ranging from 0.5, 1, 2, 3, 4, 5, 6, 7, 8, 9, 10, 15 min. A 10 µl aliquot of each types of E-CNDs (0.01 mg mL^{-1}) and U-CNDs (0.1 mg mL^{-1}) was suspended in 100 µl of Fe (III) (10 µM) and 890 µl of water. The fluorescence intensity was calculated for each time interval.

The stability of the CNDs in aqueous solution was measured for every 10 days up to 50 days using fluorescence spectrophotometer. The selectivity of the CNDs towards Fe (III) ions was determined. Briefly, 50 µM of different metal ions (Ca^{2+}, Co^{2+}, Fe^{2+}, Ag^{+}, Cu^{2+}, K^{+}, Fe^{3+}, Cr^{3+} and Mg^{2+}) were mixed with 10 µl of E-CNDs (0.01 mg mL^{-1}) and U-CNDs (0.1 mg mL^{-1}). The selectivity of the CNDs towards Fe (III) in the presence of

competitive metal ions was tested. The fluorescence spectra were measured for each type of the metal ions used.

Cyclic voltammetry was performed using a three-electrode electrochemical cell with a working gold electrode, 3 M Ag/AgCl reference electrode and platinum counter electrode. The electrolyte solution is 10 mM Fe (III) ions with different concentrations of CNDs in nitrogen-purged deionized water. The samples were run at different scan rates at room temperature.

Human serum samples were centrifuged to remove protein content and the supernatant was treated with CNDs at a concentration of 0.1 mg mL^{-1} to detect the levels of Fe (III). Then the serum samples were spiked with different concentrations of Fe (III) and recovery rates were calculated based on the standard curve of the Fe (III). Briefly, 10 µl of E-CNDs (0.01 mg mL^{-1}), 10 µl of different concentrations of Fe (III) and 80 µl of human serum were mixed together and incubated for 5 minutes at room temperature and the emission spectra was recorded using an excitation wavelength of 350 nm. Similar set of experiments were performed with U-CNDs at a concentration of 0.1 mg mL^{-1}.

Human endothelial cells (EA. Hy926) were cultured in DMEM supplemented with 10% FBS and 1% pen/strep antibiotic solution. The cells were seeded on sterilized glass cover slips in 24 well plates and incubated at 37 ºC and 5% CO_2 for 24 hours, followed by incubation with E-CNDs (0.2 mg mL^{-1}) or U-CNDs (0.5 mg mL^{-1}) for 6 hours. The cells were washed twice with 1x PBS and treated with 10 µM Fe (III) in DMEM media for different time intervals (5 min, 30 min and 1 h). As a control, no Fe (III) ions were added. The cells were washed twice with 1x PBS and fixed with 4%

paraformaldehyde for 12 min. The cells were washed twice with 1x PBS and stained with mitotracker green (stains actin filaments) 30 min. The cover slips were mounted on the glass slides using mounting media and imaged under confocal microscope (Zeiss Z1 Spinning Disk Confocal Microscope) at 20X magnification.

Results and Discussion

The AFM images show the even dispersion of E-CNDs (Figure 2.1A) on the mica surface with an average height of 7 nm. Similarly, U-CNDs (Figure 2.1C) also show an even distribution on the mica surface with an average height of 2.4 nm. Since both CNDs are smaller than the radius of curvature for the AFM probe, only the height data can be used to determine size. The TEM images demonstrate monodisperse, spherical E-CNDs (Figure 2.1B) and U-CNDs (Figure 2.1D) with sizes around 7 nm and 2.4 nm, respectively, which are in accordance with the height profiles of the AFM images. The overall yield of E-CNDs and U-CNDs was found to be 8% and 5%, respectively.

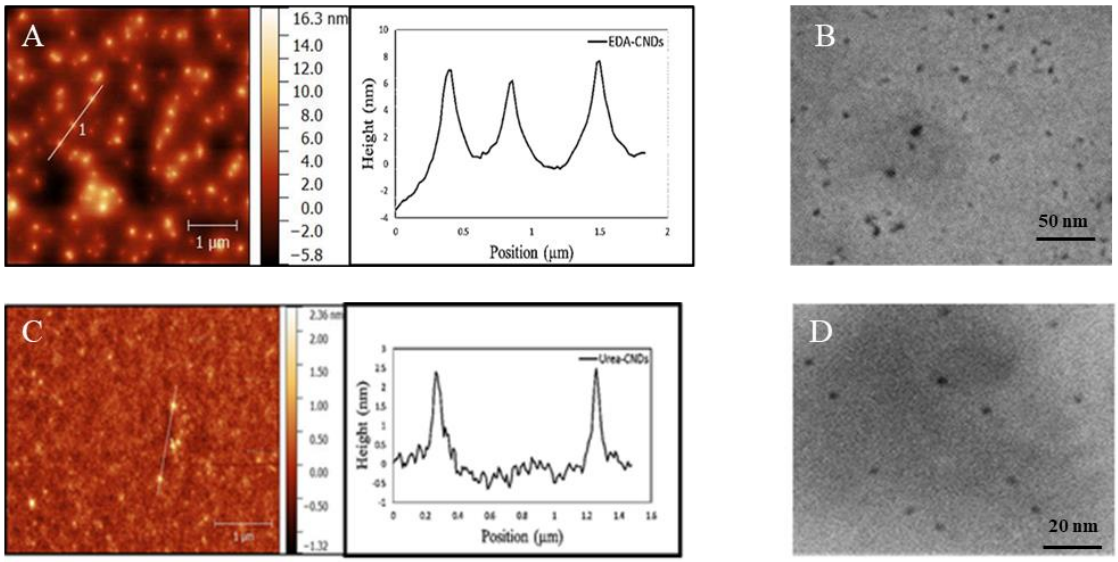

Figure 2.1. AFM and TEM of CNDs. Atomic force microscopy (AFM) images of E-CNDs (A) and U-CNDs (C) with their respective height profiles around 7 nm and 2.4 nm respectively, and the TEM images of E-CNDs (B) and U-CNDs (D), respectively.

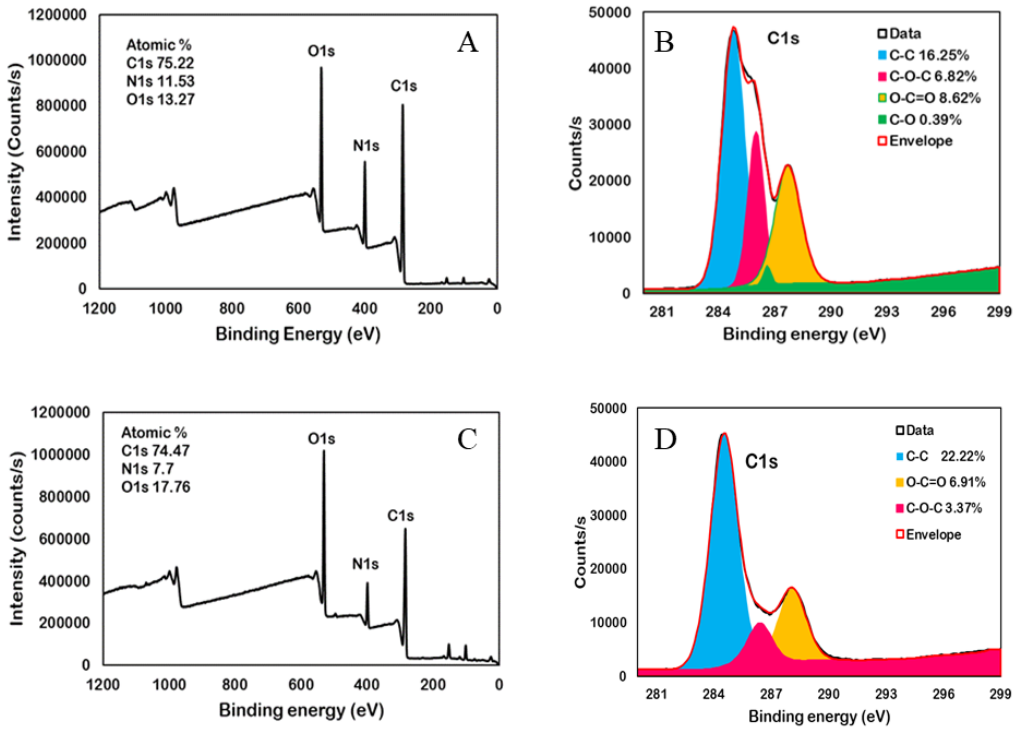

Figure 2.2. XPS Spectra of CNDs. XPS survey spectrum of E-CNDs (A) and U-CNDs (C) respectively. High resolution C1s peaks of E-CNDs (B) and U-CNDs (D).

The XPS survey spectrum of both the E-CNDs (Figure 2.2A) and U-CNDs (Figure 2.2C) show the presence of peaks at 285.0, 400.5, and 532.0 eV attributing to C1s, O1s and N1s respectively. E-CNDs present intense N1s peak (Figure 2.2A) in comparison to the U-CNDs (Figure 2.2C) depicting higher amounts of N incorporated into E-CNDs from EDA.[57] The C1s spectrum of U-CNDs (Figure 2.2B) show C-C, O-C=O and C-O-C surface groups whereas E-CNDs (Figure 2.2D) gives one more additional C-O functional group. The O1s and N1s spectra for both E-CNDs (Figure A.S2A & A.S2B) and U-CNDs (Figure A.S2C & A.S2D) are observed at 531 and 400 eV respectively. EDX analysis provides the weight and atomic ratios of C, H, O and N for both E-CNDs (Figure A.S3A) and U-CNDs (Figure A.S3B), and higher nitrogen content in E-CNDs (11.3% wt) vs. U-CNDs (8.2% wt) was observed. The reaction behind the incorporation of more nitrogen into the E-CNDs could be attributed to the faster reaction between the amines of EDA with the carboxylic groups of citric acid, compared to formation of U-CNDs. The reaction between amides of urea and carboxylic groups of citric acid is slower due to the resonance from the double bonded carbon atom of urea.[58]

The zeta potential showed the surface charge of the E-CNDs and U-CNDs to be -7.32±0.92 mV and -38.5±2.72 mV, respectively. The more negative charge of the U-CNDs is attributed to the higher ratio of COO^- groups and the less negative charge of the E-CNDs to the presence of positive charged amine groups, which is in accordance with the XPS data. The FTIR (Figure A.S4) spectra of both types of CNDs show broad absorption bands at 3000-3500 cm^{-1} assigned to stretching vibrations of O-H and N-H corresponding to the carboxylic acid and amine groups, respectively. The bands at 1538,

1432, and 1375 cm^{-1} of the E-CNDs can be assigned to the bending vibrations of N-H, C-N, and C-H, respectively.[59] U-CNDs shows a peak at 1750 cm^{-1} which can be ascribed to the stretching frequencies of –C=O derived from –COOH. Similarly, C=C bending peak at 1549 cm^{-1} and characteristic O-H bending at 1655 cm^{-1} are observed.[60] The FTIR results clearly demonstrates the presence of amino, carboxyl and hydroxyl groups on the surface of the two CNDs, which attributes to the overall hydrophilicity of the CNDs.

The UV-Visible spectrum of E-CNDs (Figure 2.3A) and U-CNDs (Figure 2.3B) shows shoulder peaks at 250 nm and 245 nm which are attributed to π- π^* transitions of C=C (aromatic sp^2 domains).[61] Strong broad peaks at 350 nm and 337 nm are assigned to n-π transitions of C=O bond involving functional groups with electron lone pairs on the E-CNDs and U-CNDs respectively.[40] The strong emission peaks of the E-CNDs (Figure 2.3A) and U-CNDs (Figure 2.3B) are centered at ~450 nm with an excitation wavelength of 350 nm. Both the CNDs exhibit yellow/brown color under daylight and emitted blue light under UV light irradiation (Figure 2.3A & 2.3B inset). The excitation dependence emission of E-CNDs and U-CNDs is observed at different wavelengths starting from 330-450 nm with an increment of 30 nm (Figure A.S5), which may be due to the fluorescence origin of the CNDs relevant to the sizes, surface states, and functional groups. The strongest emission peak is observed at an excitation wavelength of 350 nm for E-CNDs.[62] With the U-CNDs, strong emission peaks, but less than that of E-CNDs, were observed at broad range of (360-420 nm) excitation wavelengths which correspond to the broad absorption spectrum (Figure 2.3B). The highest quantum yields of E-CNDs

and U-CNDs are measured to be 64.0±1.2% and 8.4±0.7%, respectively, with reference to quinine sulfate.[63]

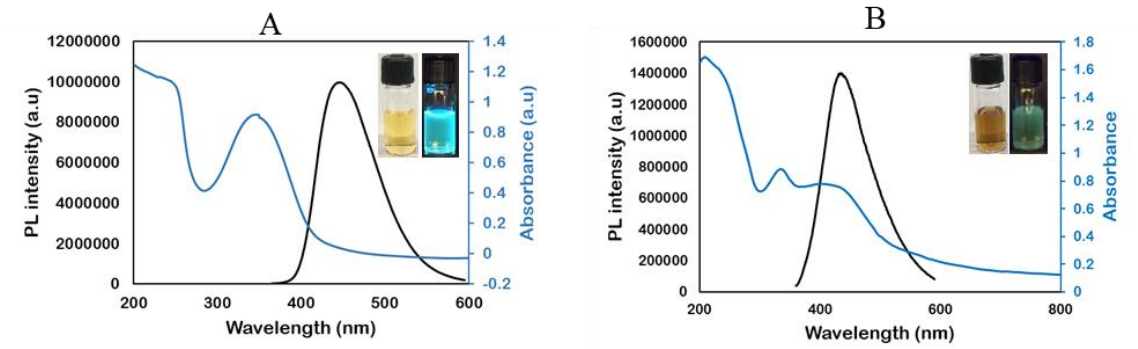

Figure 2.3. Photoluminescent Properties of CNDs. UV-Vis absorption (blue) and PL emission (black) of E-CNDs (0.01 mg mL^{-1}) (A) and U-CNDs (0.1 mg mL^{-1}) (B).

The fluorescence intensity of both the E-CNDs (Figure A.S6A) and U-CNDs (Figure A.S6B) quenches rapidly within 30 seconds upon addition of Fe (III) ions (60 µM). The excitation wavelength was 350 nm for this experiment. At the time frame of 1 minute, the decrease in the fluorescence intensity stabilized and no significant change in the fluorescence intensity was observed even after 15 minutes. This clearly shows that the CNDs can be used as a fluorescent probe in the detection of Fe (III) ions rapidly within a minute. Note that no significant change is observed in the absorption spectra of E-CNDs (Figure A.S7A) and U-CNDs (Figure A.S7B) after the addition of Fe (III) (100 µM) ions.

Figure 2.4A and 2.4B are clearly evidence that, with increase in the concentration of Fe (III) (from top to bottom: 0, 1, 2, 5, 10, 20, 50, 100, 200, 500, 1000, 2000, 5000 µM), the fluorescence intensity of both the E-CNDs and U-CNDs decreased significantly with concentration increase of Fe (III), the fluorescence intensity is negligible. Moreover,

there is a linear correlation between the quenching efficiency ($(F_0-F)/F$) and Fe (III) ion concentration in both E-CNDs (Figure 2.4C) and U-CNDs (Figure 2.4D), where F_0 and F represent the fluorescence intensity of the CNDs in the absence and presence of Fe (III) ions, respectively. The limit of detection (LOD) is calculated using the signal noise ratio S/N=3 for the CNDs based on the plots with the low concentration below sub μM (Figure A.S8). The LOD is determined to be 18 nM and 30 nM for E-CNDs and U-CNDs, respectively. Table A.S1 lists several publications using CNDs as PL probes for Fe (III) detection for a comparison to this work. This work demonstrates good performance for Fe (III) detection in terms of the lowest detection limit, sensitivity and a much larger dynamic detection range at the similar level of quantum yield to the best performance in literature, such as in refs.[40-42, 64-65]

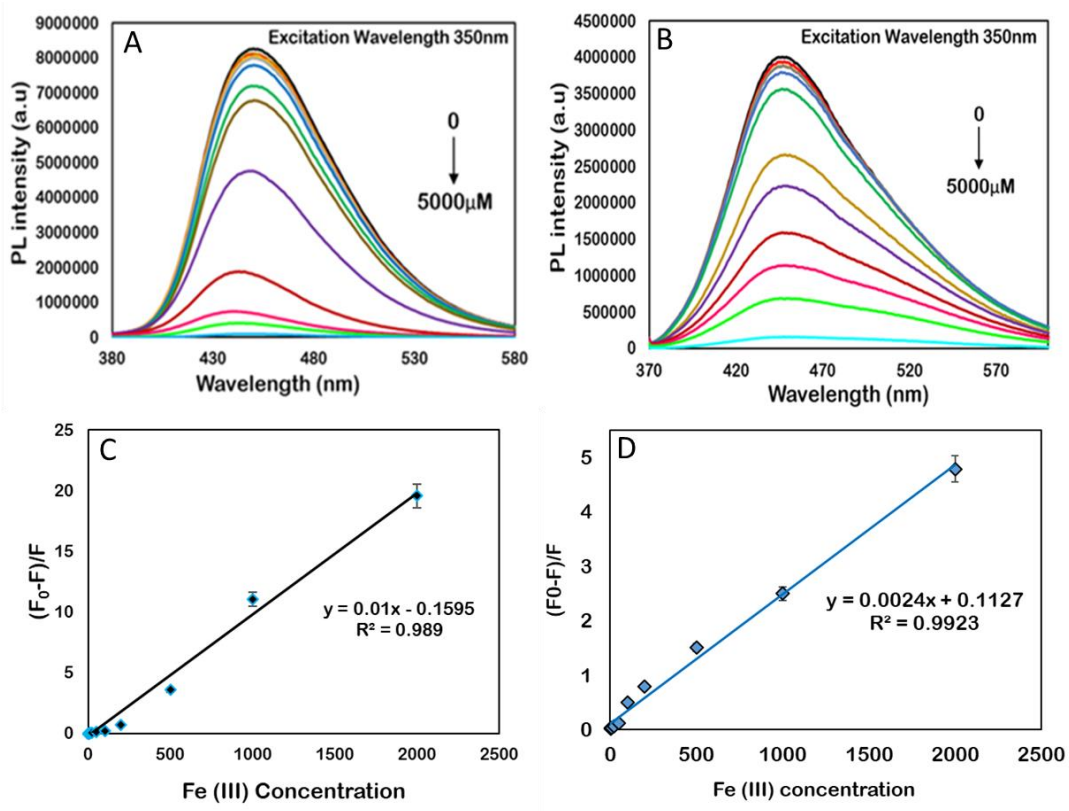

Figure 2.4. Fluorescence Quenching of CNDs upon Addition of Fe (III) Ions. PL intensity of E-CNDs (0.01 mg mL^{-1}) (A) and U-CNDs (0.1 mg mL^{-1}) (B) upon addition of different concentrations of Fe (III) ions. Linear plot of E-CNDs (C) and U-CNDs (D) fluorescence quenching, $(F_0\text{-}F)/F$, versus Fe (III) concentration at 0.5 – 2000 µM for E-CNDs and 1.0 – 2000 µM for U-CNDs. Lower concentrations of Fe (III) are ploted in Figure A.S8.

The stability of the E-CNDs (Figure 2.5A) & U-CNDs (Figure 2.5B) was observed for 50 days with an interval of 10 days at a concentration of 0.05 mg mL^{-1}. There is no significant decrease in the fluorescence intensity in both types of CNDs. This suggests the stability of the CNDs in the aqueous solution, which can be a better entity for use in biological solutions. The selectivity of the CNDs towards different metal ions (Ca^{2+}, Co^{2+}, Fe^{2+}, Ag^{+}, Cu^{2+}, K^{+}, Fe^{3+}, Cr^{3+}, and Mg^{2+}) of 50 µM concentration was demonstrated using fluorescence spectroscopic measurements. Both E-CNDs (0.05 mg

mL^{-1}) (Figure 2.5C) and U-CNDs (0.1 mg mL^{-1}) (Figure 2.5D) show significant decrease in the fluorescence intensity upon addition of Fe (III) ions in comparison to the other metal ions. The quenching efficiency of E-CNDs (Figure A.S9A) and U-CNDs (Figure A.S9B) towards Fe (III) was found to be 87±4% and 70±3%, respectively, much higher in comparison to other metal ions. The metal ions have no significant effect on the fluorescence quenching of E-CNDs (Figure A.S9C) and U-CNDs (Figure A.S9D) but in the presence of Fe (III) ions, the decrease in the intensity is obvious (Figure 2.5E & 2.5F). Note that the counter anions, such as NO^{3-}, Cl^{-} in this study show insignificant interference. The insignificance of fluorescence interference with metal ions suggests the high selectivity of both the CNDs as potential probes in the detection of Fe (III) ions.

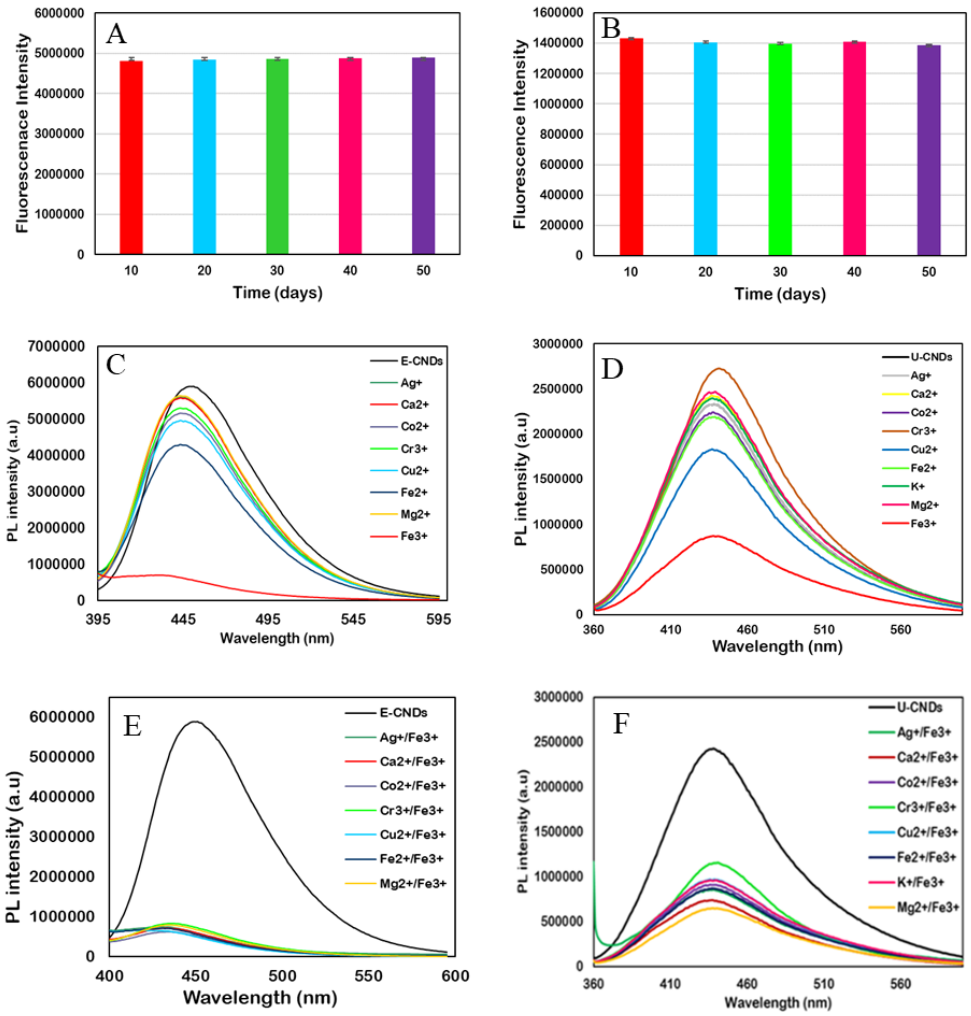

Figure 2.5. Stability of CNDs and Interference of Fluorescence in Presence of Different Cations. Stability of fluorescence intensity of 0.05 mg mL^{-1} E-CNDs (A) & 0.1 mg mL^{-1} U-CNDs (B) with time (days). Representative fluorescence emission spectra of the E-CNDs (C) and U-CNDs (D) in presence of different cations at a concentration of 50 µM in water, and (E) E-CNDs and (F) U-CNDs with mixed 50 µM Fe (III) ions with different cations (50 µM).

To demonstrate detection of Fe (III) in real samples, the iron content in both tap water and human serum samples were determined using the CNDs. When the E-CNDs (Figure A.S10A) and U-CNDs (Figure A.S10B) were added to the tap water and human serum, there is a decrease in the fluorescent intensity which indicated the presence of iron

present. With the help of the calibration curve between Fe (III) concentration and the CNDs fluorescence intensity, E-CNDs and U-CNDs were able to detect the iron content in tap water to be 3.8 µM and 1µM, respectively. The iron content in concentrated human serum sample was found to be 27.8 µM and 24.6 µM using E-CNDs and U-CNDs, respectively. The ability of the CNDs to detect the iron content in real samples was validated with inductively coupled plasma optical emission spectrophotometer (ICP OES). Standard solutions of Fe (III) (0.1, 1, 5, 10 ppm) were prepared and calibration curve was plotted with Fe (III) concentration vs. emission intensity (Figure A.S11). Samples of tap water and serum in 3% HNO_3 were analyzed with ICP for iron content and was found to be 2.56 µM and 28 µM respectively which is in accordance with the fluorescence data of the CNDs (Figure 2.4).

The high quantum yield and excellent photostability allow the as-synthesized CNDs to be used in bioimaging. The confocal images show the localization of both the CNDs inside the EA. hy926 cells with bright blue fluorescence (Figure 2.6). The cells were counter stained with Mito-tracker green (MT green) to label the actin filaments. In the absence of Fe (III) ions, no quenching of fluorescence intensity is observed in the cells incubated with either E-CNDs or U-CNDs (Figure 2.6A). Quenching of fluorescence is observed in the cells incubated with the CNDs upon the addition of Fe (III) ions. At time interval of 5 min, there is not much decrease in the fluorescence intensity when compared to the control (Figure 2.6B), but after the incubation of Fe (III) ions for 30 min, there is a significant decrease in the fluorescence intensity (Figure 2.6C).

The fluorescence is almost completely quenched after incubation of Fe (III) ions for 1 h (Figure 2.6D).

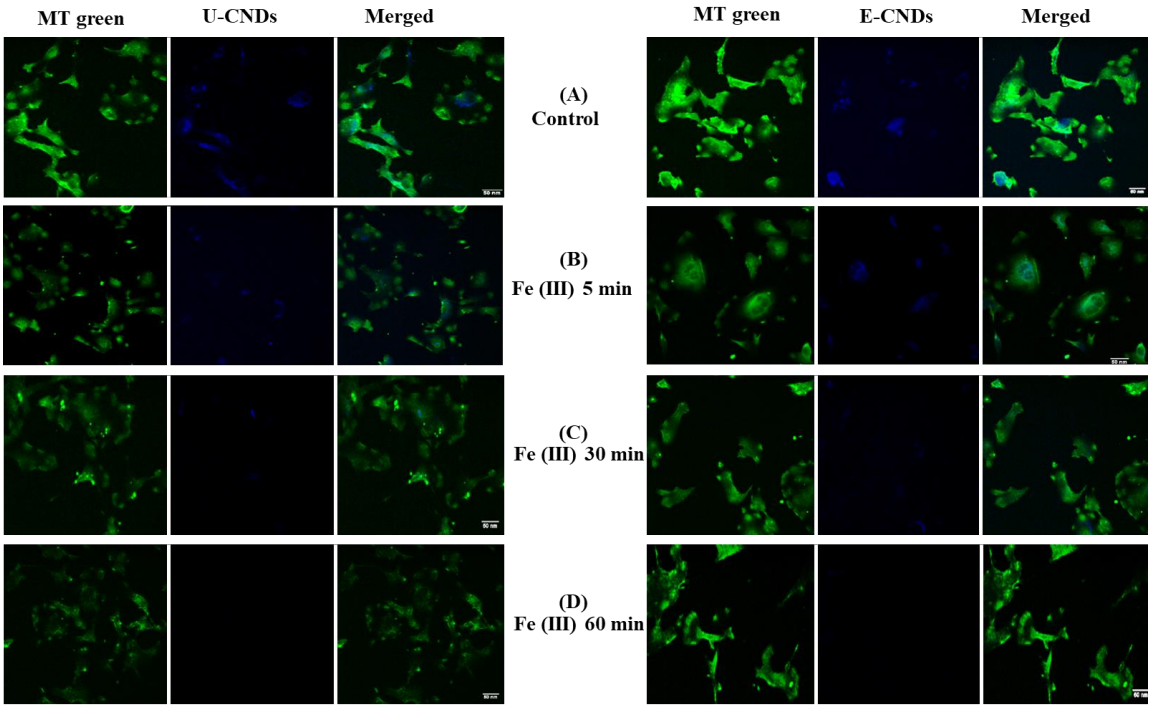

Figure 2.6. Confocal Images. Fluorescence images of EA. hy926 cells incubated with E-CNDs (0.1mg mL^{-1}, right) and U-CNDs (0.3mg mL^{-1}, left) in the absence of Fe (III) ions (A). Fluorescence images of EA. hy926 cells incubated with E-CNDs and U-CNDs in the presence of 10µM of Fe (III) for different time intervals of 5 min (B), 30 min (C) and 1 hour (D).

The possible quenching mechanism of the CNDs in presence of Fe (III) ions was investigated. The quenching process may occur due to the formation of a non-fluorescent complex, when a fluorescent molecule and a quencher interact together. The process can either be static or dynamic quenching which can be fitted to the Stern-Volmer equation.[66]

$$F_0/F = 1 + K_{sv}[Q] \quad (2.2)$$

where F_0 and F represent the fluorescence intensity of the CNDs in the absence and presence of Fe (III) ions, respectively, K_{sv} is the quenching constant, and Q is the concentration of the quencher (Fe (III) ions).

Both the CNDs show good linear correlation with the Fe (III) ion concentration following the Stern-Volmer plot. The quenching constant (K_{sv}) for the low concentration linear range (0.01 to 0.5 μM) was determined to be $5.57\times10^4\ M^{-1}$ and $3.76\times10^4\ M^{-1}$ for E-CNDs (Figure A.S8A) and U-CNDs (Figure A.S8B), respectively, by plotting the quenching efficiency ($(F_0-F)/F$) vs. Fe (III) ion concentration. The K_{sv} values for E-CNDs (Figure 2.4C) and U-CNDs (Figure 2.4D) was calculated as $1\times10^4\ M^{-1}$ and $2.3\times10^3\ M^{-1}$, respectively, for the broader linear concentration range of 0.5-2000 μM. The larger constant K_{sv} value suggests faster kinetics of the association of CNDs with Fe (III) at lower concentration of CNDs. Upon addition of Fe (III) ions to the CNDs solution, the strong blue fluorescence was quenched which was clear from the decrease in the fluorescence intensity spectra of both the CNDs (Figure 2.4A & 2.4B). In the presence of Fe (III) ions, the fluorescence intensity of the CNDs was quenched but this phenomenon was not observed upon the addition of Fe (II) ions (Figure A.S12). In the presence of Fe (III) ions, the nitrogen rich CNDs may donate an electron to the Fe (III) to an orbital in the half-filled d-shell, resulting in the formation of a low or non-fluorescent complex. Hence, a fluorescence quenching reaction is proposed that addition of CNDs to Fe (III) solution will form a complex of CNDs-Fe (III), then followed with electron transfer between the optical active sites of CNDs and Fe (III) ions where the Fe (III) is being

reduced to Fe (II). As a result, the fluorescence of CNDs in the complex CNDs-Fe (III)/(II) is quenched.

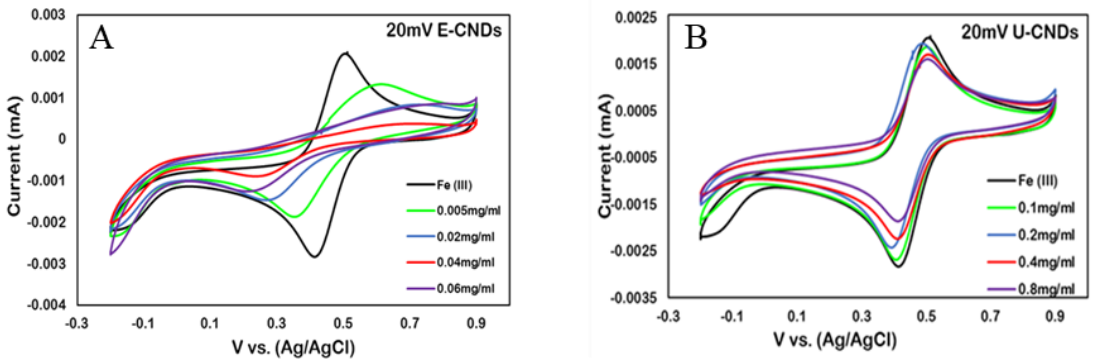

Figure 2.7. Cyclic Voltammograms. Cyclic voltammograms of Fe (III) incubated with different concentrations of E-CNDs (A) and U-CNDs (B) at a scan rate of 20 mV s^{-1}.

To further verify the proposed charge transfer quenching process, electrochemistry using cyclic voltammograms (CV) of Fe (III) ions in the presence and absence of CNDs was performed with the potential window of -0.2 to 0.9 V vs. Ag/AgCl. The CV plots of Fe (III) ions have both oxidation and reduction peaks, but the peaks started to disappear upon the addition of the CNDs. Moreover, the redox peaks disappeared with the increasing concentration of the CNDs (Figure 2.7). This clearly states that, as the concentration of the CNDs increased and more CNDs-Fe (III) complex formation, electrons from the CNDs are being transferred to the Fe (III) ions resulting in the loss of redox peaks. The CVs for E-CNDs present much more decrease in peak current than that of U-CNDs, even though the concentration of E-CNDs is much lower. The results strongly support that the fluorescence of E-CNDs quenching reaction is kinetically faster than the U-CNDs by Fe (III), a good agreement with the K_{sv} value

obtained by the Stern-Volmer equation. Based on the observation, a quenching reaction of E-CNDs with Fe (III) is as follows:

$$\mathrm{E-CND} + \mathrm{n}\big(\mathrm{Fe(III)}\big) \rightarrow \mathrm{E-CND-(Fe(III))_n} \leftrightarrow \mathrm{E-CND-}\big(\mathrm{Fe(II)}\big)_\mathrm{n} \qquad (2.3)$$

The n in Eq. 3 is the stoichiometric coefficient (a number greater than 1) of Fe ions combine to a single CND through coordinating or chelating interactions due to large number of surface functional groups for chelating.[67] When CNDs are added to the Fe (III) solution, a complex E-CND-(Fe (III))$_n$ forms and participates in the redox reaction at the working electrode, resulting in E-CND-(Fe (II))$_n$ complex. Note that, since the Fe (III) molar concentration is orders higher than the CNDs, not all Fe (III) ions form the CND-Fe (III) complex. The CV redox peaks represent an ensemble of both the free iron ions and the complex (Figure 2.7). Due to the association of E-CNDs with Fe (II) after the reaction, the diffusion of E-CND-(Fe(II))$_n$ complex to the working electrode is slower than the free iron ions in the cyclic voltammetry, consequently a broadened oxidation peak of Fe (II) in the CVs is observed. The larger separation of oxidation and reduction peaks with more CNDs in the solution suggests slower electrochemical kinetics of redox reaction of CND-(Fe (III))$_n$/CND-n(Fe (II))$_n$ at the electrode surface because of more CNDs-(Fe (II/III))$_n$ complex formation and less free Fe (III) ions in the solution.[68] In a control experiment, the cyclic voltammetry of Fe (II) treated with E-CNDs or U-CNDs presents insignificant changes of the redox reaction at electrode surfaces (Figure A.S13 and A.S14), suggesting that the chelating of CNDs to Fe (II) is weak and electron transfer from Fe (II) to CNDs is not in favor. This result indicates the fluorescence quenching

would be specifically electron transfer from the CNDs to Fe (III) ions when the complex forms, namely oxidation of CNDs and reduction of Fe (III) promoted by applied external voltage. Moreover, this control experiment also implies that it is unlikely the adhesion of CNDs or a contamination to the electrode surface to cause the slower electrochemical kinetics.

The selectivity of the CNDs can be attributed to the energy level match between the photo-excited excitons (PL centers) in CNDs and the level of valence d state orbit of the Fe (III) when the CND- $(Fe(III))_n$ complex forms, resulting the reduction of Fe(III).[67, 69] In this work, the Fe (III) valence d state level as an electron acceptor matches the CNDs' PL centers, similar to ref[67] for Fe (III) detection, while other metal ions don't, though CNDs might be able to form a complex with other metal ions via chelating interactions. This can be further elucidated by the difference of standard reduction potential of metal ions. For instance, the standard reduction potential of Fe (III) to Fe (II) and Cu (II) to Cu (I) are 0.77 V (NHE) and 0.16 V (NHE), respectively. The Fe (III) is a much stronger oxidizing agent (electron acceptor) than Cu (II). Hence, one should not expect strong fluorescence quenching with addition of Cu (II) in this case, though the CNDs-Cu (II) complex may form due to the presence of amine groups of CNDs. This was confirmed by the CVs of Cu^{2+} in water with and without addition of E-CNDs (Figure A.S15) or U-CNDs (Figure A.S16), which don't show significant changes in shape of the CVs while the redox peak currents decrease with addition of CNDs due to formation of CND- $(Cu(II)_n$, which indicates decrease of free Cu^{2+}. Similarly, this principle is applicable to other metal ions that the energy level for charge transfer doesn't match the

excitons (PL centers) in CNDs for charge transfer. As a result, no significant interference was observed from Ca^{2+}, Co^{2+}, Fe^{2+}, Ag^{+}, Cu^{2+}, K^{+}, Fe^{3+}, Cr^{3+} and Mg^{2+} *etc*.

Conclusion

In summary, E-CNDs and U-CNDs synthesized using one step microwave synthesis are able to detect Fe (III) ions with high selectivity and sensitivity. The synthesized CNDs show good aqueous solubility, excellent stability, and high PL with E-CNDs quantum yield as high as 64%. A decrease in fluorescence intensity is observed with the increase of Fe (III) ions in the CNDs solution. E-CNDs probe provide higher sensitive analysis of Fe (III) ions in comparison to U-CNDs probe with limit of detection of about 18 nM for E-CNDs and 30 nM for U-CNDs, owing to increase nitrogen content in E-CNDs. The CNDs are used as probes to detect Fe (III) in real samples such as tap water and human serum without pretreatment, and the results are validated by ICP element analysis. Both the CNDs are successfully internalized inside endothelial cells with bright blue fluorescence and the phenomenon of fluorescence quenching is observed when the cells are incubated with Fe (III), suggesting potential sensing of Fe (III) in living cells. The fluorescence quenching of CNDs attributes to the charge transfer specifically between CNDs to Fe (III) which is further verified in cyclic voltammetry studies. The energy match of the excitons (PL centers) of the CNDs for electron transfer to the metal ions is critical for allowed charge transfer quenching mechanism when the CNDs-metal ion complex forms. In conclusion, these CNDs can be valuable nanoprobes in the sensitive and selective detection of Fe (III) ions in a broad dynamic range concentration (0 – 2000 μM).

References

1. Anastassopoulou, J., Metal–DNA interactions. *J. Mol. Struct.* **2003,** *651-653*, 19-26.

2. Lynch, S. R., Interaction of Iron with Other Nutrients. *Nutr. Rev.* **1997,** *55* (4), 102-110.

3. Lieu, P. T.; Heiskala, M.; Peterson, P. A.; Yang, Y., The roles of iron in health and disease. *Mol. Aspects Med.* **2001,** *22* (1-2), 1-87.

4. Abbaspour, N.; Hurrell, R.; Kelishadi, R., Review on iron and its importance for human health. *J. Res. Med. Sci.* **2014,** *19* (2), 164-174.

5. Helman, S. L.; Anderson, G. J.; Frazer, D. M., Dietary iron absorption during early postnatal life. *BioMetals* **2019,** *32*, s10534-019-00181-9.

6. Rosenzweig, P. H.; Volpe, S. L., Iron, Thermoregulation, and Metabolic Rate. *Crit. Rev. Food Sci. Nutr.* **1999,** *39* (2), 131-148.

7. Kaplan, J.; Ward, D. M., Muscle specific iron deficiency has systemic consequences. *EBioMedicine* **2015,** *2* (11), 1582-1583.

8. Silvestri, L.; Camaschella, C., A potential pathogenetic role of iron in Alzheimer's disease. *J. Cell. Mol. Med.* **2008,** *12* (5A), 1548-1550.

9. Hirayama, T.; Nagasawa, H., Chemical tools for detecting Fe ions. *J. Clin. Biochem. Nutr.* **2017,** *60* (1), 39-48.

10. Carter, K. P.; Young, A. M.; Palmer, A. E., Fluorescent Sensors for Measuring Metal Ions in Living Systems. *Chem. Rev.* **2014,** *114* (8), 4564-4601.

11. Resch-Genger, U.; Grabolle, M.; Cavaliere-Jaricot, S.; Nitschke, R.; Nann, T., Quantum dots versus organic dyes as fluorescent labels. *Nat. Methods* **2008,** *5* (9), 763-75.

12. Lesiak, A.; Drzozga, K.; Cabaj, J.; Banski, M.; Malecha, K.; Podhorodecki, A., Optical Sensors Based on II-VI Quantum Dots. *Nanomaterials (Basel)* **2019,** *9* (2), 192.

13. Hardman, R., A toxicologic review of quantum dots: toxicity depends on physicochemical and environmental factors. *Environ. Health Perspect.* **2006,** *114* (2), 165-172.

14. Valizadeh, A.; Mikaeili, H.; Samiei, M.; Farkhani, S. M.; Zarghami, N.; Kouhi, M.; Akbarzadeh, A.; Davaran, S., Quantum dots: synthesis, bioapplications, and toxicity. *Nanoscale Res. Lett.* **2012,** *7* (1), 480-480.

15. Chan, W. H.; Shiao, N. H., Cytotoxic effect of CdSe quantum dots on mouse embryonic development. *Acta Pharmacol. Sin.* **2008,** *29* (2), 259-66.

16. Agasti, S. S.; Rana, S.; Park, M.-H.; Kim, C. K.; You, C.-C.; Rotello, V. M., Nanoparticles for detection and diagnosis. *Adv. Drug Del. Rev.* **2010,** *62* (3), 316-328.

17. Rosi, N. L.; Mirkin, C. A., Nanostructures in Biodiagnostics. *Chem. Rev.* **2005,** *105* (4), 1547-1562.

18. Baker, S. N.; Baker, G. A., Luminescent carbon nanodots: emergent nanolights. *Angew. Chem. Int. Ed.* **2010,** *49* (38), 6726-44.

19. Zheng, X. T.; Ananthanarayanan, A.; Luo, K. Q.; Chen, P., Glowing graphene quantum dots and carbon dots: properties, syntheses, and biological applications. *Small* **2015,** *11* (14), 1620-36.

20. Ahmed, M.; Faisal, M.; Ihsan, A.; Naseer, M. M., Fluorescent organic nanoparticles (FONs) as convenient probes for metal ion detection in aqueous medium. *Analyst* **2019,** *144*, 2480-2497

21. Zhu, S.; Song, Y.; Zhao, X.; Shao, J.; Zhang, J.; Yang, B., The photoluminescence mechanism in carbon dots (graphene quantum dots, carbon nanodots, and polymer dots): current state and future perspective. *Nano Res.* **2015,** *8* (2), 355-381.

22. Zheng, M.; Xie, Z.; Qu, D.; Li, D.; Du, P.; Jing, X.; Sun, Z., On–Off–On Fluorescent Carbon Dot Nanosensor for Recognition of Chromium(VI) and Ascorbic Acid Based on the Inner Filter Effect. *ACS Appl. Mater. Interfaces* **2013,** *5* (24), 13242-13247.

23. Zeng, Z.; Zhang, W.; Arvapalli, D. M.; Bloom, B.; Sheardy, A.; Mabe, T.; Liu, Y.; Ji, Z.; Chevva, H.; Waldeck, D. H.; Wei, J., A fluorescence-electrochemical study of carbon nanodots (CNDs) in bio- and photoelectronic applications and energy gap investigation. *Phys. Chem. Chem. Phys.* **2017,** *19* (30), 20101-20109.

24. Ray, S. C.; Saha, A.; Jana, N. R.; Sarkar, R., Fluorescent Carbon Nanoparticles: Synthesis, Characterization, and Bioimaging Application. *J. Phys. Chem. C* **2009,** *113* (43), 18546-18551.

25. Roy, P.; Chen, P.-C.; Periasamy, A. P.; Chen, Y.-N.; Chang, H.-T., Photoluminescent carbon nanodots: synthesis, physicochemical properties and analytical applications. *Mater. Today* **2015,** *18* (8), 447-458.

26. Wei, W.; Xu, C.; Ren, J.; Xu, B.; Qu, X., Sensing metal ions with ion selectivity of a crown ether and fluorescence resonance energy transfer between carbon dots and graphene. *Chem. Commun.* **2012,** *48* (9), 1284-1286.

27. Kong, B.; Zhu, A.; Ding, C.; Zhao, X.; Li, B.; Tian, Y., Carbon dot-based inorganic-organic nanosystem for two-photon imaging and biosensing of pH variation in living cells and tissues. *Adv. Mater.* **2012,** *24* (43), 5844-5848.

28. Hu, S.; Trinchi, A.; Atkin, P.; Cole, I., Tunable photoluminescence across the entire visible spectrum from carbon dots excited by white light. *Angew. Chem. Int. Ed.* **2015,** *54* (10), 2970-4.

29. Lee, H. U.; Park, S. Y.; Park, E. S.; Son, B.; Lee, S. C.; Lee, J. W.; Lee, Y.-C.; Kang, K. S.; Kim, M. I.; Park, H. G.; Choi, S.; Huh, Y. S.; Lee, S.-Y.; Lee, K.-B.; Oh, Y.-K.; Lee, J., Photoluminescent carbon nanotags from harmful cyanobacteria for drug delivery and imaging in cancer cells. *Sci. Rep.* **2014,** *4*, 4665.

30. Sun, X.; Lei, Y., Fluorescent carbon dots and their sensing applications. *Trends Anal. Chem.* **2017,** *89*, 163-180.

31. He, G.; Xu, M.; Shu, M.; Li, X.; Yang, Z.; Zhang, L.; Su, Y.; Hu, N.; Zhang, Y., Rapid solid-phase microwave synthesis of highly photoluminescent nitrogen-doped carbon dots for Fe^{3+} detection and cellular bioimaging. *Nanotechnology* **2016,** *27* (39), 395706.

32. Karali, K. K.; Sygellou, L.; Stalikas, C. D., Highly fluorescent N-doped carbon nanodots as an effective multi-probe quenching system for the determination of nitrite, nitrate and ferric ions in food matrices. *Talanta* **2018,** *189*, 480-488.

33. Omer, K. M.; Tofiq, D. I.; Hassan, A. Q., Solvothermal synthesis of phosphorus and nitrogen doped carbon quantum dots as a fluorescent probe for iron(III). *Microchim. Acta* **2018,** *185* (10), 466.

34. Rao, L.; Tang, Y.; Li, Z.; Ding, X.; Liang, G.; Lu, H.; Yan, C.; Tang, K.; Yu, B., Efficient synthesis of highly fluorescent carbon dots by microreactor method and their

application in Fe^{3+} ion detection. *Mater. Sci. Eng. C Mater. Biol. Appl.* **2017,** *81*, 213-223.

35. Ye, Q.; Yan, F.; Luo, Y.; Wang, Y.; Zhou, X.; Chen, L., Formation of N, S-codoped fluorescent carbon dots from biomass and their application for the selective detection of mercury and iron ion. *Spectrochim. Acta. A Mol. Biomol. Spectrosc.* **2017,** *173*, 854-862.

36. Feng, J.; Chen, Y.; Han, Y.; Liu, J.; Ren, C.; Chen, X., Fluorescent carbon nanoparticles: A low-temperature trypsin-assisted preparation and Fe^{3+} sensing. *Anal. Chim. Acta* **2016,** *926* (5), 107-117.

37. Song, Y.; Zhu, C.; Song, J.; Li, H.; Du, D.; Lin, Y., Drug-Derived Bright and Color-Tunable N-Doped Carbon Dots for Cell Imaging and Sensitive Detection of Fe^{3+} in Living Cells. *ACS Appl. Mater. Interfaces* **2017,** *9* (8), 7399-7405.

38. Li, C.; Wang, Y.; Zhang, X.; Guo, X.; Kang, X.; Du, L.; Liu, Y., Red fluorescent carbon dots with phenylboronic acid tags for quick detection of Fe(III) in PC12 cells. *J. Colloid Interface Sci.* **2018,** *526*, 487-496.

39. Zhang, J.; Yan, J.; Wang, Y.; Zhang, Y., One-Step Hydrothermal Approach to Synthesis Carbon Dots from D-Sorbitol for Detection of Iron(III) and Cell Imaging. *J. Nanosci. Nanotechnol.* **2018,** *18* (7), 4457-4463.

40. Shi, B.; Su, Y.; Zhang, L.; Huang, M.; Liu, R.; Zhao, S., Nitrogen and Phosphorus Co-Doped Carbon Nanodots as a Novel Fluorescent Probe for Highly Sensitive Detection of Fe^{3+} in Human Serum and Living Cells. *ACS Appl. Mater. Interfaces* **2016,** *8* (17), 10717-10725.

41. Zhang, H.; Chen, Y.; Liang, M.; Xu, L.; Qi, S.; Chen, H.; Chen, X., Solid-Phase Synthesis of Highly Fluorescent Nitrogen-Doped Carbon Dots for Sensitive and Selective Probing Ferric Ions in Living Cells. *Anal. Chem.* **2014,** *86* (19), 9846-9852.

42. Li, S.; Li, Y.; Cao, J.; Zhu, J.; Fan, L.; Li, X., Sulfur-Doped Graphene Quantum Dots as a Novel Fluorescent Probe for Highly Selective and Sensitive Detection of Fe^{3+}. *Anal. Chem.* **2014,** *86* (20), 10201-10207.

43. Du, F.; Gong, X.; Lu, W.; Liu, Y.; Gao, Y.; Shuang, S.; Xian, M.; Dong, C., Bright-green-emissive nitrogen-doped carbon dots as a nanoprobe for bifunctional sensing, its logic gate operation and cellular imaging. *Talanta* **2018,** *179*, 554-562.

44. Sarkar, C.; Chowdhuri, A. R.; Kumar, A.; Laha, D.; Garai, S.; Chakraborty, J.; Sahu, S. K., One pot synthesis of carbon dots decorated carboxymethyl cellulose-

hydroxyapatite nanocomposite for drug delivery, tissue engineering and Fe^{3+} ion sensing. *Carbohydr. Polym.* **2018,** *181*, 710-718.

45. Wang, C.; Hu, T.; Wen, Z.; Zhou, J.; Wang, X.; Wu, Q.; Wang, C., Concentration-dependent color tunability of nitrogen-doped carbon dots and their application for iron(III) detection and multicolor bioimaging. *J. Colloid Interface Sci.* **2018,** *521*, 33-41.

46. Patidar, R.; Rebary, B.; Sanghani, D. A.; Bhadu, G. R.; Paul, P., Fluorescent carbon nanoparticles obtained from charcoal via green methods and their application for sensing Fe^{3+} in an aqueous medium. *Luminescence* **2017,** *32* (8), 1466-1472.

47. Suvarnaphaet, P.; Tiwary, C. S.; Wetcharungsri, J.; Porntheeraphat, S.; Hoonsawat, R.; Ajayan, P. M.; Tang, I. M.; Asanithi, P., Blue photoluminescent carbon nanodots from limeade. *Mater. Sci. Eng. C Mater. Biol. Appl.* **2016,** *69*, 914-21.

48. Li, H.; Shao, F.-Q.; Zou, S.-Y.; Yang, Q.-J.; Huang, H.; Feng, J.-J.; Wang, A.-J., Microwave-assisted synthesis of N,P-doped carbon dots for fluorescent cell imaging. *Microchim. Acta* **2016,** *183* (2), 821-826.

49. Wang, L.; Li, B.; Li, L.; Xu, F.; Xu, Z.; Wei, D.; Feng, Y.; Wang, Y.; Jia, D.; Zhou, Y., Ultrahigh-yield synthesis of N-doped carbon nanodots that down-regulate ROS in zebrafish. *Journal of Materials Chemistry B* **2017,** *5* (38), 7848-7860.

50. Xiao, D.; Yuan, D.; He, H.; Lu, J., Microwave-assisted one-step green synthesis of amino-functionalized fluorescent carbon nitride dots from chitosan. *Luminescence* **2013,** *28* (4), 612-615.

51. Liu, G.; Li, B.; Liu, Y.; Feng, Y.; Jia, D.; Zhou, Y., Rapid and high yield synthesis of carbon dots with chelating ability derived from acrylamide/chitosan for selective detection of ferrous ions. *Appl. Surf. Sci.* **2019,** *487*, 1167-1175.

52. Wang, L.; Li, B.; Xu, F.; Shi, X.; Feng, D.; Wei, D.; Li, Y.; Feng, Y.; Wang, Y.; Jia, D.; Zhou, Y., High-yield synthesis of strong photoluminescent N-doped carbon nanodots derived from hydrosoluble chitosan for mercury ion sensing via smartphone APP. *Biosens. Bioelectron.* **2016,** *79*, 1-8.

53. Zhu, S.; Meng, Q.; Wang, L.; Zhang, J.; Song, Y.; Jin, H.; Zhang, K.; Sun, H.; Wang, H.; Yang, B., Highly Photoluminescent Carbon Dots for Multicolor Patterning, Sensors, and Bioimaging. *Angew. Chem. Int. Ed.* **2013,** *52* (14), 3953-3957.

54. Zhu, X.; Wang, J.; Zhu, Y.; Jiang, H.; Tan, D.; Xu, Z.; Mei, T.; Li, J.; Xue, L.; Wang, X., Green emitting N,S-co-doped carbon dots for sensitive fluorometric

determination of Fe(III) and Ag(I) ions, and as a solvatochromic probe. *Microchim. Acta* **2018,** *185* (11), 510.

55. Zhai, X.; Zhang, P.; Liu, C.; Bai, T.; Li, W.; Dai, L.; Liu, W., Highly luminescent carbon nanodots by microwave-assisted pyrolysis. *Chem. Commun.* **2012,** *48* (64), 7955-7957.

56. Mintz, K. J.; Zhou, Y.; Leblanc, R. M., Recent development of carbon quantum dots regarding their optical properties, photoluminescence mechanism, and core structure. *Nanoscale* **2019,** *11* (11), 4634-4652.

57. Gong, X.; Lu, W.; Paau, M. C.; Hu, Q.; Wu, X.; Shuang, S.; Dong, C.; Choi, M. M. F., Facile synthesis of nitrogen-doped carbon dots for Fe^{3+} sensing and cellular imaging. *Anal. Chim. Acta* **2015,** *861*, 74-84.

58. L. G. Wade, J., *Organic Chemistry*. 6 ed.; Prentice Hall: 2005; p 1328.

59. Hu, Q.; Paau, M. C.; Zhang, Y.; Chan, W.; Gong, X.; Zhang, L.; Choi, M. M. F., Capillary electrophoretic study of amine/carboxylic acid-functionalized carbon nanodots. *J. Chromatogr. A* **2013,** *1304*, 234-240.

60. Qu, S.; Wang, X.; Lu, Q.; Liu, X.; Wang, L., A biocompatible fluorescent ink based on water-soluble luminescent carbon nanodots. *Angew. Chem. Int. Ed.* **2012,** *51* (49), 12215-8.

61. Zhu, X.; Zhang, Z.; Xue, Z.; Huang, C.; Shan, Y.; Liu, C.; Qin, X.; Yang, W.; Chen, X.; Wang, T., Understanding the Selective Detection of Fe^{3+} Based on Graphene Quantum Dots as Fluorescent Probes: The Ksp of a Metal Hydroxide-Assisted Mechanism. *Anal. Chem.* **2017,** *89* (22), 12054-12058.

62. Dong, Y.; Pang, H.; Yang, H. B.; Guo, C.; Shao, J.; Chi, Y.; Li, C. M.; Yu, T., Carbon-based dots co-doped with nitrogen and sulfur for high quantum yield and excitation-independent emission. *Angew. Chem. Int. Ed.* **2013,** *52* (30), 7800-4.

63. Heller, C. A.; Henry, R. A.; McLaughlin, B. A.; Bliss, D. E., Fluorescence spectra and quantum yields. Quinine, uranine, 9,10-diphenylanthracene, and 9,10-bis(phenylethynyl)anthracenes. *Journal of Chemical & Engineering Data* **1974,** *19* (3), 214-219.

64. Liu, Y.; Duan, W.; Song, W.; Liu, J.; Ren, C.; Wu, J.; Liu, D.; Chen, H., Red Emission B, N, S-co-Doped Carbon Dots for Colorimetric and Fluorescent Dual Mode Detection of Fe^{3+} Ions in Complex Biological Fluids and Living Cells. *ACS Appl. Mater. Interfaces* **2017,** *9* (14), 12663-12672.

65. Zhou, X.; Zhao, G.; Tan, X.; Qian, X.; Zhang, T.; Gui, J.; Yang, L.; Xie, X., Nitrogen-doped carbon dots with high quantum yield for colorimetric and fluorometric detection of ferric ions and in a fluorescent ink. *Microchimica Acta* **2019,** *186* (2), 67.

66. Boaz, H.; Rollefson, G. K., The Quenching of Fluorescence. Deviations from the Stern-Volmer Law. *J. Am. Chem. Soc.* **1950,** *72* (8), 3435-3443.

67. Wang, Y.; Chang, Q.; Hu, S., Carbon dots with concentration-tunable multicolored photoluminescence for simultaneous detection of Fe3+ and Cu2+ ions. *Sensors and Actuators B: Chemical* **2017,** *253*, 928-933.

68. Wei, J.; Liu, H.; Dick, A. R.; Yamamoto, H.; He, Y.; Waldeck, D. H., Direct Wiring of Cytochrome c's Heme Unit to an Electrode: Electrochemical Studies. *J. Am. Chem. Soc.* **2002,** *124* (32), 9591-9599.

69. Gao, X.; Du, C.; Zhuang, Z.; Chen, W., Carbon quantum dot-based nanoprobes for metal ion detection. *Journal of Materials Chemistry C* **2016,** *4* (29), 6927-6945.

CHAPTER III

DESIGN OF CURCUMIN LOADED CARBON NANODOTS DELIVERY SYSTEM: ENHANCED BIOAVAILABILITY, RELEASE KINETICS AND ANTICANCER ACTIVITY

This chapter has been submitted for publication as: Arvapalli, Durga; Sheardy, Alex; Allado, Kokougan; Chevva, Harish; Wei, Jianjun, Design of Curcumin loaded Carbon Nanodots Delivery System: Enhanced Bioavailability, Release Kinetics and Anticancer Activity. 2020.

Overview

Despite the potential health benefits of curcumin (Curc) such as antioxidant, anticancer and anti-inflammatory, antimicrobial properties, its usage is limited by poor bioavailability and low aqueous solubility. Nano–formulations of curcumin has gained lot of attention due to their increased bioavailability, solubility, circulation times, targeted specificity, decreased biodegradation, better stability, and improved cellular uptake. The current study aimed to enhance the bioavailability of curcumin by using carbon nanodots (CNDs) as loading vehicles to deliver curcumin due to their excellent biocompatibility, aqueous solubility and photoluminescence properties. Two types of CNDs (E-CNDs and U-CNDs) were used for curcumin loading and characterized for particle size, morphology, encapsulation efficiency, stability, photoluminescence properties, in-vitro drug release studies, cellular uptake and anticancer activity. The prepared Curc-loading CNDs displayed size around or below 10 nm with good stability. The Curc-E-CNDs

demonstrated an encapsulation efficiency of 91%, while the Curc-U-CNDs have an encapsulation efficiency of 82%. Curcumin release followed a controlled sustained pattern, where a total of 59% and 68% of curcumin was released at 72 hours from Curc-E-CNDs and Curc-U-CNDs, respectively. Both the Curc-CNDs were uptaken by cells and exhibited prominent cytotoxicity towards cancer cells. The results clearly depict the role of CNDs as an efficient carrier for curcumin delivery with prolonged release, and enhanced bioavailability thereby improving the overall antitumor activity.

Introduction

Curcumin, a natural polyphenolic spice obtained from tropical southeast Asian plant Curcuma Longa (turmeric) has its applications dated back centuries as a dietary supplement[1-2] with its anti-inflammatory, analgesic, antiseptic and antioxidant properties.[1, 3] Phase I clinical trials in humans showed no side effects upon administration of curcumin (8 g/day). Curcumin can inhibit cell cycle progression, induce apoptosis and halt cell proliferation process in cancer cell lines thereby establishing its potential role as an anti-tumor agent. However, the poor bioavailability, low aqueous solubility, poor absorption, rapid degradation, fast metabolism, and systemic elimination hinders this elixir drug usage as a chemotherapeutic agent. Moreover, the intracellular uptake of curcumin is limited by its hydrophobicity, where curcumin binds to the lipids of the cell membrane without entering the cytoplasm.

Structural and chemical modifications have been implemented to increase the bioavailability of curcumin, but are limited due to the low potency of the derivates compared to the native curcumin, therefore requiring higher doses to elicit therapeutic

responses.[16-17] Nano-based drug delivery systems have emerged as an eminent solution to overcome the limitations and increase the bioavailability and targetability of curcumin, thereby improving the overall anticancer activity.[18] Nanoparticles size, shape, and surface chemistry plays an important role in the selection of drug delivery vehicles for cancer therapy.[19] Various nano-formulation based drug delivery systems such as liposomes,[20-24] polymeric nanoparticles,[25-27] and hydrogels[28-29] showed promising curcumin delivery, however also exhibit some drawbacks. Specifically, use of liposomes is limited by low drug entrapment and instability,[30] polymeric nanoparticles offer toxicity of unreacted monomers and initial burst release of curcumin respectively.[31] Encapsulation of curcumin into nanoparticles improve the solubility and stability of the hydrophobic drug overcoming rapid drug metabolism and transports the drug to the target site and reduces adverse side effects.[32]

Carbon nanodots (CNDs) are spherical low molecular weight luminescent particles (<10 nm) with excellent photostability against photobleaching, and possess tunable emission spectra, photo-electric activities,[33-34] good biocompatibility,[35] and low toxicity.[36-37] These desirable properties of the CNDs opened up several applications in photocatalysis,[38] bio-sensing,[39] bioimaging,[40-42] and anti- or pro-oxidation.[43-46] While tremendous progresses have been made on designing drug carrying nano-vehicles for cancer therapy,[47-52] limited light is shed on the CNDs.[53-56] Due to their superior chemical and physical properties, CNDs with large number of surface functional groups offer high surface area for drug loading, thereby increasing the solubility of hydrophobic drug

which can be used as drug loading vehicles to reach cancer site with better targeting and delivery efficiency, thereby reducing the side effects and improving drug tolerance.

The work is to synthesize curcumin-loaded CNDs with enhance bioavailability, loading efficiency and anti-cancer properties along with incorporating the unique properties, such as photoluminescence, small size (~10 nm), and stability. In the present study, two types of CNDs (E-CNDs and U-CNDs) are functionalized with curcumin for examining the bioavailability and eliciting the therapeutic effects. The Curc-CNDs are characterized regarding the structure, composite and optical properties. Curcumin release kinetics from the complex was investigated using Korsmeyer and Peppas equation. The kinetics studies provide information about the pH dependent release of curcumin as a function of time. Intracellular and anticancer activities of Curc-CNDs were tested in two cancer cell lines, HepG2 and A549 cells, and one normal cell lines, EA. hy926. Curcumin loading onto the CNDs increases the bioavailability of in cells compared to native curcumin, thereby meeting low concentrations required to elicit anti-cancer effects.

Methods and Materials

Citric acid (ACROS Organics), Ethylenediamine, Urea (Fisher Scientific), Curcumin (Chem Cruz), phosphate buffer solution (PBS) (Life Tech), quinine sulfate dihydrate, methanol (Fisher Scientific), A549 cell line, HepG2 cell line, EA. hy926 cell line, DMEM (Dulbecco’s minimum essential medium), EMEM (Eagle’s minimum essential medium), and F12 K (Ham's F-12K (Kaighn's) Medium), (ATCC), pen/strep solution, tryplE, fetal bovine serum and CCK-8 assay kit (Sigma Aldrich), alamar blue (Thermo scientific).

E-CNDs and U-CNDs were synthesized as mentioned in our previous work.[37] Briefly, E-CNDs were prepared by dissolving 960 mg of citric acid in 1 mL each of DI water and ethylene diamine (EDA) were added. The mixture was pyrolyzed by 300 W microwave (CEM Corp 908005 Microwave Reactor) for 18 min at temperature below 150 ºC. The resulting brown foamy solution was dissolved in 5 mL of DI water for purification. U-CNDs were prepared by pyrolyzing urea (1 gram) and citric acid (1 gram) in 1 mL of DI water at 110 ºC for 12 min at 150 W power. Large aggregated particles were removed by centrifugation. Both samples were purified by dialysis against DI water (1000 MWCO) and solid powders were obtained by lyophilization.

The synthesized E-CNDs and U-CNDs were loaded with curcumin. Briefly, curcumin was dissolved in methanol (1:1 w/v) and the solution was added dropwise to either E-CNDs or U-CNDs at a concentration of 2 mg/mL. The reactant mixture was ultra-sonicated in a water bath for 20 min and shaken on rotary shaker (500 rpm) overnight at room temperature. The methanol was evaporated by using rotary evaporation and the Curc-CNDs were centrifuged. The pellet was dissolved in known amount of methanol and quantified using UV-Vis spectrophotometer (Varian Cary 6000i) at 425 nm. Curcumin standard curve was plotted with known concentrations. The curcumin encapsulation and loading efficiency % was calculated using the formula as follows

$$\text{Encapsulation efficiency} = \frac{\text{Total curcumin added} - \text{free curcumin in solution}}{\text{Total curcumin added}} \quad (3.1)$$

$$\text{Loading efficiency \%} = \frac{\text{Weight of curcumin CNDs}}{\text{weight of CNDs}} * 100 \quad (3.2)$$

Atomic Force Microscopy (Agilent 5600LS AFM), Transmission Electron Microscopy (TEM, Carl Zeiss Libra 120 Plus), and zeta potentiometer (Malvern Zetasizer ZEN3600) were used for the determination of the size and charge of the CNDs before and after functionalization with Curcumin respectively. The samples were analyzed by FT-IR spectroscopy (Agilent FTIR) to identify the functional groups of curcumin in the functionalized Curc-CNDS. Chemical structure and elemental composition of the Curc-CNDs were characterized using XPS (Thermo Scientific ESCALAB Xi^+) and Raman spectroscopy (Horiba XploRA One Raman Confocal Microscope System) respectively. Ultraviolet-visible spectrophotometer (Varian Cary 6000i) and fluorescence spectrophotometer (Varian Cary Eclipse) were used to investigate the optical properties of the Curc-CNDs, respectively. The fluorescence quantum yield (QY) of the CNDs before and after Curcumin functionalization was determined using Quinine Sulfate (QS) as a standard fluorescent compound in 0.1 M H_2SO_4 using the following equation:[57-58]

$$\Phi_C = \Phi_{QS} \times \frac{Grad_C}{Grad_{QS}} \times \frac{{\eta_C}^2}{{\eta_{QS}}^2} \quad (3.3)$$

where, Φ represent the quantum yield, Grad is the gradient from the plot of integrated fluorescence intensity vs absorbance and η, refractive index (aqueous solution 1.33). The subscript QS and C denoted quinine sulfate and CNDs before and after functionalization with curcumin respectively.

The Curc-CNDs were dissolved in 10mM PBS and incubated at 37 ºC at a pH of 5 and 7. Samples were taken at different time intervals (0, 0.5, 1, 2, 4, 8, 16, 24, 48, and 72 h) and centrifuged for 3 min at 1200 rpm to pelletize released curcumin. Concentrations of released curcumin was calculated from the curcumin standard curve. Curcumin release studies were also carried out in cell culture media to determine the release pattern. The release % was calculated using the formula

$$\text{Release } \% = \frac{\text{Curcumin released}}{\text{Total curcumin in CNDs}} * 100 \tag{3.4}$$

The release pattern of the curcumin was analyzed using the formulation derived by Korsmeyer and Peppas to analyze the release pattern of drugs, which is given by

$$M_t/M_\infty = kt^n \tag{3.5}$$

$$\text{Log}\left(\frac{M_t}{M_\infty}\right) = \text{Log}(k) + n\text{Log}(t) \tag{3.6}$$

Where, M_t and M_∞ are the fraction of drug released at time t and infinite time, respectively, k is a kinetic constant, and n is the release exponent, indicative of transport mechanism of drug.[59]

HepG2 cells (human hepatocellular cancer cells) were maintained in EMEM supplemented with 10% FBS and 1% pen/strep antibiotic solution, A549 cells (adenocarcinomic human alveolar basal epithelial cells) were maintained in F12K media supplemented with 10% FBS and 1% pen/strep antibiotic solution and EA. hy926 cells

were maintained in DMEM media supplemented with 10% FBS and 1% pen/strep antibiotic solution. All the cells were kept in an incubator with 5% CO_2 at 37 ºC.

The biocompatibility of E-CNDs, U-CNDs and Curc-CNDs were determined using CCK-8 assay. The assay is based on the conversion of WST-8 [2-(2-methoxy-4-nitrophenyl)-3-(4-nitrophenyl)-5-(2,4disulfophenyl)-2H-tetrazolium, monosodium salt] dye to a water-soluble orange colored formazan complex due to the cellular dehydrogenase activity. The cell viability is measured at an optical density of 450 nm.[60] The EA. hy926 cells were pre-seeded in 96-well plate overnight and starved in low serum media for 24 hours. The respective medium with different concentrations of the CNDs and Curc-CNDs (0, 0.1, 0.2, 0.4, 0.8, 1.6, and 3.2 mg/mL) were added to investigate their biocompatibility towards both the cancerous cells and normal cells incubated for 24 hours. Viability of the cells was examined by measuring absorption at 450 nm after 1 hr. Equation used for calculating viability % is

$$\text{Viability } \% = \frac{\left(\text{OD}_{\text{sample}} - \text{OD}_{\text{blank}}\right)}{\text{OD}_{\text{control}} - \text{OD}_{\text{blank}}} * 100 \qquad (3.7)$$

10,000 cells of HepG2 and A549 were pre-seeded in 96-well plate overnight and starved in low serum media for 24 hours. Different concentrations (0, 0.1, 0.2, 0.4, 0.8, 1.6, and 3.2 mg/mL) of the CNDs and Curc-CNDs were added to HepG2 and A549 cells and incubated for 24 hours. Viability was determined using alamar blue assay and % of living cells was calculated using the above-mentioned formula.

Live/Dead assay were conducted on HepG2 and A549 cells. Cells (1×10^5) were seeded on coverslips that were placed in 12 well plates overnight. The medium was replaced with different concentrations (0, 0.4, 0.8, and, 1.6 mg/ml) of Curc-E-CNDs and Curc-U-CNDs and incubated for 12 hours. The growth medium was replaced with live dead reagent (calcein AM and ethidium homodimer-1) dissolved in sterile phosphate buffer saline (PBS), and incubated for 45 minutes. The cells were washed thrice with PBS and the coverslip was placed on the slide. The cells were imaged under confocal microscope (Zeiss Z1 Spinning Disk Confocal Microscope) for intracellular localization of thCurc-E-CNDs. The images were collected at 20X magnification. The live cells uptake calcein AM and stain green, whereas the dead cells uptake ethidium homodimer-1 and stain red.

All data were expressed as mean ± standard error. Each experiment was repeated in triplicates and significance was analyzed by multifactor analysis of variance (ANOVA) with accepted statistical significance at a level of $p < 0.05$.

Results and Discussion

The successful conjugation of CNDs with curcumin was validated using different characterization techniques. The AFM images of Curc-E-CNDs (Figure 3.1A) and Curc-U-CNDs (Figure 3.1B) showed an even dispersion with average height of 9 nm and 4 nm, respectively. Since the radius of curvature of the AFM probe is bigger compared to both the Curc-CNDs, only the height data can be used to determine the size. The average diameter of the curcumin functionalized Curc-E-CNDs (Figure 3.1C) and Curc-U-CNDs (Figure 3.1D) is around 10 nm and 5 nm, respectively, from the TEM images, which is in

accordance with the AFM data. The zeta potential of E-CNDs is -7.32±0.9 mV, and upon functionalization with curcumin changed to -11.7±1.3 mV at a physiological pH of 7.4. Upon functionalization of U-CNDs with curcumin, the zeta potential has changed from -38.5±2.7 mV to -32.9±3.8 mV. The zeta potential trends observed in both the Curc-CNDs suggest the successful adsorption of curcumin onto the CNDs. The higher negative zeta potential indicates better stability in aqueous solution.[61] This property allows for the longer circulation time of the Curc-U-CNDs in the tumor microenvironment, due to reduced interaction between serum proteins and the Curc-CNDs.[62]

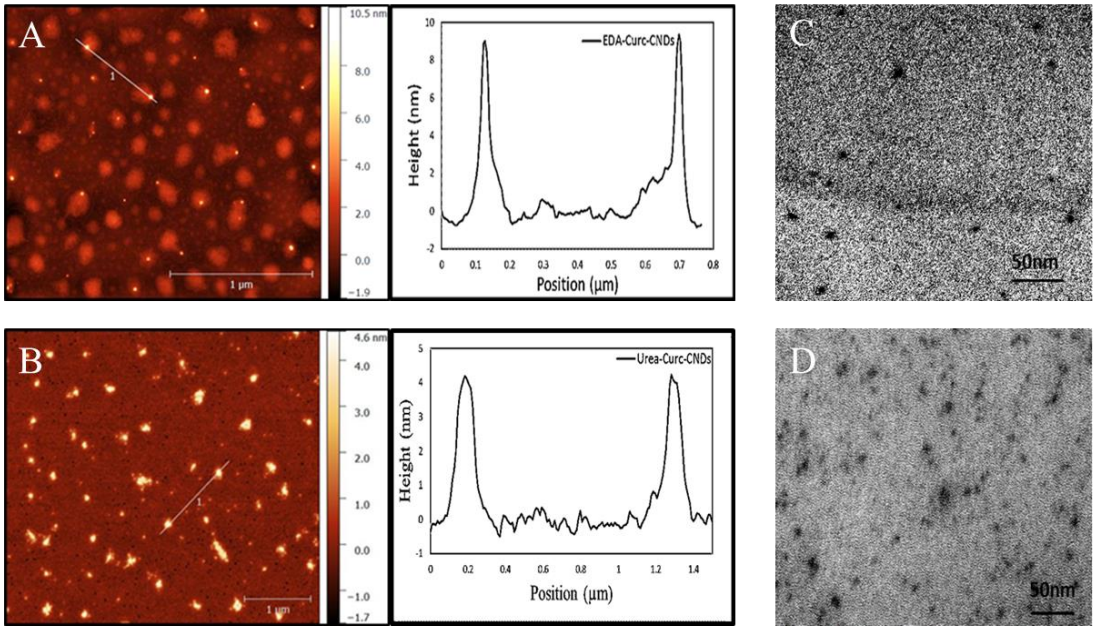

Figure 3.1. AFM and TEM of Curc-CNDs. Atomic force microscopy (AFM) images of Curc-E-CNDs (A) and Curc-U-CNDs (C) with their respective height profiles around 9 nm and 4 nm respectively, and the TEM images of Curc-E-CNDs (B) and Curc-U-CNDs (D), respectively.

The FTIR analysis further confirmed the functionalization of the CNDs with curcumin. Native curcumin exhibits characteristic peaks at 3509 cm^{-1}, 3024 cm^{-1}, 1624

cm^{-1}, 1275 cm^{-1} which corresponds to OH stretching of phenol, CH stretching, C=O, C=C stretching mode, C-O enol stretching, respectively.[63] Both E-CNDs and U-CNDs, after functionalization with curcumin exhibit similar characteristic peaks to that of curcumin confirming the successful conjugation of CNDs and curcumin (Figure 3.2). Moreover, the O-H and N-H stretching of the E-CNDs and U-CNDs is conserved in the Curc-CNDs after functionalization (Figure B.S1).[39] Raman spectra of both the CNDs shows the increase in D band intensity after functionalization with curcumin which can be attributed to the carbon atoms excited from sp^2 to sp^3 hybridization due to the introduction of oxygenated functional groups (Figure B.S2).[64]

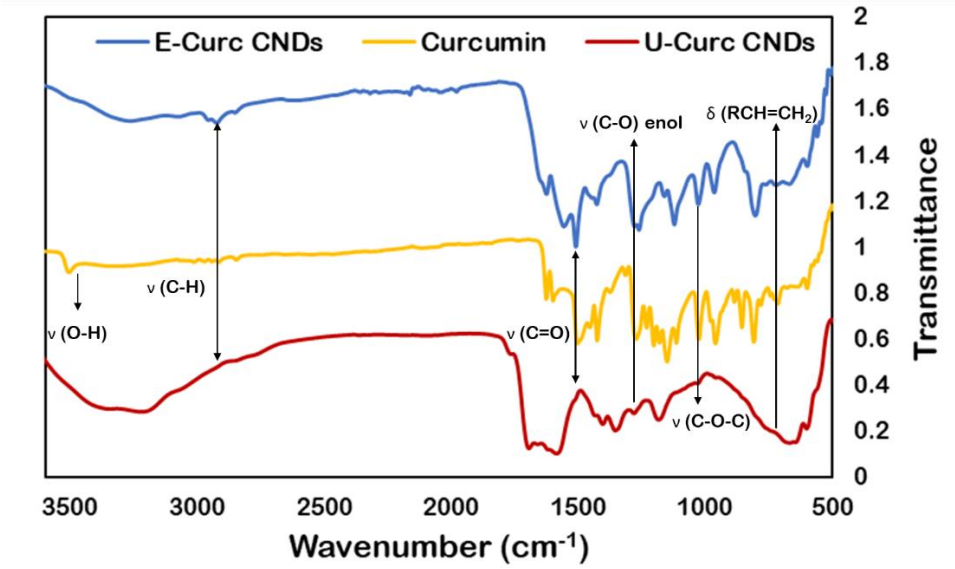

Figure 3.2. FTIR Spectra of Curc-CNDs. FTIR spectra of Curc-E-CNDs (A) and Curc-U-CNDs (B) with their characteristic curcumin and CNDs spectra.

XPS spectrum of curcumin depicts the presence of two elements carbon at 285.0 eV and oxygen at 532.0 eV, respectively (Figure S3A). The XPS spectra of both E-CNDs (Figure 3.3A) and U-CNDs (Figure 3.3C) after functionalization with curcumin show the

presence of carbon, nitrogen, and oxygen at 285.0, 400.5, and 532.0 eV. The curve fitting C1s spectra of Curc-E-CNDs (Figure 3.3B) and Curc-U-CNDs (Figure 3.3D) have chemical states at corresponding to C-C, C-O-C, O-C=O and O=C-OH, similar to that of the curcumin C1s spectra (Figure B.S3). Similarly, the C1s characteristic peaks of E-CNDs and U-CNDs are conserved after functionalization with curcumin (Figure B.S4).[56] The additional peak O=C-OH is observed in both the types of CNDs after functionalization with curcumin (Figure 3.3B & 3.3D). The O1s spectra of Curc-E-CNDs depicts O-H and C=O peaks (Figure B.S5A) and Curc-U-CNDs have presented peaks corresponding to O-H and O-C=O (Figure B.S5C), whereas the individual high resolution N1s spectra of both the Curc-E-CNDs (Figure B.S5B) and Curc-U-CNDs (Figure B.S5D) showed the presence of C-N-C and N-H peaks.

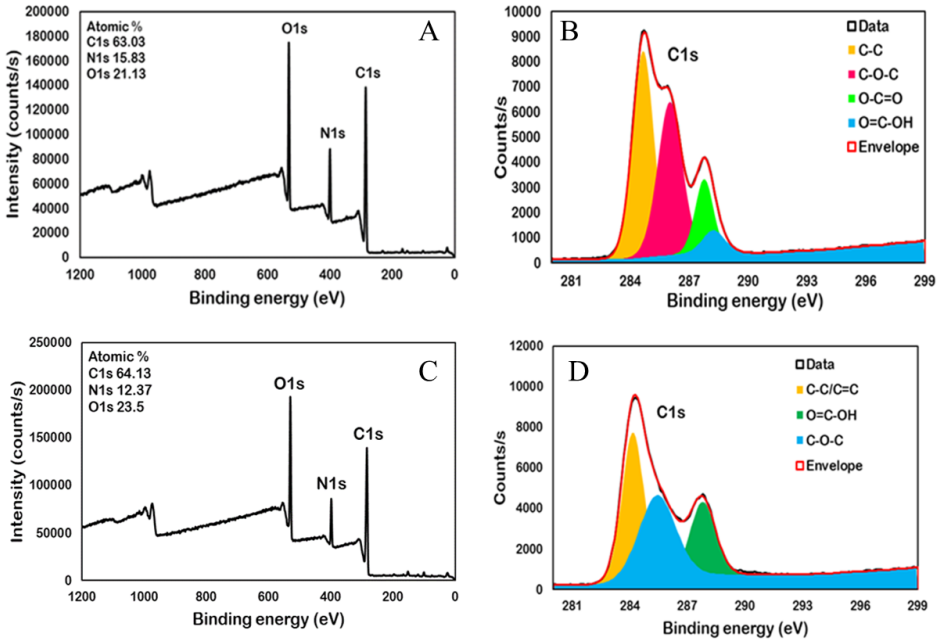

Figure 3.3. XPS Spectra of Curc-CNDs. XPS survey spectra of Curc-E-CNDs (A) and Curc-U-CNDs (C). High resolution C1s (B, D) XPS spectra of Curc-E-CNDs and Curc-U-CNDs respectively.

In UV-Vis (Figure 3.4A), E-CNDs and U-CNDs have shoulder peaks located at 250 nm and 245 nm which are attributed to π- π* transitions of C=C (aromatic sp^2 domains). The E-CNDs and U-CNDs shows strong broad peaks at 350 nm and 337 nm, respectively, which are assigned to n-π transitions of C=O bond involving functional groups with electron lone pairs.[37] The UV-Vis spectrum of curcumin shows two distinct peaks at ~268 nm and ~426 nm corresponding to n–π* and π–π* transitions, respectively (Figure 3.4A).[65] The UV-Vis spectrum of Curc-E-CNDs depicts strong peak at 356 nm and shoulder peak at 240 nm, respectively. Curc-U-CNDs exhibits two peaks at 343 nm and 427 nm (Figure 3.4A). The excitation dependent behavior at different excitation wavelengths gives information about the strong emission peaks. Curc-E-CNDs (Figure 3.4B) and Curc-U-CNDs (Figure 3.4C) exhibited strong emission peaks at an excitation

wavelength of 360 nm and 450 nm, respectively. Unlike curcumin, both the Curc-CNDs are readily dispersed in water and exhibited good fluorescence stability over a time period of 50 days (Figure B.S6). The quantum yields of the Curc-E-CNDs (48.74%) and Curc-U-CNDs (6.54%) is calculated with reference to quinine sulfate (Table B.S1).[66]

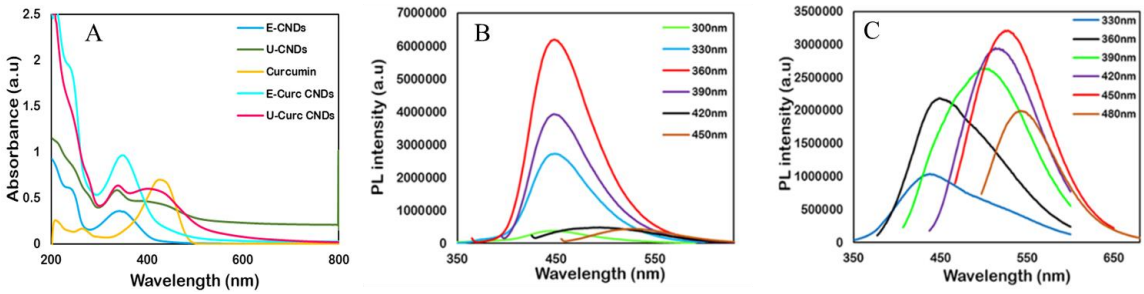

Figure 3.4. Photoluminescence Properties of Curc-CNDs. UV-Vis absorption spectra of E-CNDs, U-CNDs, curcumin, Curc-E-CNDs, and l-U-CNDs (A). Excitation dependent fluorescence spectra of Curc-E-CNDs (0.5 mg/mL) (B) and Curc-U-CNDs (0.5 mg/mL) (C), respectively.

The curcumin loading capacity and encapsulation efficiency for Curc-E-CNDs were determined to be 91.5±1.5% and 3.8±0.8% and for Curc-U-CNDs to be 81.9±1.9% and 3.4±0.6%, respectively. These results demonstrate good loading capacity of both CNDs. The curcumin release pattern of both the Curc -CNDs was firstly studied in PBS at two different pH (7.4 and 5) over a time course of 72 hours. High curcumin release (%) is observed at a pH 5 in a gradual controlled manner for both the Curc-CNDs (Figure 3.5A-B). The enhanced drug release at pH 5 may be due to weaker interactions of Curc-CNDs in acidic environment, which will be beneficial for curcumin to elicit it's therapeutic effects in the tumor microenvironment. Slow release rate of curcumin in solution of pH 7.4 can be attributed to the stronger electrostatic interactions between

CNDs and curcumin. Initial curcumin burst release of Curc-E-CNDs and Curc-U-CNDs was found to be 33.1% and 33.5%, respectively at 2 hours at pH 5 using curcumin standard curve (Figure B.S7), which might be due to the desorption and release of surface curcumin into the surrounding media. Thereafter, the curcumin release from both the Curc-CNDs followed a controlled sustained release pattern which can be attributed to the lipophilic nature of curcumin (Figure 3.5). A total of 59.9% and 74.3% of curcumin was released at 72 hours from Curc-E-CNDs and, Curc-U-CNDs, respectively. The slower controlled release of curcumin from Curc-E-CNDs can be exlained by the stronger interactions between the E-CNDs and curcumin in comparison to U-CNDs and curcumin due to more amine groups in E-CNDs. The drug release behavior was studied by fitting the curcumin release with kinetic models. The curcumin release data were plotted using Korsmeyer and Peppas equation with R^2 values of 0.98-0.99 and n values below 0.45 for both the types of Curc CNDs at pH of 5 and 7.4 (Figure B.S8 & B.S9). The n values less than 0.45 ($n<0.45$) confirms the fickian diffusion of the solute molecule (curcumin) from Curc-CNDs complex into the surrounding media due to chemical gradient. A similar release trend is observed when the Curc CNDs are suspended in EMEM cell culture media, with n values less than 0.45 (Figure 3.5C-D). Almost 90 % of curcumin is released into the media within 96 hours.

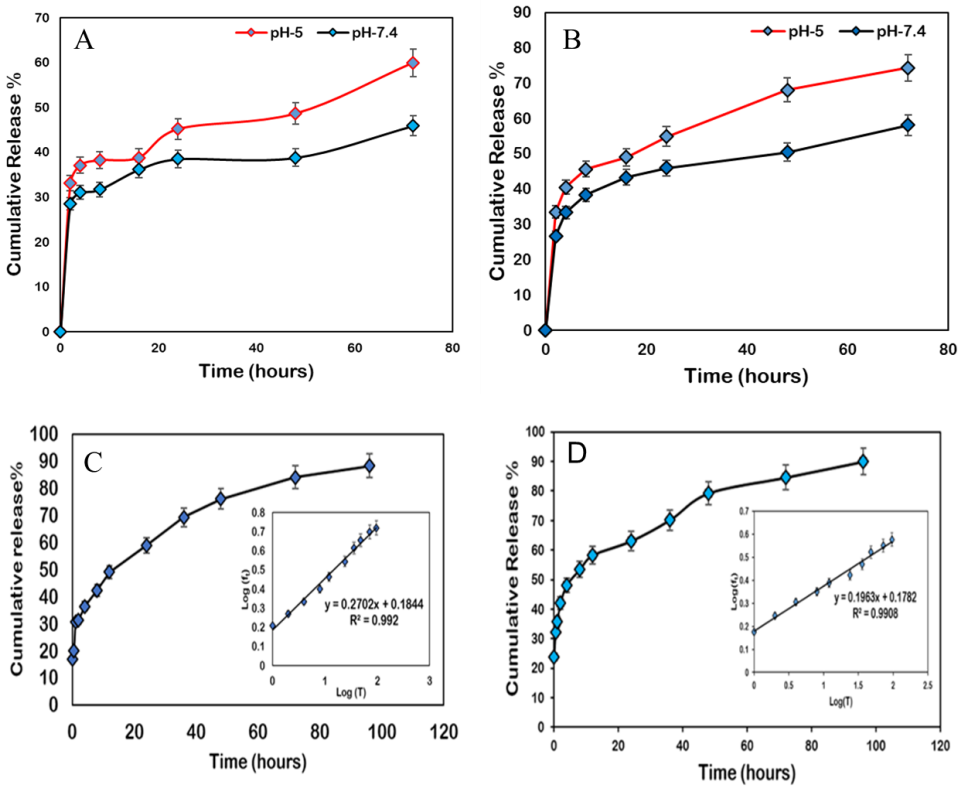

Figure 3.5. Release Profile. Curcumin release profile of Curc-E-CNDs (A) and Curc-U-CNDs (B) under two different pH-5 & 7.4 in PBS and Curc-E-CNDs (C) and Curc-U-CNDs (D)in EMEM media. Inserts in (C) and (D) are Korsmeyer-Peppas release model of Curcumin. All the data values were done in triplicates with mean ±SDs.

Biocompatibility of the CNDs and Curc-CNDs were analyzed using CCK-8viability assay for the normal cell line EA. hy926. The cells showed no significant signs of cellular toxicity on treatment with the CNDs and Curc-CNDs even at high concentration of 3.2 mg/mL (Figure 3.6A). In concert, HepG2 and A549 cells were treated with CNDs and Curc-CNDs at concentrations of 0.1, 0.2, 0.4, 0.8, 1.6, and 3.2 mg/mL for 24 hours. The number of viable cells decreased in Curc CNDs treated HepG2 and A549 cells in comparison to the CNDs treated cells (Figure 3.6B-C) from the alamar blue assay. At a concentration of 3.2 mg/mL, the cell viability is around 40% and 30%

for the HepG2 cells treated with Curc-E-CNDs and Curc-U-CNDs (Figure 3.6B), respectively. A549 cells displayed a cell viability of ~38% and ~18% when treated with Curc-E-CNDs and Curc-U-CNDs (Figure 3.6C) at a maximum concentration of 3.2 mg/mL for 24 hours, respectively. A more rapid decrease in the number of viable cells is observed in both the cells treated with Curc-U-CNDs in comparison to Curc-E-CNDs (Figure 3.6C). The A549 cell viability assay was carried on for an extended period of 48 and 72 hours to observe the effects of Curc-CNDs on cell viabilty. Curc-E-CNDs treated cells shows a cell viability of ~30% and ~25%, while Curc-U-CNDs depicts ~5% and ~2% at a concentration of 3.2 mg/mL, at time period of 48 and 72 hours, respectively (Figure B.S10). Cancer cells treated with the Curc-CNDs showed cytotoxicity due to the higher uptake and release of curcumin compared to normal cells. This might be attributed to membrane structure and protein composition differences and low pH in the cells.[67] The presence of high levels of glutathione in tumor cells enhances the sensitivity of tumor cells to curcumin.[68] Upon treatment with Curc-CNDs, both HepG2 and A549 cells showed dose-dependent increase in cellular toxicity, high cellular toxicity of the Curc-U-CNDs can be attributed to the more release of curcumin, which was observed from the release profile. The mechanism of cytotoxicity of curcumin in cancer cells is dependent on the type of cancer being treated. Specifically, in liver cancer cell lines curcumin suppress tumor cell survival and proliferation through inhibition of NF-κB signaling pathway.[69] Whereas in lung cancer cells, curcumin inhibits cell proliferation and induces apoptosis through supression of PI3K/Akt signaling pathway.[70]

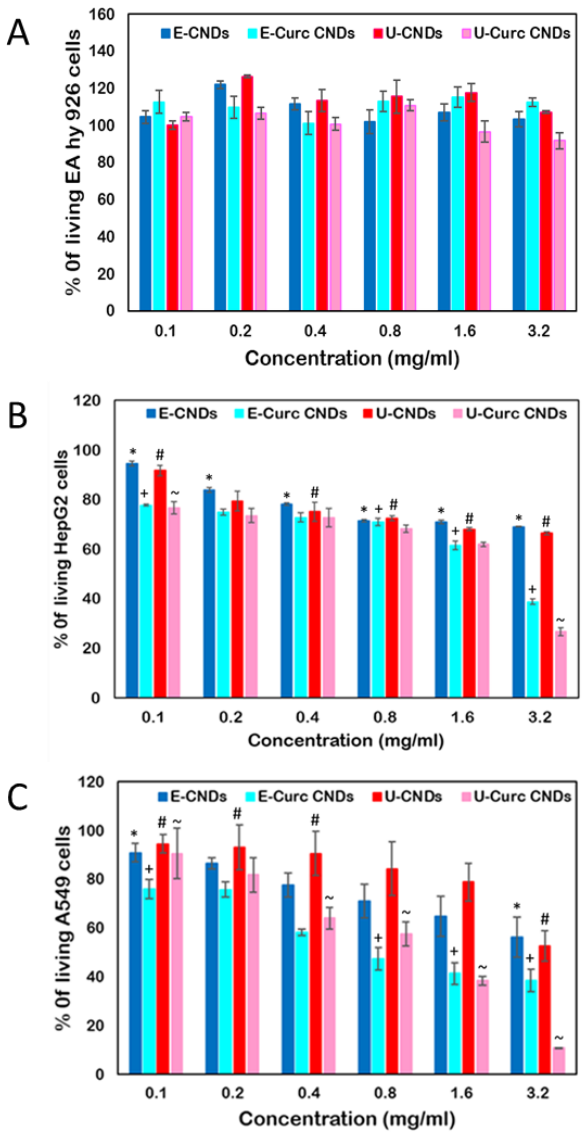

Figure 3.6. Cell Viability Assays. Cell viability assays of EA. hy926 (A), HepG2 (B) and A549 (C) cells treated with different concentrations of E-CNDs & Curc-E-CNDs and U-CNDs & Curc-U-CNDs for 24 hrs.

The cellular uptake studies of Curc-E-CNDs and Curc-U-CNDs were conducted using two cell lines HepG2 and A549 at concentrations of 0.4, 0.8, and, 1.6 mg/mL. Both the types of Curc-CNDs show good cellular uptake in HepG2 and A549 cells (Figure 3.7

& 3.8). Cells treated with Curc-E-CNDs exhibited high fluorescence intensity compared to Curc-U-CNDs, which is due to the high quantum yield of Curc-E-CNDs.

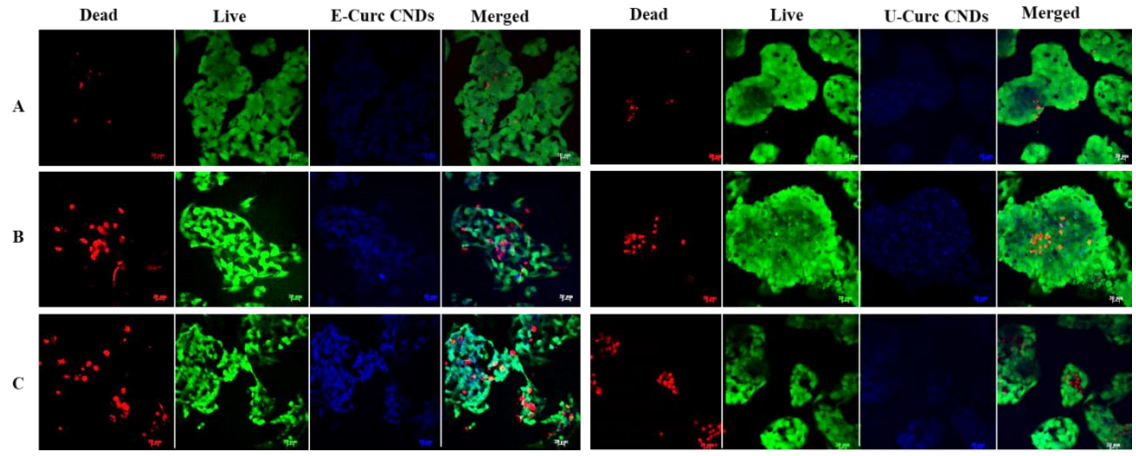

Figure 3.7. Confocal Images of HepG2 Cells. Fluorescence images of live and dead HepG2 cells incubated with E-Curc & Curc-U-CNDs at different concentrations (0.4 (A), 0.8 (B), and 1.6 (C) mg/mL) for 12 hours.

The cellular toxicity of Curc-CNDs was evaluated using live dead assay in two cell lines HepG2 and A549. Curc-CNDs exhibited cytotoxicity in a dose dependent manner in both the cell types. As the concentration of Curc-CNDs was increased, the number of dead cells increased gradually. At a concentration of 1.6 mg/mL, both the Curc CNDs showed significant decrease in number of viable cells (Figure 3.7 & 3.8) and A549 cells showed change in the cell morphology (Figure 3.8C). 3.2 mg/mL concentration was also tested, but the cells were all detached from the cover slip after the treatment, due to the high toxicity of Curc CNDs. The fluorescent microscope images show Curc-CNDs are found to be distributed both in cytoplasm and nucleus (Figure 3.7 & 3.8). With increase in concentration of Curc-CNDs, the cellular toxicity increased along with cellular uptake which is evident from live/dead assay. The results in more

amounts of curcumin localized in the cells, which might induce dose dependent DNA damage to nuclear as well as mitochondrial genome with increase of ROS levels and lipid peroxidation.[71]

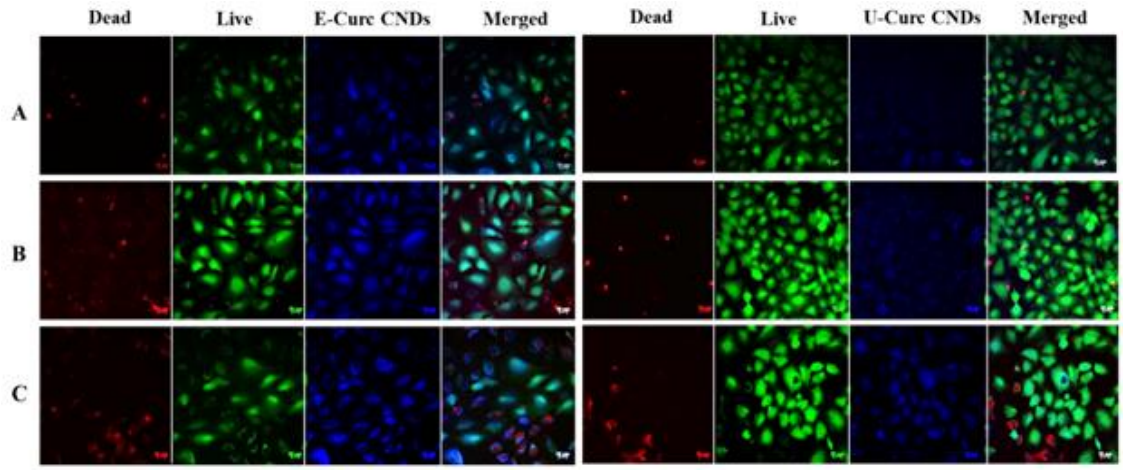

Figure 3.8. Confocal Images of A549 Cells. Fluorescence images of live and dead A549 cells incubated with Curc-E- & Curc-U-CNDs at different concentrations (0.4 (A), 0.8 (B), and 1.6 (C) mg/mL) for 12 hours.

Conclusion

In the current study, curcumin loaded CNDs were prepared in an cost-effective manner, to enhance the bioavailability of curcumin and explore the antiproliferative effects of encapsulated curcumin. The characterization studies confirmed the successful conjugation of curcumin with CNDs with overall small size, high loading capacity, good photoluminescence properties and stability. The curcumin release studies have shown better release of curcumin in solution with pH-5, inferring more amount of drug might be released in tumor microenvironment compared to normal tissues. The CNDs used for curcumin loading shown to be non-toxic to normal cells, thereby proving a better vehicle

for curcumin delivery. Curc-U-CNDs have shown enhanced cellular toxicity even at low concentrations which is further supported by the zeta potential measurements (longer circulation times) and drug release profile of curcumin, and can be attributed to the effective loading of curcumin onto the functional group rich CNDs. In conclusion, the CNDs can be valuable vehicles for curcumin delivery with enhanced bioavailability, small size, high encapsulation capacity, better photoluminescence, and biocompatibility, eliciting improved anticancer properties at low concentrations.

References

1. Shishodia, S.; Sethi, G.; Aggarwal, B. B., Curcumin: getting back to the roots. *Annals of the New York Academy of Sciences* **2005,** *1056*, 206-17.

2. Wilken, R.; Veena, M. S.; Wang, M. B.; Srivatsan, E. S., Curcumin: A review of anti-cancer properties and therapeutic activity in head and neck squamous cell carcinoma. *Mol Cancer* **2011,** *10*, 12-12.

3. Rao, C. V.; Rivenson, A.; Simi, B.; Reddy, B. S., Chemoprevention of colon carcinogenesis by dietary curcumin, a naturally occurring plant phenolic compound. *Cancer research* **1995,** *55* (2), 259-66.

4. Gupta, S. C.; Patchva, S.; Aggarwal, B. B., Therapeutic roles of curcumin: lessons learned from clinical trials. *AAPS J* **2013,** *15* (1), 195-218.

5. Moos, P. J.; Edes, K.; Mullally, J. E.; Fitzpatrick, F. A., Curcumin impairs tumor suppressor p53 function in colon cancer cells. *Carcinogenesis* **2004,** *25* (9), 1611-7.

6. Choudhuri, T.; Pal, S.; Das, T.; Sa, G., Curcumin selectively induces apoptosis in deregulated cyclin D1-expressed cells at G2 phase of cell cycle in a p53-dependent manner. *The Journal of biological chemistry* **2005,** *280* (20), 20059-68.

7. Hassan, F.-U.; Rehman, M. S.-U.; Khan, M. S.; Ali, M. A.; Javed, A.; Nawaz, A.; Yang, C., Curcumin as an Alternative Epigenetic Modulator: Mechanism of Action and Potential Effects. *Front Genet* **2019,** *10*, 514-514.

8. Huminiecki, L.; Horbanczuk, J.; Atanasov, A. G., The functional genomic studies of curcumin. *Seminars in cancer biology* **2017,** *46*, 107-118.

9. Kunnumakkara, A. B.; Bordoloi, D.; Padmavathi, G.; Monisha, J.; Roy, N. K.; Prasad, S.; Aggarwal, B. B., Curcumin, the golden nutraceutical: multitargeting for multiple chronic diseases. *Br. J. Pharmacol.* **2017,** *174* (11), 1325-1348.

10. Mirzaei, H.; Khoi, M. J.; Azizi, M.; Goodarzi, M., Can curcumin and its analogs be a new treatment option in cancer therapy? *Cancer gene therapy* **2016,** *23* (11), 410.

11. Panda, A. K.; Chakraborty, D.; Sarkar, I.; Khan, T.; Sa, G., New insights into therapeutic activity and anticancer properties of curcumin. *J Exp Pharmacol* **2017,** *9*, 31-45.

12. Kundu, M.; Sadhukhan, P.; Ghosh, N.; Chatterjee, S.; Manna, P.; Das, J.; Sil, P. C., pH-responsive and targeted delivery of curcumin via phenylboronic acid-functionalized ZnO nanoparticles for breast cancer therapy. *Journal of Advanced Research* **2019,** *18*, 161-172.

13. Anand, P.; Kunnumakkara, A. B.; Newman, R. A.; Aggarwal, B. B., Bioavailability of curcumin: problems and promises. *Molecular pharmaceutics* **2007,** *4* (6), 807-18.

14. Barry, J.; Fritz, M.; Brender, J. R.; Smith, P. E.; Lee, D. K.; Ramamoorthy, A., Determining the effects of lipophilic drugs on membrane structure by solid-state NMR spectroscopy: the case of the antioxidant curcumin. *Journal of the American Chemical Society* **2009,** *131* (12), 4490-8.

15. Tsukamoto, M.; Kuroda, K.; Ramamoorthy, A.; Yasuhara, K., Modulation of raft domains in a lipid bilayer by boundary-active curcumin. *Chemical Communications* **2014,** *50* (26), 3427-3430.

16. Tomeh, M. A.; Hadianamrei, R.; Zhao, X., A Review of Curcumin and Its Derivatives as Anticancer Agents. *Int. J. Mol. Sci.* **2019,** *20* (5), 1033.

17. Shoji, M.; Nakagawa, K.; Watanabe, A.; Tsuduki, T.; Yamada, T.; Kuwahara, S.; Kimura, F.; Miyazawa, T., Comparison of the effects of curcumin and curcumin glucuronide in human hepatocellular carcinoma HepG2 cells. *Food Chem* **2014,** *151*, 126-32.

18. Gera, M.; Sharma, N.; Ghosh, M.; Huynh, D. L.; Lee, S. J.; Min, T.; Kwon, T.; Jeong, D. K., Nanoformulations of curcumin: an emerging paradigm for improved remedial application. *Oncotarget* **2017,** *8* (39), 66680-66698.

19. Davis, M. E.; Chen, Z. G.; Shin, D. M., Nanoparticle therapeutics: an emerging treatment modality for cancer. *Nature reviews. Drug discovery* **2008,** *7* (9), 771-82.

20. Wang, D.; Veena, M. S.; Stevenson, K.; Tang, C.; Ho, B.; Suh, J. D.; Duarte, V. M.; Faull, K. F.; Mehta, K.; Srivatsan, E. S.; Wang, M. B., Liposome-encapsulated curcumin suppresses growth of head and neck squamous cell carcinoma in vitro and in xenografts through the inhibition of nuclear factor kappaB by an AKT-independent pathway. *Clinical cancer research : an official journal of the American Association for Cancer Research* **2008,** *14* (19), 6228-36.

21. Thangapazham, R. L.; Puri, A.; Tele, S.; Blumenthal, R.; Maheshwari, R. K., Evaluation of a nanotechnology-based carrier for delivery of curcumin in prostate cancer cells. *International journal of oncology* **2008,** *32* (5), 1119-23.

22. Karewicz, A.; Bielska, D.; Loboda, A.; Gzyl-Malcher, B.; Bednar, J.; Jozkowicz, A.; Dulak, J.; Nowakowska, M., Curcumin-containing liposomes stabilized by thin layers of chitosan derivatives. *Colloids and surfaces. B, Biointerfaces* **2013,** *109*, 307-16.

23. Li, C.; Zhang, Y.; Su, T.; Feng, L.; Long, Y.; Chen, Z., Silica-coated flexible liposomes as a nanohybrid delivery system for enhanced oral bioavailability of curcumin. *Int J Nanomedicine* **2012,** *7*, 5995-6002.

24. Li, L.; Braiteh, F. S.; Kurzrock, R., Liposome-encapsulated curcumin: in vitro and in vivo effects on proliferation, apoptosis, signaling, and angiogenesis. *Cancer* **2005,** *104* (6), 1322-31.

25. Akl, M. A.; Kartal-Hodzic, A.; Suutari, T.; Oksanen, T.; Montagner, I. M.; Rosato, A.; Ismael, H. R.; Afouna, M. I.; Caliceti, P.; Yliperttula, M.; Samy, A. M.; Mastrotto, F.; Salmaso, S.; Viitala, T., Real-Time Label-Free Targeting Assessment and in Vitro Characterization of Curcumin-Loaded Poly-lactic-co-glycolic Acid Nanoparticles for Oral Colon Targeting. *ACS Omega* **2019,** *4* (16), 16878-16890.

26. Rejinold, N. S.; Yoo, J.; Jon, S.; Kim, Y. C., Curcumin as a Novel Nanocarrier System for Doxorubicin Delivery to MDR Cancer Cells: In Vitro and In Vivo Evaluation. *ACS Appl Mater Interfaces* **2018,** *10* (34), 28458-28470.

27. Bisht, S.; Feldmann, G.; Soni, S.; Ravi, R.; Karikar, C.; Maitra, A.; Maitra, A., Polymeric nanoparticle-encapsulated curcumin ("nanocurcumin"): a novel strategy for human cancer therapy. *Journal of nanobiotechnology* **2007,** *5*, 3.

28. Liu, J.; Chen, Z.; Wang, J.; Li, R.; Li, T.; Chang, M.; Yan, F.; Wang, Y., Encapsulation of Curcumin Nanoparticles with MMP9-Responsive and Thermos-Sensitive Hydrogel Improves Diabetic Wound Healing. *ACS Appl Mater Interfaces* **2018,** *10* (19), 16315-16326.

29. Altunbas, A.; Lee, S. J.; Rajasekaran, S. A.; Schneider, J. P.; Pochan, D. J., Encapsulation of curcumin in self-assembling peptide hydrogels as injectable drug delivery vehicles. *Biomaterials* **2011,** *32* (25), 5906-5914.

30. Sharma, A.; Sharma, U. S., Liposomes in drug delivery: Progress and limitations. *International Journal of Pharmaceutics* **1997,** *154* (2), 123-140.

31. Hatefi, A.; Amsden, B., Biodegradable injectable in situ forming drug delivery systems. *Journal of Controlled Release* **2002,** *80* (1), 9-28.

32. Yallapu, M. M.; Nagesh, P. K.; Jaggi, M.; Chauhan, S. C., Therapeutic Applications of Curcumin Nanoformulations. *AAPS J* **2015,** *17* (6), 1341-56.

33. Zeng, Z.; Zhang, W.; Arvapalli, D. M.; Bloom, B.; Sheardy, A.; Mabe, T.; Liu, Y.; Ji, Z.; Chevva, H.; Waldeck, D. H.; Wei, J., A fluorescence-electrochemical study of carbon nanodots (CNDs) in bio- and photoelectronic applications and energy gap investigation. *Phys. Chem. Chem. Phys.* **2017,** *19* (30), 20101-20109.

34. Sheardy, A. T.; Arvapalli, D. M.; Wei, J., Experimental and Time-Dependent Density Functional Theory Modeling Studies on the Optical Properties of Carbon Nanodots. *The Journal of Physical Chemistry C* **2020**.

35. Baker, S.; Baker, G., Luminescent Carbon Nanodots: Emergent Nanolights. *Angewandte Chemie (International ed. in English)* **2010,** *49*, 6726-44.

36. Sun, Y.-P.; Zhou, B.; Lin, Y.; Wang, W.; Fernando, K. A. S.; Pathak, P.; Meziani, M. J.; Harruff, B. A.; Wang, X.; Wang, H.; Luo, P. G.; Yang, H.; Kose, M. E.; Chen, B.; Veca, L. M.; Xie, S.-Y., Quantum-Sized Carbon Dots for Bright and Colorful Photoluminescence. *J. Am. Chem. Soc.* **2006,** *128* (24), 7756-7757.

37. Wang, Q.; Huang, X.; Long, Y.; Wang, X.; Zhang, H.; Zhu, R.; Liang, L.; Teng, P.; Zheng, H., Hollow luminescent carbon dots for drug delivery. *Carbon* **2013,** *59*, 192-199.

38. Cao, L.; Sahu, S.; Anilkumar, P.; Bunker, C. E.; Xu, J.; Fernando, K. A. S.; Wang, P.; Guliants, E. A.; Tackett, K. N.; Sun, Y.-P., Carbon Nanoparticles as Visible-Light Photocatalysts for Efficient CO2 Conversion and Beyond. *Journal of the American Chemical Society* **2011,** *133* (13), 4754-4757.

39. Arvapalli, D. M.; Sheardy, A. T.; Alapati, K. C.; Wei, J., High Quantum Yield Fluorescent Carbon Nanodots for detection of Fe (III) Ions and Electrochemical Study of Quenching Mechanism. *Talanta* **2020,** *209*, 120538.

40. Cao, L.; Wang, X.; Meziani, M. J.; Lu, F.; Wang, H.; Luo, P. G.; Lin, Y.; Harruff, B. A.; Veca, L. M.; Murray, D.; Xie, S.-Y.; Sun, Y.-P., Carbon Dots for Multiphoton Bioimaging. *J. Am. Chem. Soc.* **2007,** *129* (37), 11318-11319.

41. Sun, Y.-P.; Wang, X.; Lu, F.; Cao, L.; Meziani, M. J.; Luo, P. G.; Gu, L.; Veca, L. M., Doped Carbon Nanoparticles as a New Platform for Highly Photoluminescent Dots. *The Journal of Physical Chemistry C* **2008,** *112* (47), 18295-18298.

42. Yang, S.-T.; Cao, L.; Luo, P. G.; Lu, F.; Wang, X.; Wang, H.; Meziani, M. J.; Liu, Y.; Qi, G.; Sun, Y.-P., Carbon Dots for Optical Imaging in Vivo. *J. Am. Chem. Soc.* **2009,** *131* (32), 11308-11309.

43. Zhang, W.; Zeng, Z.; Wei, J., Electrochemical Study of DPPH Radical Scavenging for Evaluating the Antioxidant Capacity of Carbon Nanodots. *The Journal of Physical Chemistry C* **2017,** *121* (34), 18635-18642.

44. Zhang, W.; Chavez, J.; Zeng, Z.; Bloom, B.; Sheardy, A.; Ji, Z.; Yin, Z.; Waldeck, D. H.; Jia, Z.; Wei, J., Antioxidant Capacity of Nitrogen and Sulfur Codoped Carbon Nanodots. *ACS Appl. Nano Mater.* **2018,** *1* (6), 2699-2708.

45. Ji, Z.; Sheardy, A.; Zeng, Z.; Zhang, W.; Chevva, H.; Allado, K.; Yin, Z.; Wei, J., Tuning the Functional Groups on Carbon Nanodots and Antioxidant Studies. *Molecules* **2019,** *24* (1), 152.

46. Ji, Z.; Arvapalli, D. M.; Zhang, W.; Yin, Z.; Wei, J., Nitrogen and sulfur co-doped carbon nanodots in living EA.hy926 and A549 cells: oxidative stress effect and mitochondria targeting. *Journal of Materials Science* **2020**.

47. Cho, H. S.; Dong, Z.; Pauletti, G. M.; Zhang, J.; Xu, H.; Gu, H.; Wang, L.; Ewing, R. C.; Huth, C.; Wang, F.; Shi, D., Fluorescent, superparamagnetic nanospheres for drug storage, targeting, and imaging: a multifunctional nanocarrier system for cancer diagnosis and treatment. *ACS nano* **2010,** *4* (9), 5398-404.

48. Bae, K. H.; Lee, K.; Kim, C.; Park, T. G., Surface functionalized hollow manganese oxide nanoparticles for cancer targeted siRNA delivery and magnetic resonance imaging. *Biomaterials* **2011,** *32* (1), 176-84.

49. Cho, H.-Y.; Mavi, A.; Chueng, S.-T. D.; Pongkulapa, T.; Pasquale, N.; Rabie, H.; Han, J.; Kim, J. H.; Kim, T.-H.; Choi, J.-W.; Lee, K.-B., Tumor Homing Reactive Oxygen Species Nanoparticle for Enhanced Cancer Therapy. *ACS Appl. Mater. Interfaces* **2019,** *11* (27), 23909-23918.

50. Sztandera, K.; Gorzkiewicz, M.; Klajnert-Maculewicz, B., Gold Nanoparticles in Cancer Treatment. *Mol. Pharm.* **2019,** *16* (1), 1-23.

51. El-Sawy, H. S.; Al-Abd, A. M.; Ahmed, T. A.; El-Say, K. M.; Torchilin, V. P., Stimuli-Responsive Nano-Architecture Drug-Delivery Systems to Solid Tumor Micromilieu: Past, Present, and Future Perspectives. *ACS Nano* **2018,** *12* (11), 10636-10664.

52. Taghavi, S.; Abnous, K.; Taghdisi, S. M.; Ramezani, M.; Alibolandi, M., Hybrid carbon-based materials for gene delivery in cancer therapy. *J. Controlled Release* **2020,** *318*, 158-175.

53. Kong, T.; Hao, L.; Wei, Y.; Cai, X.; Zhu, B., Doxorubicin conjugated carbon dots as a drug delivery system for human breast cancer therapy. *Cell Prolif* **2018,** *51* (5), e12488.

54. Hettiarachchi, S. D.; Graham, R. M.; Mintz, K. J.; Zhou, Y.; Vanni, S.; Peng, Z.; Leblanc, R. M., Triple conjugated carbon dots as a nano-drug delivery model for glioblastoma brain tumors. *Nanoscale* **2019,** *11* (13), 6192-6205.

55. Feng, T.; Ai, X.; An, G.; Yang, P.; Zhao, Y., Charge-Convertible Carbon Dots for Imaging-Guided Drug Delivery with Enhanced in Vivo Cancer Therapeutic Efficiency. *ACS nano* **2016,** *10* (4), 4410-4420.

56. Yuan, Y.; Guo, B.; Hao, L.; Liu, N.; Lin, Y.; Guo, W.; Li, X.; Gu, B., Doxorubicin-loaded environmentally friendly carbon dots as a novel drug delivery system for nucleus targeted cancer therapy. *Colloids and Surfaces B: Biointerfaces* **2017,** *159*, 349-359.

57. Mintz, K. J.; Zhou, Y.; Leblanc, R. M., Recent development of carbon quantum dots regarding their optical properties, photoluminescence mechanism, and core structure. *Nanoscale* **2019,** *11* (11), 4634-4652.

58. Meng, Q.; Wang, L.; Zhang, J.; Song, Y.; Jin, H.; Zhang, K.; Hongchen, S.; Wang, H.; Yang, B., Highly Photoluminescent Carbon Dots for Multicolor Patterning, Sensors, and Bioimaging. *Angewandte Chemie (International ed. in English)* **2013,** *52*.

59. Korsmeyer, R. W.; Gurny, R.; Doelker, E.; Buri, P.; Peppas, N. A., Mechanisms of solute release from porous hydrophilic polymers. *International Journal of Pharmaceutics* **1983,** *15* (1), 25-35.

60. Cai, L.; Qin, X.; Xu, Z.; Song, Y.; Jiang, H.; Wu, Y.; Ruan, H.; Chen, J., Comparison of Cytotoxicity Evaluation of Anticancer Drugs between Real-Time Cell Analysis and CCK-8 Method. *ACS omega* **2019,** *4* (7), 12036-12042.

61. Terence, *Colloid Science Principles*. 2 ed.; Wiley: New York, 2010.

62. Alexis, F.; Pridgen, E.; Molnar, L. K.; Farokhzad, O. C., Factors affecting the clearance and biodistribution of polymeric nanoparticles. *Molecular pharmaceutics* **2008,** *5* (4), 505-15.

63. Muthoosamy, K.; Abubakar, I. B.; Bai, R. G.; Loh, H.-S.; Manickam, S., Exceedingly Higher co-loading of Curcumin and Paclitaxel onto Polymer-functionalized Reduced Graphene Oxide for Highly Potent Synergistic Anticancer Treatment. *Scientific Reports* **2016,** *6* (1), 32808.

64. Hussain, S.; Shah, K. A.; Islam, S. S., Investigation of effects produced by chemical functionalization in single-walled and multi-walled carbon nanotubes using Raman spectroscopy. *Materials Science-Poland* **2013,** *31* (2), 276-280.

65. Jagannathan, R.; Abraham, P. M.; Poddar, P., Temperature-Dependent Spectroscopic Evidences of Curcumin in Aqueous Medium: A Mechanistic Study of Its Solubility and Stability. *The Journal of Physical Chemistry B* **2012,** *116* (50), 14533-14540.

66. Heller, C. A.; Henry, R. A.; McLaughlin, B. A.; Bliss, D. E., Fluorescence spectra and quantum yields. Quinine, uranine, 9,10-diphenylanthracene, and 9,10-bis(phenylethynyl)anthracenes. *Journal of Chemical & Engineering Data* **1974,** *19* (3), 214-219.

67. Kunwar, A.; Barik, A.; Mishra, B.; Rathinasamy, K.; Pandey, R.; Priyadarsini, K. I., Quantitative cellular uptake, localization and cytotoxicity of curcumin in normal and tumor cells. *Biochimica et Biophysica Acta (BBA) - General Subjects* **2008,** *1780* (4), 673-679.

68. Syng-ai, C.; Kumari, A. L.; Khar, A., Effect of curcumin on normal and tumor cells: Role of glutathione and bcl-2. *Mol. Cancer Ther.* **2004,** *3* (9), 1101.

69. Marquardt, J. U.; Gomez-Quiroz, L.; Arreguin Camacho, L. O.; Pinna, F.; Lee, Y. H.; Kitade, M.; Dominguez, M. P.; Castven, D.; Breuhahn, K.; Conner, E. A.; Galle, P. R.; Andersen, J. B.; Factor, V. M.; Thorgeirsson, S. S., Curcumin effectively inhibits oncogenic NF-kappaB signaling and restrains stemness features in liver cancer. *J. Hepatol.* **2015,** *63* (3), 661-9.

70. Wang, M.; Jiang, S.; Zhou, L.; Yu, F.; Ding, H.; Li, P.; Zhou, M.; Wang, K., Potential Mechanisms of Action of Curcumin for Cancer Prevention: Focus on Cellular Signaling Pathways and miRNAs. *Int. J. Biol. Sci.* **2019,** *15* (6), 1200-1214.

71. Cao, J.; Jia, L.; Zhou, H.-M.; Liu, Y.; Zhong, L.-F., Mitochondrial and Nuclear DNA Damage Induced by Curcumin in Human Hepatoma G2 Cells. *Toxicological Sciences* **2006,** *91* (2), 476-483.

CHAPTER IV

ELUCIDATION OF ANTI-PROLIFERATIVE AND ROS REGULATION ACTIVITY OF PHOTOLUMINESCENT CURCUMIN NANOPARTICLES

Overview

Recently, various types of nanomaterials have been employed to design delivery vehicles for curcumin to address the problems of poor bioavailability, low aqueous solubility, and rapid metabolism. The present study focussed on the direct one pot synthesis of curcumin nanoparticles (E-Curc dots) without delivery vehicles and elucidate it's therapeutic properties. E-Curc dots were synthesized using three precursor molecules, curcumin, ethylene diamine (EDA) and citric acid and characterized. The as-synthesized E-Curc dots exhibited bright blue fluorescence due to the incorporation of nitrogen from EDA precursor molecule. The characterization studies showed even distribution of dots with size less than 10 nm and reatined some of the major characteristic peaks of native curcumin. The synthesized E-Curc dots showed antioxidation activity at low concentrations (0.01-0.04 mg/mL) with low levels of ROS generation. At high concentrations, the dots exhibited pro-oxidant effects on both the cancer cells and normal cells through the generation of more ROS and dose dependent cytotoxicity is observed. The E-Curc dots showed better cytotoxicity towards cancer cells compared to native curcumin. The dots were uptaken by both the cancer and normal cells. The results clearly

showed the efficacy of E-Curc dots as an anti-proliferative and ROS regulator with possible applications in bioimaging.

Introduction

Reactive oxygen species (ROS) such as H_2O_2, NO, O_2^-, HOCl, and OH^- contain reactive oxygen molecule and are produced not only when the cells are under stress but also during the cellular metabolism.[1-2] Cellular immune responses release free radicals, which in low amounts[1] are beneficial to cells by inhibiting growth of viruses, pathogens and tumors.[3] ROS also plays an important role as regulatory mediators in signaling pathways such as cell proliferation, activation and migration.[2] The detrimental effects of ROS are observed only in high amounts, causing irreparable damage to cellular structures such as carbohydrates, proteins, nucleic acids (DNA and RNA), and lipids.[4] Inbuilt antioxidant mechanisms, effective against blocking the damaging effects of ROS are altered during oxidative stress leading to various pathological conditions such as cancer, neurological disorders,[5] asthma,[6] atherosclerosis and hypertension.[4] Widely used exogenous antioxidants such as butylated hydroxyanisole (BHA), butylated hydroxytoluene (BHT) are toxic and causes liver damage and carcinogenesis.[7] So, the search for natural, safe and effective atioxidants to counterbalance the ROS effects is extensive.

Curcumin, a natural polyphenolic spice obtained from tropical southeast Asian plant Curcuma Longa (turmeric) has its applications dated back to centuries as a dietary supplement[8] with its anti-inflammatory,[9] analgesic, antiseptic and antioxidant properties.[10-13] Curcumin has been reported to play an important role in radical

scavenging,[14] metal chelation and inhibition of lipid peroxidation.[12] Antioxidant genes such as HO-1, γ-GCS has been upregulated by curcumin during oxidative stress.[10, 15] Although, curcumin's role as an antioxidant is well studied, few reports suggest curcumin can also act as pro-oxidant through the production of ROS.[16-18] Phase I clinical trials in humans showed no side effects upon administration of curcumin (8 g/day).[19] Despite all these pleiotropic effects of curcumin, the low aqueous solubility, poor bioavailability,[20] and rapid degradation, fast metabolism,[21] and systemic elimination renders this elixir drug usage as a therapeutic agent.[22-23]

Extensive research has been focussed on enhancement of curcumin bioavailability using various formulations such as micelles,[24] phospholipids,[25] liposomes,[26] emulsions,[27] and polymers.[26] However, low encapsulation efficiency, carrier instability, poor drug loading capacity and drug release are the challenges that need to be addressed.[28-30] Recently, nanoformulations of curcumin has gained lot of attention due to their increased bioavailability, solubility, circulation times, targeted specificity, decreased biodegradation, better photostability, and improved cellular uptake.[31-38] Metallic nanoparticles were used as vehicles for curcumin delivery,[39] but their usage is limited by particle instability, impurities, longer retention time and biocompatibility issues. Carbon nanodots (CNDs) are minute fluorescent particles in the size range of 1-10 nm with some unique characteristics such as aqueous solubility, chemical inertness, stable photoluminescence, and better biocompatibility. Small size, large surface area and oxygen containing functional groups (-OH and -COOH) of the CNDs acts as a better platform for the encapsulation and targeted delivery of curcumin.

The work is focussed on economical one pot synthesis of curcumin nanoparticles (E-Curc dots) using three precursors, ethylene diamine (EDA), citric acid and curcumin to enhance the bioavialability and efficacy of curcumin. E-CNDS from our previous study, showed high quantum yield of 64% when EDA and citric acid were used as precursor molecules.[40] In the present study, EDA acts as a nitrogen dopant in the synthesis process making E-Curc dots photoluminescent and provides applications in bioimaging. The as-synthesized E-Curc dots were well characterized and antioxidant properties were investigated using DPPH. EA. hy926 (normal cell line) and A549 (lung cancer cell line) were used for biocompatibilty, ROS levels measurement, and intracellular studies. The synthesized E-Curc dots exhibited both antioxidant and pro-oxidant activity in a concentration dependent manner.

Methods and Materials

Citric acid (ACROS Organics), Ethylenediamine (Fisher Scientific), Curcumin (Chem Cruz), α, α-diphenyl-β-picrylhydrazyl (DPPH), and dichloromethane (DCM) (Alfa Aesar), phosphate buffer solution (PBS) (Life Tech), quinine sulfate dihydrate, DCF-DA (Sigma), methanol, gold electrode, Ag/AgCl reference electrode, and platinum electrode (Fisher Scientific), A549 cell line, EA. hy 926 cell line, DMEM media, and F12 K, (ATCC), pen/strep solution, fetal bovine serum and alamar blue, dimethylsulfoxide (DMSO) (Thermo Fisher Scientific), tryplE (Gibco).

E-Curc dots were synthesized using ethylene diamine (EDA), curcumin and citric acid using one step microwave synthesizer (CEM Corp 908005 Microwave Reactor). Briefly, 960 mg of citric acid was dissolved in 1 ml of deionized water followed by

addition of 1 ml of EDA. To this solution, 2 ml of curcumin dissolved in dicholoromethane (10 mg/mL) was added and the mixture was pyrolyzed for 15 min at temperature below 150 ºC and 300 W power. The brown colored solution was dissolved in 5 ml of deionized water and dialyzed through MWCO 1000 membrane (Scientific Fisher) for 24 hrs. The solution was lyophilized for 24 hours using a freeze drier (Labconco Free Zone 6 Freeze Dryer).

Atomic Force Microscopy (AFM, Agilent 5600LS AFM) in tapping mode and Transmission Electron Microscopy (TEM, Carl Zeiss Libra 120 Plus) were used for the size characterization and distribution of the synthesized dots respectively. Surface functional groups were investigated using fourier transform infrared (FTIR) spectra (Agilent FTIR). XPS (Thermo Scientific ESCALAB Xi^+) and EDX (Bruker Nano XFlash Detector 5030) were used for the elemental composition and surface states of the as prepared E-Curc dots, respectively. Zeta potential of the E-Curc dots (0.01mg/mL) was measured using Malvern Zetasizer ZEN3600. The optical properties were measured using UV-Visible spectroscopy (Varian Cary 6000i) and fluorescence spectrophotometer (Horiba FluoroMax-4). Excitation-dependent behavior of the as prepared E-Curc dots (0.01 mg/mL) was determined using a fluorescence spectroscopy at different excitation wavelengths ranging from 300-480 nm. The quantum yield of the E-Curc dots was calculated with quinine sulfate as a standard using the formula:[41-42]

$$\Phi_C = \Phi_{QS} \times \frac{Grad_C}{Grad_{QS}} \times \frac{{\eta_C}^2}{{\eta_{QS}}^2} \quad (4.1)$$

where, Φ represent the quantum yield, Grad is the slope from the plot (integrated fluorescence intensity vs absorbance) and η, refractive index (water, 1.33). The subscript QS and C denoted quinine sulfate and E-Curc dots respectively.

2,2- Diphenyl-1-icrylhydrazyl (DPPH) free radical assay was carried out to study the antioxidant activity of E-Curc dots. 50 µM of DPPH in methanol was added to different concentrations (0, 0.005, 0.01, 0.02, 0.04, 0.05 mg/mL) of E-Curc dots and incubated in dark environment for 1.5 hours with appropriate controls. Later the samples were analyzed for decrease in absorbance at 517 nm using UV-vis spectrophotometer with increase in the concentration. Antioxidant activity was calculated using the following formula.

$$\% \text{ Anti} - \text{oxiadtion activity} = 1 - \frac{A_c}{A_0} * 100 \qquad (4.2)$$

where A_0 and A_C corresponds to absorbance of DPPH without and with presence of E-Curc dots respectively.

Cyclic Voltammetric (CV) experiments were performed using a three-electrode system, with gold working electrode, Ag/AgCl reference electrode and a platinum counter electrode. Methanol and 40mM PBS in 1:1 ratio was used as an electrolyte for all the experimental runs. A final concentration of 50 µM DPPH was added to each concentration of the E-Curc dots to be tested. Prior to the CV run, the samples were incubated in dark environment for 60 min. DPPD in methanolic PBS without E-Curc dots was used as a control. All the samples were run at seven different scan rates.

A549 and EA. hy926 cells were cultured in F12K medium and Dulbecco's Modified Eagles Medium (DMEM) supplemented with 10% fetal bovine serum (FBS) and 1% pencillin/streptomycin solution respectively. All the cell lines were maintained in an incubator with 5% CO_2 and 37 ºC in a humidified atmosphere.

Cellular cytotoxicity studies were carried out for the synthesized E-Curc dots using EA. hy926 and A549 cell lines. Briefly, 10,000 cells were plated per each well in 96 plate supplemented with the complete media and incubated for overnight. Cells were treated with different concentrations (0, ,0.1, 0.2, 0.4, 0.8, 1.6 mg/mL) of E-Curc dots for 24 hours. The cells were treated with native curcumin dissolved in DMSO (0.2 mg/mL) for comparison with the E-Curc dots treatment group. Alamar blue assay determines the quantitative measurement of cell proliferation by reducing blue non-fluorescent resazurin to fluorescent resorufin in presence of cellular metabolic reactions.[43] The cell viability was determined by measuring the fluorescence at an excitation wavelength of 560 nm and emission wavelength of 590 nm which is proportional to the number of living cells. % of living cells is calculated using the below formula, where Fl is the fluorescence intensity

$$\text{Viability } \% = \frac{\text{Fl}_{\text{sample}} - \text{Fl}_{\text{blank}}}{\text{Fl}_{\text{control}} - \text{Fl}_{\text{blank}}} * 100 \qquad (4.3)$$

Intracellular ROS levels were monitored in A549 and EA. hy926 cells using DCFH-DA, a peroxide/hydroperoxide probe. Briefly, 10,000 cells were plated in 96 well plate per each well and grown for 24 hours. The cell culture medium was replaced with 20 μM of Dichloro-dihydro-fluorescein diacetate (DCF-DA) in FBS free media and

incubated for 30 minutes at 37 ºC. The cells were washed with 1x PBS twice and treated with different concentrations of E-Curc dots for 8 hours. The cells were washed twice with 1x PBS and the fluorescence intensity resulting from the oxidation of DCF-DA to DCF was measured at an excitation of 485 nm and emission wavelength of 530 nm. As controls, the cells without E-Curc dots treatment and the E-Curc dots treated cells without DCF-DA were used. As negative control, cells were treated with ascorbic acid (AA) for comparison. The effect of E-Curc dots on H_2O_2 induced ROS production was observed by treating the cells with 200 μM of H_2O_2 after treatment with E-Curc dots and before the addition of DCF-DA. Normalized fluorescence intensity was calculated.

E-Curc dots intracellular uptake was observed using confocal microscopy. Briefly, 1×10^5 cells (EA. hy926 and 549) were plated on cover slip in each well of 12 well plate and incubated overnight. The medium was replaced with different concentrations of E-Curc dots () and incubated for 12 hours. The images were collected at 20X magnification using confocal microscope (Zeiss Z1 Spinning Disk Confocal Microscope).

Results and Discussion

The size of the E-Curc dots is around 6 nm from the height profile of AFM with an even dispersion (Figure 4.1A & 4.1B). Since the radius of curvature for the AFM probe is smaller, only height data is used for the size determination. The TEM analysis show spherical monodisperse E-Curc dots of sizes ranging from 4-6.5 nm (Figure 4.1C & 4.1D).

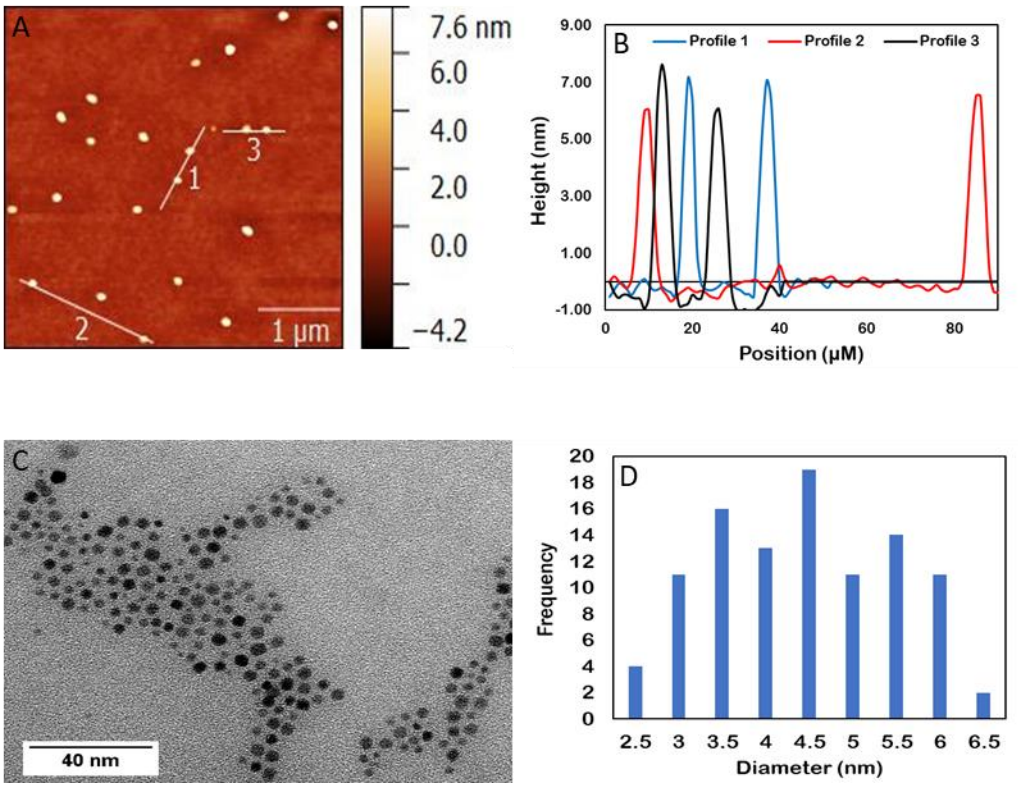

Figure 4.1. AFM and TEM of E-Curc Dots. AFM image of E-Curc dots (A) and the respective height profile (B). TEM image of E-Curc dots (C) with size histogram (D).

The XPS survey spectrum of E-Curc dots demonstrate the presence of C1s, N1s and O1s peaks at 285.0, 400.5, and 532.0 eV respectively (Figure 4.2A). High resolution C1s spectrum of E-Curc dots depicts three surface groups corresponding to C=C, C-C/C-H, C-OH, and O-C=O at 284.0 eV, 285.5 eV, 286.8 eV, and 288.8 eV respectively (Figure 4.2B). The appearance of C=C peak in the synthesized E-Curc dots indicates the presence of curcumin.[44] Moreover, the peaks C-OH and O-C=O confirms the presence of alcoholic and carbonyl (keto) functional groups of curcumin (Figure C.S1).[45] The high resolution O1s spectra shows four deconvolution peaks at 530.4 eV, 532.4 eV, and 534.3 eV, correlate to adsorbed oxygen, O=C, and O-H respectively (Figure C.S2A). The

HRN1s spectrum depicts two peaks corresponding to N=C and N-C (Figure C.S2B). The XRD pattern of the E-Curc dots showed similar elemental compositions as of the XPS spectra (Figure C.S3).

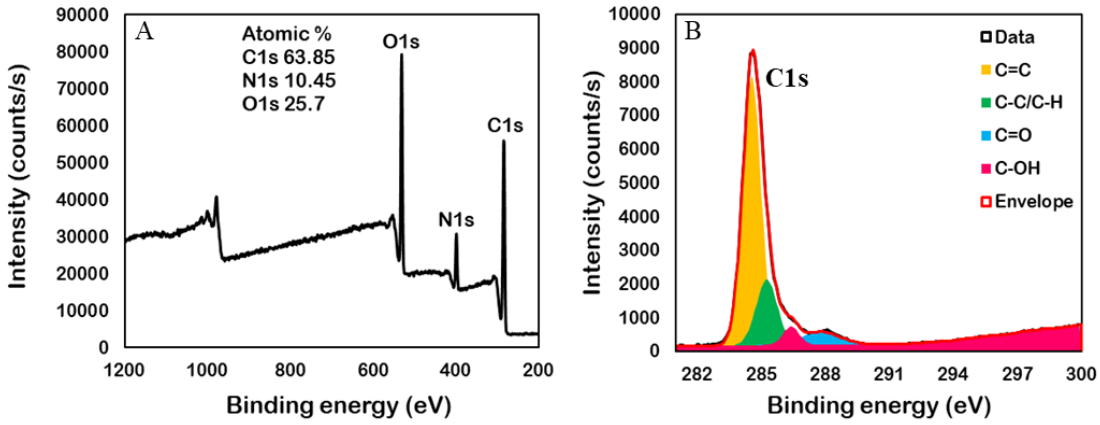

Figure 4.2. XPS Spectra. XPS survey spectra (A) and high resolution C1s spectra (B) of E-Curc dots.

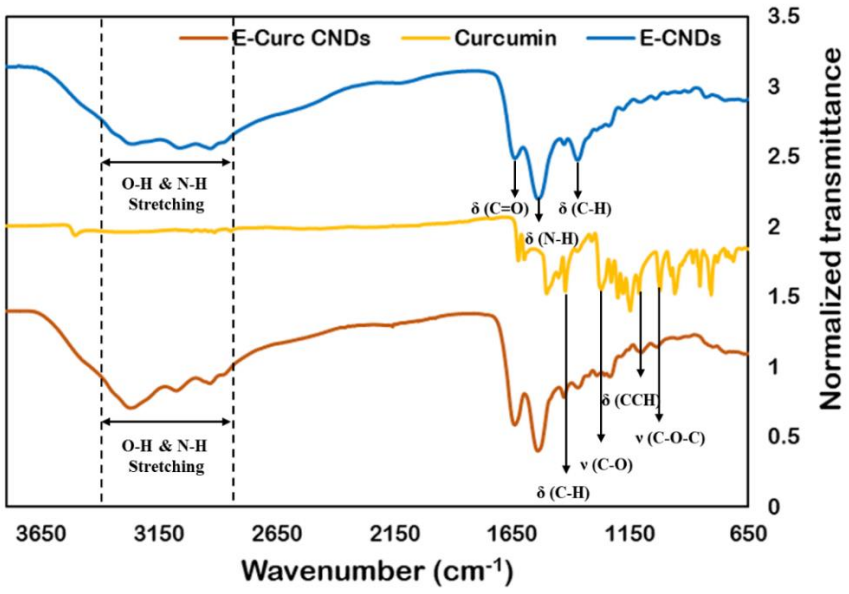

Figure 4.3. FTIR Spectra. FTIR spectra of E-CNDs, Curcumin and E-Curc dots.

The zeta potential of the synthesized E-Curc dots is found to be -15.9±1.07 mV, while the E-CNDs has a potential of -25.3±1.54 mV. FTIR spectral analysis of the curcumin (Figure 4.3) shows its characteristic peaks at 3505 cm^{-1} (phenolic O-H stretching), 1625 cm^{-1} (aromatic C=C stretching), 1427 cm^{-1} (olefinic C-H bending), 1270 cm^{-1} (aromatic C-O stretching), and 1025 cm^{-1} (C-O-C stretching). The characteristic bands of the E-CNDs at 3000-3400 cm^{-1} (stretching vibrations of O-H and N-H), 1538 cm^{-1}, 1432 cm^{-1}, and 1375 cm^{-1} corresponds to the bending vibrations of N-H, C-N, and C-H respectively. The synthesized E-Curc dots (Figure 4.3) retained major bands of the curcumin and E-CNDs, clearly indicating the incorporation of curcumin. The disappearance of peak at 3505 cm^{-1} in the E-Curc dots may be due to the interaction of phenolic O-H of curcumin with COOH of the citric acid.

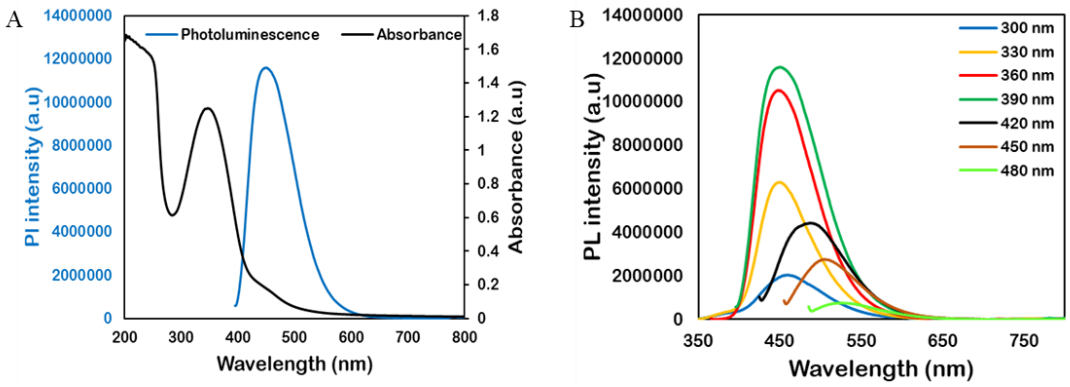

Figure 4.4. Photoluminescent Properties of E-Curc Dots. UV-Vis absorption (blue) and PL emission (black) spectra of E-Curc dots (0.01 mg/mL) at an excitation of 390 nm (A). Wavelength dependence of E-Curc dots at different excitation wavelengths (B).

E-Curc dots show strong absorption peak at 350 nm corresponding to the n-π transitions and shoulder peak at 250 nm attributing to the π- π* transitions of C=C (aromatic sp^2 domains) (Figure 4.4A). The shoulder peak at 460 nm attributes to the

curcumin incorporated into the CNDs. The emission peak was observed at 450 nm with an excitation wavelength of 390 nm (Figure 4.4A). The wavelength dependence of E-Curc dots was performed at different excitation wavelengths ranging from 300-480 nm (Figure 4.4B). The high intensity emission peak occurs at an excitation wavelength of 390 nm. The quantum yield of the as-synthesized E-Curc dots is 45.5±2.1% with reference to quinine sulfate (54%).

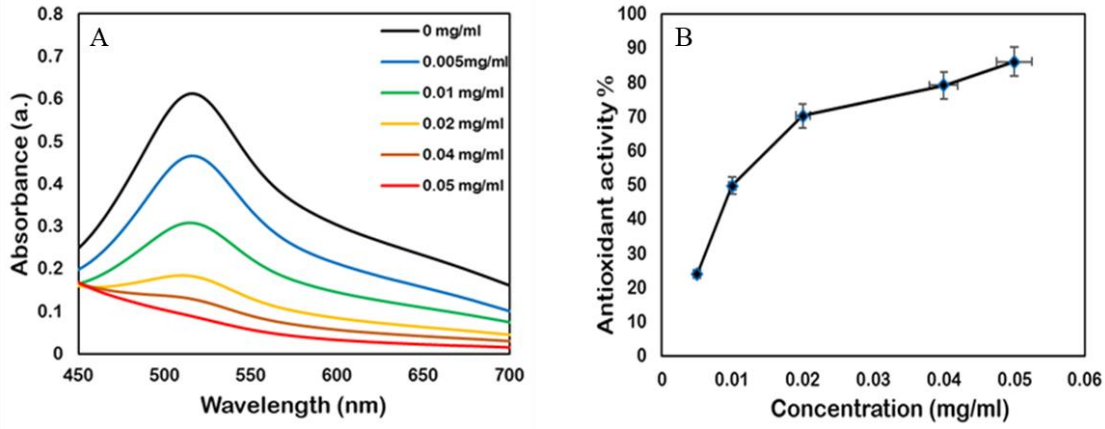

Figure 4.5. DPPH Antioxidation Assay. UV-Vis spectra of DPPH in methanolic solution at various concentrations of E-Curc dots (0, 0.005, 0.01, 0.02, 0.04, 0.05 mg/mL) (A). Antioxidant activity of E-Curc dots with their respective concentrations (B).

E-Curc dots antioxidation activity was assessed with DPPH assay using UV-Vis spectrophotometer. DPPH is a stable free radical with an unpaired valence electron at nitrogen bridge and has a bright purple color when dissolved in methanol. The basic principle is scavenging of antioxidant compounds, through the transfer of hydrogen atom of the antioxidant molecule to the hydrazine of the DPPH, thereby changing it's color from deep purple to yellow.[46] With increase in the concentrations of E-Curc dots, the absorption peak decreases at 515 nm (Figure 4.5A). The antioxidant activity % of E-Curc

dots is found to be 24.0, 49.6, 70.1, 79.0, 87.2% at concentrations of 0.005, 0.01, 0.02, 0.04, 0.05 mg/mL respectively (Figure 4.5B). At a concentration of 0.05 mg/mL the absorption peak flattened with 87.2% antioxidant activity and the color of the DPPH solution turned yellow. The rapid decrease in the absorbance peak might be attributed to the anti-oxidant nature of curcumin incorporated into the dots.

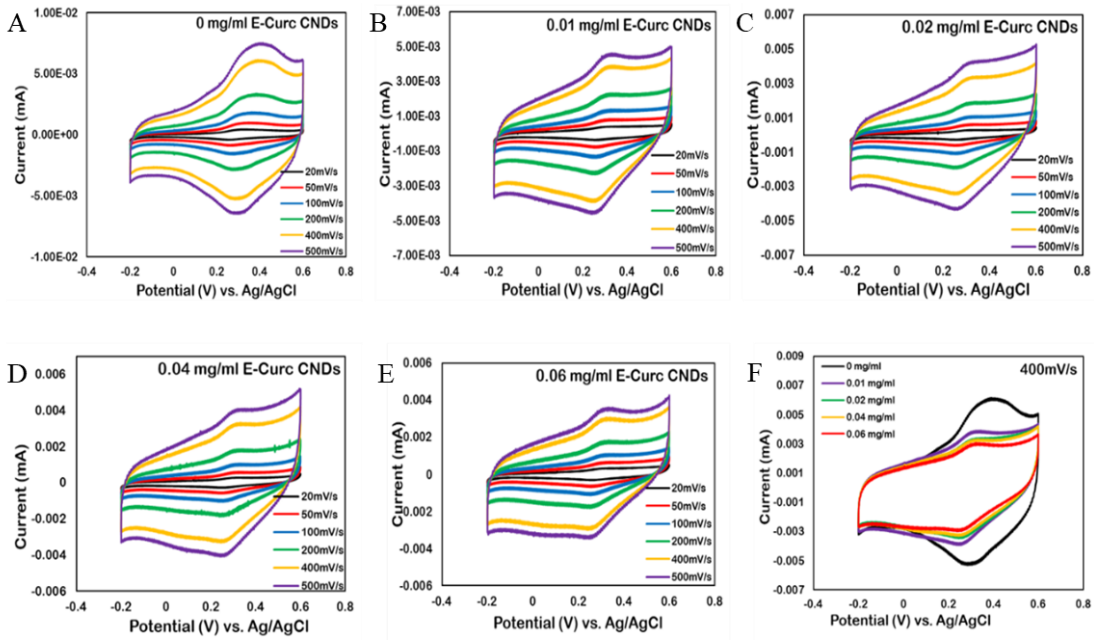

Figure 4.6. Cyclic Voltammograms of E-Curc Dots. Cyclic voltammograms of E-Curc dots in methanolic DPPH at different concentrations of 0 (A), 0.01 (B), 0.02 (C), 0.04 (D), 0.06 mg/mL (E) at scan rates of 0, 20, 50, 100, 200, 400 and 500 mV/s. Cyclic voltammograms of E-Curc dots in methanolic DPPH at different concentrations (0, 0.01, 0.02, 0.04, 0.06 mg/mL) at a scan rate of 400 mV/s (F).

The antioxidant activity of E-Curc dots is further supported with cyclic voltammetric analysis. DPPH can either act as an oxidizing or a reducing agent and most of the antioxidant studies showed DPPH exclusively acts as an oxidising agent.[47]

$$DPPH^{*} \leftrightarrow DPPH - H + e^{-} \qquad (4.4)$$

$$DPPH^{*} + e^{-} \leftrightarrow DPPH^{-} \quad (4.5)$$

In the absence of E-curc dots, the redox peaks in methanolic DPPH are intact (Figure 4.6A), but with increase in the concentration of E-Curc dots, the redox peaks started to decrease (Figure 4.6B-E). The clear decrease in tendency of redox peaks is observed with increasing concentration sof E-Curc dots at a scan rate of 400 mV/s (Figure 4.6F). This is due to the proton transfer from the E-Curc dots to DPPH*, converting free radical DPPH* to neutral stable DPPH-H. With increase in E-Curc dots, the available DPPH* is decreased at the electrode surface, thereby reducing the redox peaks. The underlying mechanism might be the hydrogen atom transfer (HAT) from the O-methoxy phenolic group of nanocurcumin molecule to the DPPH* free radical.

$$E - \text{Curc dots} + DPPH^{*} \rightarrow DPPH - H + E - \text{Curc dots}^{*} \quad (4.6)$$

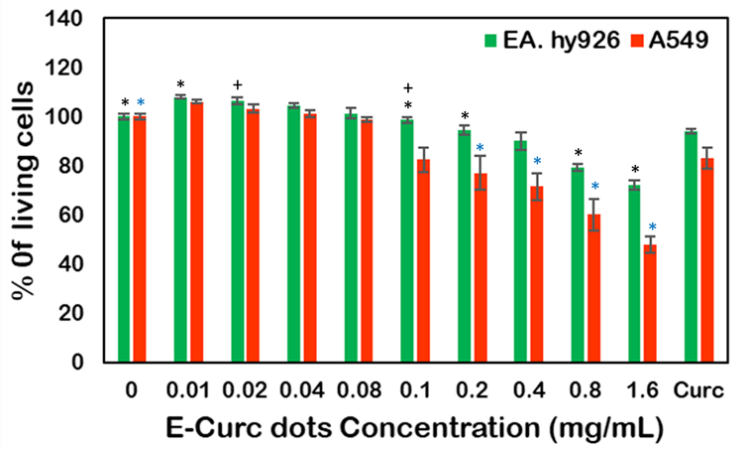

Figure 4.7. Biocompatibility of E-Curc Dots. Biocompatibility of E-Curc dots tested at different concentrations in EA. hy926 and A549 cells.

The cell viability of E-Curc dots was assessed using alamar blue assay for two cell lines EA. hy926 and A549. There is an increase in cell viability upon treatment with E-Curc dots in a concentration range 0.01-0.08 mg/mL in both the cell lines. Thereafter, with increase in the concentration of E-Curc dots, the cell viability decreased significantly in both the cell lines. A549 cells showed higher levels of cell toxicity compared to the EA. hy926 cells (Figure 4.7). Statistically, the cell viability is around 72% for A549 cells and 48% for EA. hy926 cells, after incubated for 24 hours at higher concentration of 1.6 mg/mL. The control native curcumin in DMSO (0.2 mg/mL) showed 93% and 83% cell viability for EA. hy926 and A549 cells respectively. The nano-curcumin (E-Curc dots) showed better cytotoxicity towards the cancer cells at low concentrations (0.2 mg/mL) compared to native curcumin, suggesting the efficacy of the synthesized E-Curc dots. The increased cellular toxicity of the 549 cells compared to EA. hy926 upon treatment with E-Curc dots can be due to increased cellular uptake in cancer cells and moreover, cancer cells are more sensitive to oxidative stress.[48] The different trends observed in the cell viability with E-Curc dots treatment might be attributed to the different cellular responses to E-Curc dots.

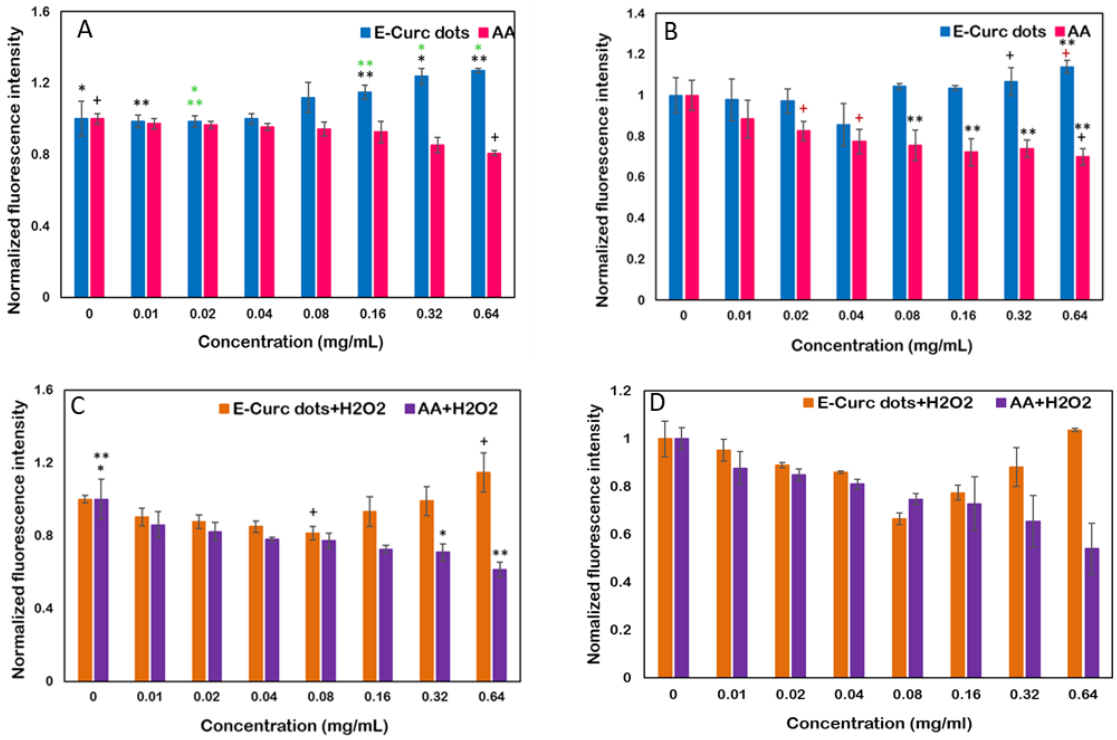

Figure 4.8. ROS Levels Measurement. ROS levels measurement in EA. hy926 (A) and A549 cells (B) on addition of E-Curc dots and ascorbic acid (AA) at different concentrations using DCF-DA assay. Effects of E-Curc dots at different concentrations on H_2O_2 (200 μM) treated EA. hy926 (C) and A549 cells (D).

Intracellular ROS levels of EA. hy926 and A549 cells were measured using DCFH-DA assay upon treatment with E-Curc dots. DCFH-DA is a cell permeable non-fluorescent probe for intarcellular oxidative stress measurement. Intracellular esterases cleave ester bonds of DCFH-DA into non-fluorescent impermeable $DCFH_2$, which on subsequent oxidation produces highly fluorescent DCF. Accumulation of DCF in cells is proportional to concentration of hydrogen peroxide (H_2O_2) can be measured with increase in fluorescence 530 nm when excited at 485 nm.[49] Upon treatment with E-Curc dots, the ROS levels are almost similar to that of control (Cells with no E-Curc dots treatment) in EA. hy926 cells with in a concentrtaion range of 0.01-0.04 mg/mL. Increase

in ROS levels were observed after 0.08 mg/mL in a concentration dependent manner. But, the treatment with AA (0.01, 0.02, 0.04, 0.08, 0.16, 0.32, and 0.64 mg/mL), steadily decreased the ROS levels in EA. hy926 cells (Figure 4.8A). Similar trend is observed with A549 cells, except for the ROS levels increased after treatment with E-Curc dots at a concenration of 0.04 mg/mL (Figure 4.8B). The protective effects of E-Curc dots pretreatment on cells were identified by treating the cells with 200 μM H_2O_2, a ROS inducer. Pretreatment with E-Curc dots remarkably inhibited cell cytotoxcity caused by H_2O_2 up to a concentration of 0.08 mg/mL, in both the cell lines (Figure 4.8C & 4.8D). With increase in E-Curc dots concentration beyond 0.08 mg/mL, the ROS levels increased, leading to cellular toxicity. AA showed dose dependent decrease in ROS levels with increase in concentration in both the cell lines (Figure 4.8C & 4.8D).

In the present study, E-Curc dots are synthesized from curcumin precursors and the reduction in particle size of active ingredients to nano size might have increased the solubility and efficacy.[50] Previous studies showed at low concentrations curcumin acts an antioxidant through ROS scavenging by preventing depletion of glutathione (GSH), a natural cellular antioxidant and at high concentrations acts an pro-oxidant with increase in ROS production.[51] The antioxidant or pro-oxidant activity depends on structure modification, curcumin concentration, presence of metal ions at free radical generation.[52] The results from ROS measurement are in accordance with the cell viability data, which suggest the increased cytotoxicity upon treatment with higher concentrations of E-Curc dots might be due to the excess ROS production, making it a promising anti-cancer agent leading to cell death. And the high viability at low concentrations of E-Curc dots might

be attributed to the ROS scavenging activity. The decrease in ROS generation can be attributed to the abstraction of H-atom from the O-methoxy phenolic rings of curc dots to free radicals.[53] The high ROS generation at higher concentrations of E-Curc dots ascribes to the presence of α,β- unsaturated ketone groups, which might alkylate active sites of thioredoxin reductase enzyme, rendering the enzyme from reducing thioredoxin, which plays an important role in regulation of ROS.[17] As a result, more ROS generates within the system leading to cell cytotoxicity.

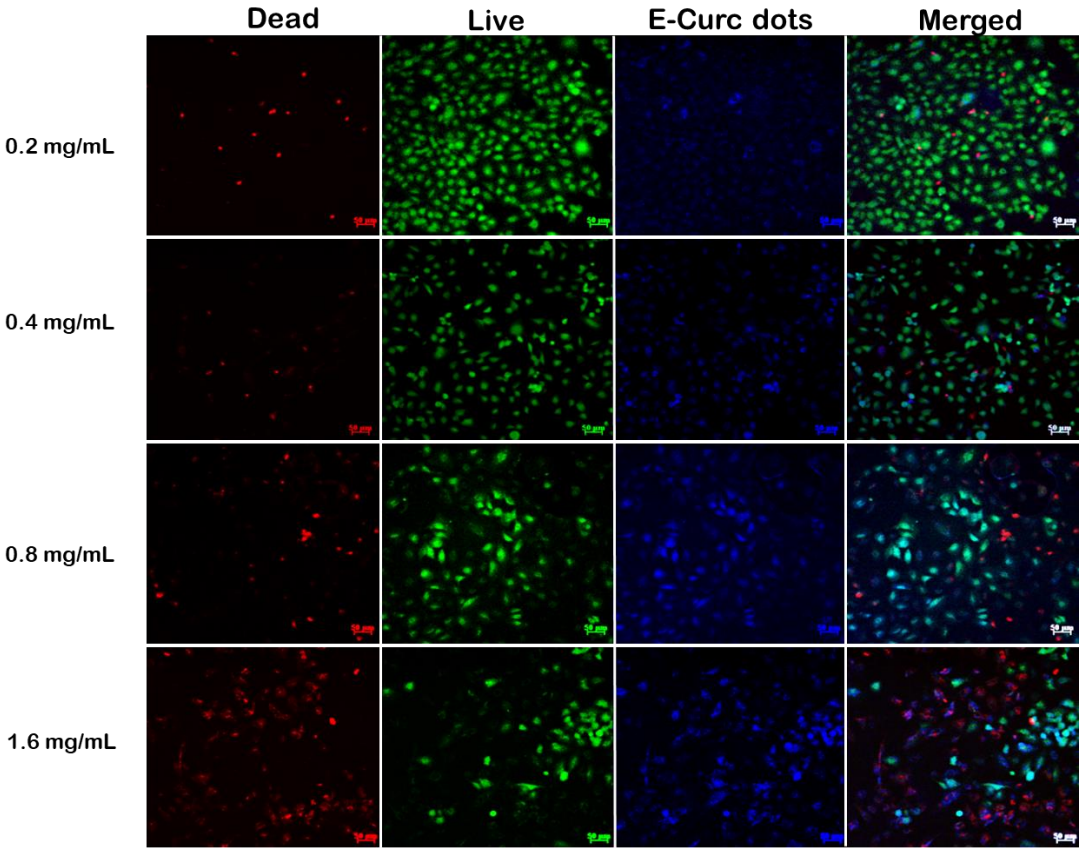

Figure 4.9. Confocal Images. Live/dead assay of A549 cells treated with different concentrations of E-Curc dots.

Live/dead assay was used to determine the cellular toxicity towards E-Curc dots. The A549 cells were treated with different concentrations of E-Curc dots (0.2, 0.4, 0.8, and 1.6 mg/mL) for 24 hours. E-Curc dots were found to be sub-cellularly localized inside the A549 (Figure 4.9) with bright blue fluorescence. As the concentration of the E-Curc dots increased, the fluorescence intensity increased (Figure 4.9). EA. hy926 cells also showed good sub-cellular localization of E-Curc dots (Figure C.S4). The cellular toxicity of A549 cells increased in a dose dependent manner upon treatment with E-Curc dots compared to controls (Figure C.S5), which can be ascribed to the more uptake of E-Curc dots. At 1.6 mg/mL concentration, more than 50% of cells were dead, indicating the production of high levels of ROS (Figure 4.9). Positive control includes the cells with no treatment and negative control has cells teated with 200 μM H_2O_2.

Conclusion

Although curcumin offers exclusive therapeutic applications as anti-cancer, antioxidant, pro-oxidant, anti-microbial, and anti-inflammatory agent, it's usage is limited by poor bioavailability and aqueous solubility, and rapid metabolism. In oder to overcome the issues, various drug delivery vehicles for carrying curcumin are developed using nanoparticles. In the present study, curcumin nanoparticles were synthesized in a cost-effective way using curcumin and ethylene diamine (EDA) as precursor molecules. EDA acts as a nitrogen dopant in the synthesis process making E-Curc dots photoluminescent and provides applications in bioimaging. The synthesized E-Curc dots retained some of the functional groups of native curcumin and demonstrated stable photoluminescence, with size less than 10 nm. The curcumin dots showed excellent

antioxidation capacity at very low concentrations (0.05 mg/mL) as measured by DPPPH assay. In terms of therapeutic efficacy, E-Curc dots proved to act as both antioxidant and pro-oxidant at low and high concentrations respectively, which is in accordance with the cell viability data. Chemo-protective nature of E-Curc dots was observed when the cells were treated with H_2O_2. Moreover, the E-Curc dots were successfully uptaken by cancer cells with bright blue fluorescence. Overall, the synthesized E-Curc dots retained the characteristics of native curcumin a ROS regulator with stable photoluminescence and showed anti-proliferative effects on cancer cells at low concentrations compared to native curcumin.

References

1. Valko, M.; Leibfritz, D.; Moncol, J.; Cronin, M. T.; Mazur, M.; Telser, J., Free radicals and antioxidants in normal physiological functions and human disease. *The international journal of biochemistry & cell biology* **2007,** *39* (1), 44-84.

2. Droge, W., Free radicals in the physiological control of cell function. *Physiological reviews* **2002,** *82* (1), 47-95.

3. Pacher, P.; Beckman, J. S.; Liaudet, L., Nitric oxide and peroxynitrite in health and disease. *Physiological reviews* **2007,** *87* (1), 315-424.

4. Birben, E.; Sahiner, U.; Sackesen, C.; Erzurum, S.; Kalayci, O., Oxidative Stress and Antioxidant Defense. *World Allergy Organization Journal* **2012,** *5*, 9-19.

5. Jenner, P., Oxidative stress in Parkinson's disease. *Annals of neurology* **2003,** *53 Suppl 3*, S26-36; discussion S36-8.

6. Comhair, S.; Ricci, K.; Arroliga, M.; Lara, A.; Dweik, R.; Song, W.; Hazen, S.; Bleecker, E.; Busse, W.; Chung, K. F.; Gaston, B.; Hastie, A.; Hew, M.; Jarjour, N.; Moore, W.; Peters, S.; Teague, W.; Wenzel, S.; Erzurum, S., Correlation of Systemic Superoxide Dismutase Deficiency to Airflow Obstruction in Asthma. *American journal of respiratory and critical care medicine* **2005,** *172*, 306-13.

7. Witschi, H. P., Enhanced tumour development by butylated hydroxytoluene (BHT) in the liver, lung and gastro-intestinal tract. *Food and chemical toxicology : an international journal published for the British Industrial Biological Research Association* **1986,** *24* (10-11), 1127-30.

8. Shishodia, S.; Sethi, G.; Aggarwal, B. B., Curcumin: getting back to the roots. *Annals of the New York Academy of Sciences* **2005,** *1056*, 206-17.

9. Abe, Y.; Hashimoto, S.; Horie, T., Curcumin inhibition of inflammatory cytokine production by human peripheral blood monocytes and alveolar macrophages. *Pharmacological research* **1999,** *39* (1), 41-7.

10. Motterlini, R.; Foresti, R.; Bassi, R.; Green, C. J., Curcumin, an antioxidant and anti-inflammatory agent, induces heme oxygenase-1 and protects endothelial cells against oxidative stress. *Free Radical Biology and Medicine* **2000,** *28* (8), 1303-1312.

11. Sharma, O. P., Antioxidant activity of curcumin and related compounds. *Biochemical pharmacology* **1976,** *25* (15), 1811-2.

12. Ruby, A. J.; Kuttan, G.; Babu, K. D.; Rajasekharan, K. N.; Kuttan, R., Anti-tumour and antioxidant activity of natural curcuminoids. *Cancer letters* **1995,** *94* (1), 79-83.

13. Alisi, I. O.; Uzairu, A.; Abechi, S. E.; Idris, S. O., Evaluation of the antioxidant properties of curcumin derivatives by genetic function algorithm. *Journal of Advanced Research* **2018,** *12*, 47-54.

14. Kunchandy, E.; Rao, M. N. A., Oxygen radical scavenging activity of curcumin. *International Journal of Pharmaceutics* **1990,** *58* (3), 237-240.

15. Rahman, I.; Biswas, S. K.; Kirkham, P. A., Regulation of inflammation and redox signaling by dietary polyphenols. *Biochemical pharmacology* **2006,** *72* (11), 1439-52.

16. Bhaumik, S.; Anjum, R.; Rangaraj, N.; Pardhasaradhi, B. V.; Khar, A., Curcumin mediated apoptosis in AK-5 tumor cells involves the production of reactive oxygen intermediates. *FEBS letters* **1999,** *456* (2), 311-4.

17. Fang, J.; Lu, J.; Holmgren, A., Thioredoxin reductase is irreversibly modified by curcumin: a novel molecular mechanism for its anticancer activity. *The Journal of biological chemistry* **2005,** *280* (26), 25284-90.

18. Khan, M. A.; Gahlot, S.; Majumdar, S., Oxidative stress induced by curcumin promotes the death of cutaneous T-cell lymphoma (HuT-78) by disrupting the function of several molecular targets. *Molecular cancer therapeutics* **2012,** *11* (9), 1873-83.

19. Gupta, S. C.; Patchva, S.; Aggarwal, B. B., Therapeutic roles of curcumin: lessons learned from clinical trials. *AAPS J* **2013,** *15* (1), 195-218.

20. Lopresti, A. L., The Problem of Curcumin and Its Bioavailability: Could Its Gastrointestinal Influence Contribute to Its Overall Health-Enhancing Effects? *Advances in Nutrition* **2018,** *9* (1), 41-50.

21. Ireson, C. R.; Jones, D. J.; Orr, S.; Coughtrie, M. W.; Boocock, D. J.; Williams, M. L.; Farmer, P. B.; Steward, W. P.; Gescher, A. J., Metabolism of the cancer chemopreventive agent curcumin in human and rat intestine. *Cancer epidemiology, biomarkers & prevention : a publication of the American Association for Cancer Research, cosponsored by the American Society of Preventive Oncology* **2002,** *11* (1), 105-11.

22. Anand, P.; Kunnumakkara, A. B.; Newman, R. A.; Aggarwal, B. B., Bioavailability of curcumin: problems and promises. *Molecular pharmaceutics* **2007,** *4* (6), 807-18.

23. Prasad, S.; Tyagi, A. K.; Aggarwal, B. B., Recent developments in delivery, bioavailability, absorption and metabolism of curcumin: the golden pigment from golden spice. *Cancer Res Treat* **2014,** *46* (1), 2-18.

24. Li, X.; Chen, T.; Xu, L.; Zhang, Z.; Li, L.; Chen, H., Preparation of curcumin micelles and the in vitro and in vivo evaluation for cancer therapy. *Journal of biomedical nanotechnology* **2014,** *10* (8), 1458-68.

25. Maiti, K.; Mukherjee, K.; Gantait, A.; Saha, B. P.; Mukherjee, P. K., Curcumin–phospholipid complex: Preparation, therapeutic evaluation and pharmacokinetic study in rats. *International Journal of Pharmaceutics* **2007,** *330* (1), 155-163.

26. Kotha, R. R.; Luthria, D. L., Curcumin: Biological, Pharmaceutical, Nutraceutical, and Analytical Aspects. *Molecules (Basel, Switzerland)* **2019,** *24* (16).

27. Cui, J.; Yu, B.; Zhao, Y.; Zhu, W.; Li, H.; Lou, H.; Zhai, G., Enhancement of oral absorption of curcumin by self-microemulsifying drug delivery systems. *International Journal of Pharmaceutics* **2009,** *371* (1), 148-155.

28. Alexander-Bryant, A. A.; Vanden Berg-Foels, W. S.; Wen, X., Bioengineering strategies for designing targeted cancer therapies. *Advances in cancer research* **2013,** *118*, 1-59.

29. Das, M.; Mohanty, C.; Sahoo, S. K., Ligand-based targeted therapy for cancer tissue. *Expert opinion on drug delivery* **2009,** *6* (3), 285-304.

30. Kim, S.; Shi, Y.; Kim, J. Y.; Park, K.; Cheng, J. X., Overcoming the barriers in micellar drug delivery: loading efficiency, in vivo stability, and micelle-cell interaction. *Expert opinion on drug delivery* **2010,** *7* (1), 49-62.

31. Carolina Alves, R.; Perosa Fernandes, R.; Fonseca-Santos, B.; Damiani Victorelli, F.; Chorilli, M., A Critical Review of the Properties and Analytical Methods for the Determination of Curcumin in Biological and Pharmaceutical Matrices. *Critical reviews in analytical chemistry* **2019,** *49* (2), 138-149.

32. Wong, K. E.; Ngai, S. C.; Chan, K.-G.; Lee, L.-H.; Goh, B.-H.; Chuah, L.-H., Curcumin Nanoformulations for Colorectal Cancer: A Review. *Frontiers in Pharmacology* **2019,** *10* (152).

33. Yavarpour-Bali, H.; Ghasemi-Kasman, M.; Pirzadeh, M., Curcumin-loaded nanoparticles: a novel therapeutic strategy in treatment of central nervous system disorders. *Int J Nanomedicine* **2019,** *14*, 4449-4460.

34. Ban, C.; Jo, M.; Park, Y. H.; Kim, J. H.; Han, J. Y.; Lee, K. W.; Kweon, D.-H.; Choi, Y. J., Enhancing the oral bioavailability of curcumin using solid lipid nanoparticles. *Food Chemistry* **2020,** *302*, 125328.

35. Ghalandarlaki, N.; Alizadeh, A. M.; Ashkani-Esfahani, S., Nanotechnology-Applied Curcumin for Different Diseases Therapy. *BioMed Research International* **2014,** *2014*, 23.

36. Bhawana; Basniwal, R. K.; Buttar, H. S.; Jain, V. K.; Jain, N., Curcumin Nanoparticles: Preparation, Characterization, and Antimicrobial Study. *Journal of Agricultural and Food Chemistry* **2011,** *59* (5), 2056-2061.

37. Montalban, M. G.; Coburn, J. M.; Lozano-Perez, A. A.; Cenis, J. L.; Villora, G.; Kaplan, D. L., Production of Curcumin-Loaded Silk Fibroin Nanoparticles for Cancer Therapy. *Nanomaterials (Basel, Switzerland)* **2018,** *8* (2).

38. Xie, J.; Yong, Y.; Dong, X.; Du, J.; Guo, Z.; Gong, L.; Zhu, S.; Tian, G.; Yu, S.; Gu, Z.; Zhao, Y., Therapeutic Nanoparticles Based on Curcumin and Bamboo Charcoal Nanoparticles for Chemo-Photothermal Synergistic Treatment of Cancer and Radioprotection of Normal Cells. *ACS Applied Materials & Interfaces* **2017,** *9* (16), 14281-14291.

39. Alsammarraie, F. K.; Wang, W.; Zhou, P.; Mustapha, A.; Lin, M., Green synthesis of silver nanoparticles using turmeric extracts and investigation of their antibacterial activities. *Colloids and Surfaces B: Biointerfaces* **2018,** *171*, 398-405.

40. Arvapalli, D. M.; Sheardy, A. T.; Alapati, K. C.; Wei, J., High Quantum Yield Fluorescent Carbon Nanodots for detection of Fe (III) Ions and Electrochemical Study of Quenching Mechanism. *Talanta* **2019**, 120538.

41. Arvapalli, D. M.; Sheardy, A. T.; Alapati, K. C.; Wei, J., High Quantum Yield Fluorescent Carbon Nanodots for detection of Fe (III) Ions and Electrochemical Study of Quenching Mechanism. *Talanta* **2020,** *209*, 120538.

42. Zhai, X.; Zhang, P.; Liu, C.; Bai, T.; Li, W.; Dai, L.; Liu, W., Highly luminescent carbon nanodots by microwave-assisted pyrolysis. *Chemical Communications* **2012,** *48* (64), 7955-7957.

43. Bonnier, F.; Keating, M. E.; Wróbel, T. P.; Majzner, K.; Baranska, M.; Garcia-Munoz, A.; Blanco, A.; Byrne, H. J., Cell viability assessment using the Alamar blue

assay: A comparison of 2D and 3D cell culture models. *Toxicology in Vitro* **2015,** *29* (1), 124-131.

44. Pan, C. J.; Tang, J. J.; Weng, Y. J.; Wang, J.; Huang, N., Preparation, characterization and anticoagulation of curcumin-eluting controlled biodegradable coating stents. *Journal of Controlled Release* **2006,** *116* (1), 42-49.

45. Singh, A.; Yadav, S.; Sharma, K.; Firdaus, Z.; Aditi, P.; Neogi, K.; Bansal, M.; Gupta, M.; Shanker, A.; Singh, R.; Prakash, P., Quantum curcumin mediated inhibition of gingipains and mixed-biofilm of Porphyromonas gingivalis causing chronic periodontitis. *RSC Advances* **2018,** *8*, 40426-40445.

46. Mishra, K.; Ojha, H.; Chaudhury, N. K., Estimation of antiradical properties of antioxidants using DPPH assay: A critical review and results. *Food Chemistry* **2012,** *130* (4), 1036-1043.

47. Solon, E.; Bard, A. J., The Electrochemistry of Diphenylpicrylhydrazyl. *Journal of the American Chemical Society* **1964,** *86* (10), 1926-1928.

48. Kunwar, A.; Barik, A.; Mishra, B.; Rathinasamy, K.; Pandey, R.; Priyadarsini, K. I., Quantitative cellular uptake, localization and cytotoxicity of curcumin in normal and tumor cells. *Biochimica et biophysica acta* **2008,** *1780* (4), 673-9.

49. Eruslanov, E.; Kusmartsev, S., Identification of ROS Using Oxidized DCFDA and Flow-Cytometry. In *Advanced Protocols in Oxidative Stress II*, Armstrong, D., Ed. Humana Press: Totowa, NJ, 2010; pp 57-72.

50. Gigliobianco, M. R.; Casadidio, C.; Censi, R.; Di Martino, P., Nanocrystals of Poorly Soluble Drugs: Drug Bioavailability and Physicochemical Stability. *Pharmaceutics* **2018,** *10* (3).

51. Banerjee, A.; Kunwar, A.; Mishra, B.; Priyadarsini, K. I., Concentration dependent antioxidant/pro-oxidant activity of curcumin: Studies from AAPH induced hemolysis of RBCs. *Chemico-Biological Interactions* **2008,** *174* (2), 134-139.

52. Yoshino, M.; Haneda, M.; Naruse, M.; Htay, H. H.; Tsubouchi, R.; Qiao, S. L.; Li, W. H.; Murakami, K.; Yokochi, T., Prooxidant activity of curcumin: copper-dependent formation of 8-hydroxy-2'-deoxyguanosine in DNA and induction of apoptotic cell death. *Toxicology in vitro : an international journal published in association with BIBRA* **2004,** *18* (6), 783-9.

53. Del Prado-Audelo, M. L.; Caballero-Floran, I. H.; Meza-Toledo, J. A.; Mendoza-Munoz, N.; Gonzalez-Torres, M.; Floran, B.; Cortes, H.; Leyva-Gomez, G., Formulations of Curcumin Nanoparticles for Brain Diseases. Biomolecules 2019, 9 (2).

CHAPTER V

CONCLUSIONS

The thesis work concentrates on the various applications of CNDs in the fields of biosensing, drug delivery and radical regulation utilizing their unique properties.

With distinct advantages of high sensitivity, selectivity, biocompatibility, simple and cost-effective synthesis, CNDs finds its application in metal ion detection. Chapter II signifies the role of CNDs in iron biosensing and the underlying detection mechanism was studied using cyclic voltammetry, an electrochemical technique for the first time. The photoluminescence phenomenon of CNDs is utilized for the detection of iron. Up on addition of Fe (III) ions, the fluorescence intensity of CNDs decreased in a dose dependent manner with a short response of 1 minute. The quenching efficiency displayed a linear relationship with Fe (III) ion concentration in a broad range of 1-2000 μM. The synthesized nanoprobes showed excellent selectivity with no interference with the other metal ions. Iron content in real samples such as tap water and human serum was detected using the nanoprobes. The Fe (III) content in living cells was also monitored, which can serve as an effective nanosensor for intracellular Fe (III) sensing. The quenching mechanism of CNDs up on addition of Fe (III) was elucidated using cyclic voltammetry. Charge transfer (electron transfer) occurs at the working electrode between the CNDs and Fe (III) ions upon formation of CND-$(Fe\ (III))_n$ complex and results in the formation of

E-CND-(Fe (II))$_n$ complex. The diffusion of E-CND-(Fe (II))$_n$ complex to the working electrode slows down compared to the free available Fe (III) in the solution thereby decreasing the redox peaks. This proposed mechanism provides a better understanding of the detection of different biologically significant metal ions.

In chapter III, CNDs were used as a drug delivery vehicle to load curcumin to deliver to the target site with minimal side effects. Curcumin, a natural antioxidant with anti-cancer, and anti-inflammatory properties confounds its therapeutic efficiency due to poor bioavailability, rapid metabolism and poor pharmacokinetics. Various delivery vehicles have been formulated for enhancement of curcumin, but the stability and low drug loading capacity is often questionable. For the first time, photoluminescent CNDs were employed for the loading of curcumin and to enhance its bioavailability. CNDs showed an encapsulation efficiency of about 92% with enhanced release in acidic media, which confers the high release of curcumin at tumor site to elicit its anti-cancer effects. The slow controlled release pattern of curcumin observed allows curcumin to reach its target site without getting wasted in the biological system. Curc CNDs were well internalized inside the cancer cells and showed dose dependent cytotoxicity in cancer cells without affecting normal cells. This new approach-based CNDs delivery systems could improve the bioavailability, and stability of several other hydrophobic drugs to elicit their therapeutic effects.

In chapter IV, curcumin nanoparticles (Curc dots) were synthesized from native curcumin using two precursor molecules EDA and citric acid. EDA acted as a nitrogen dopant in the synthesis making these dots photoluminescent and finds applications in

bioimaging. The antioxidant properties were evaluated using DPPH assay and verified by cyclic voltammetry. Curc dots elicited better anti-proliferative effects on cancer cells compared to native curcumin which might be due to the reduction in particle size of active ingredients to nano size thereby increasing the solubility and efficacy. The concentration dependent antioxidant and pro-oxidant effects of synthesized curc dots were in accordance with the cell viability assays, which suggest the increased cytotoxicity upon treatment with higher concentrations of Curc dots might be due to the excess ROS production, making it a promising anti-cancer agent leading to cell death. The mechanism behind the excess ROS generation might be due to the alkylation of active site of thioredoxin reductase enzyme by E-Curc dots. The depletion of the enzyme could not reduce thioredoxin, a compound that regulates ROS levels. And as a result, pro-oxidant radicals are generated leading to cell death.

APPENDIX A

HIGH QUANTUM YIELD FLUORESCENT CARBON NANODOTS FOR DETECTION OF FE (III) IONS AND ELECTROCHEMISTRY STUDY OF QUENCHING MECHANISM

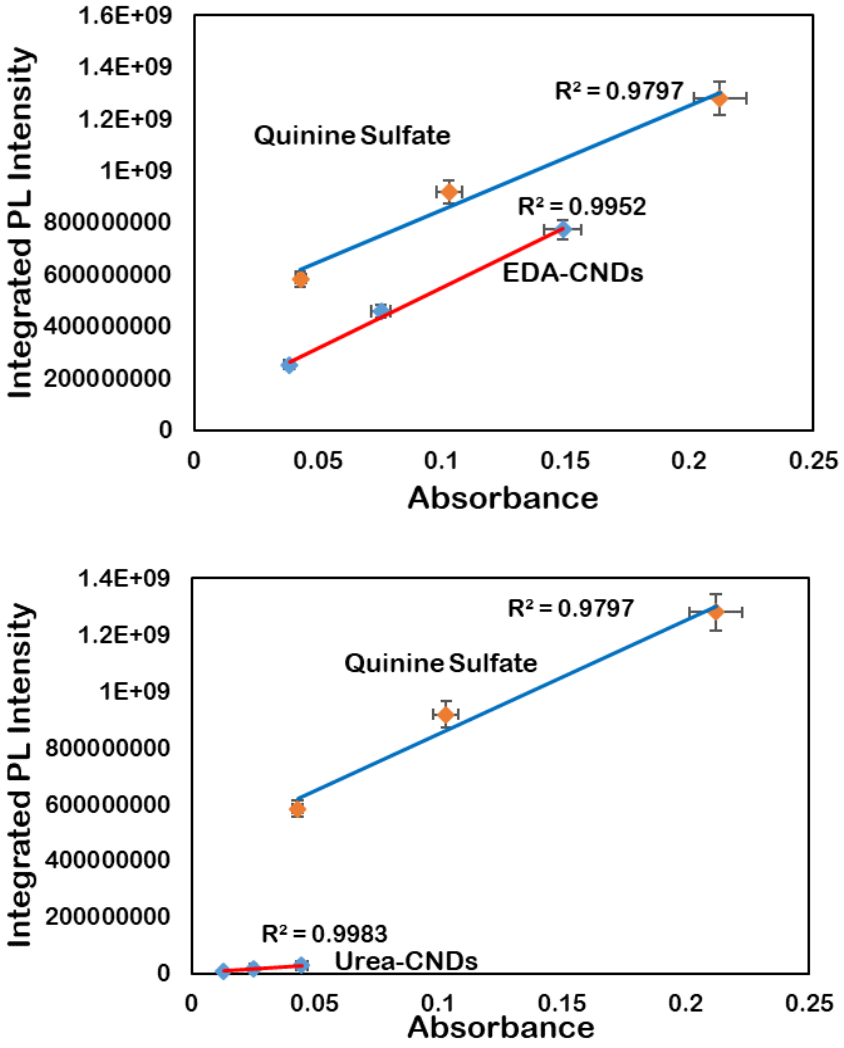

Figure A.S1. The Plot of Integrated Fluorescence Intensity vs Absorbance as a Comparison to Standard Quinine Sulfate

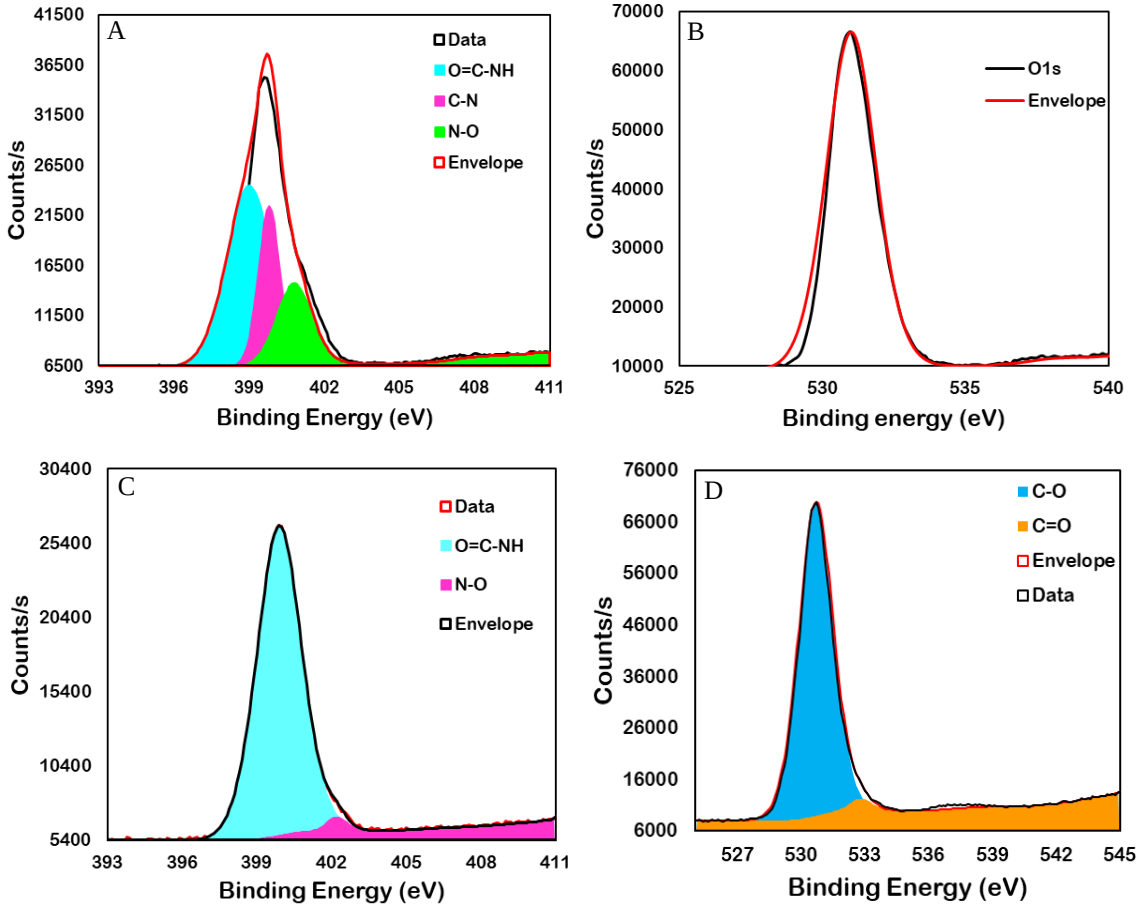

Figure A.S2. N1s and O1s XPS Peaks of CNDs. N1s and O1s XPS peaks of E-CNDs (A, B) and U-CNDs (C, D) respectively.

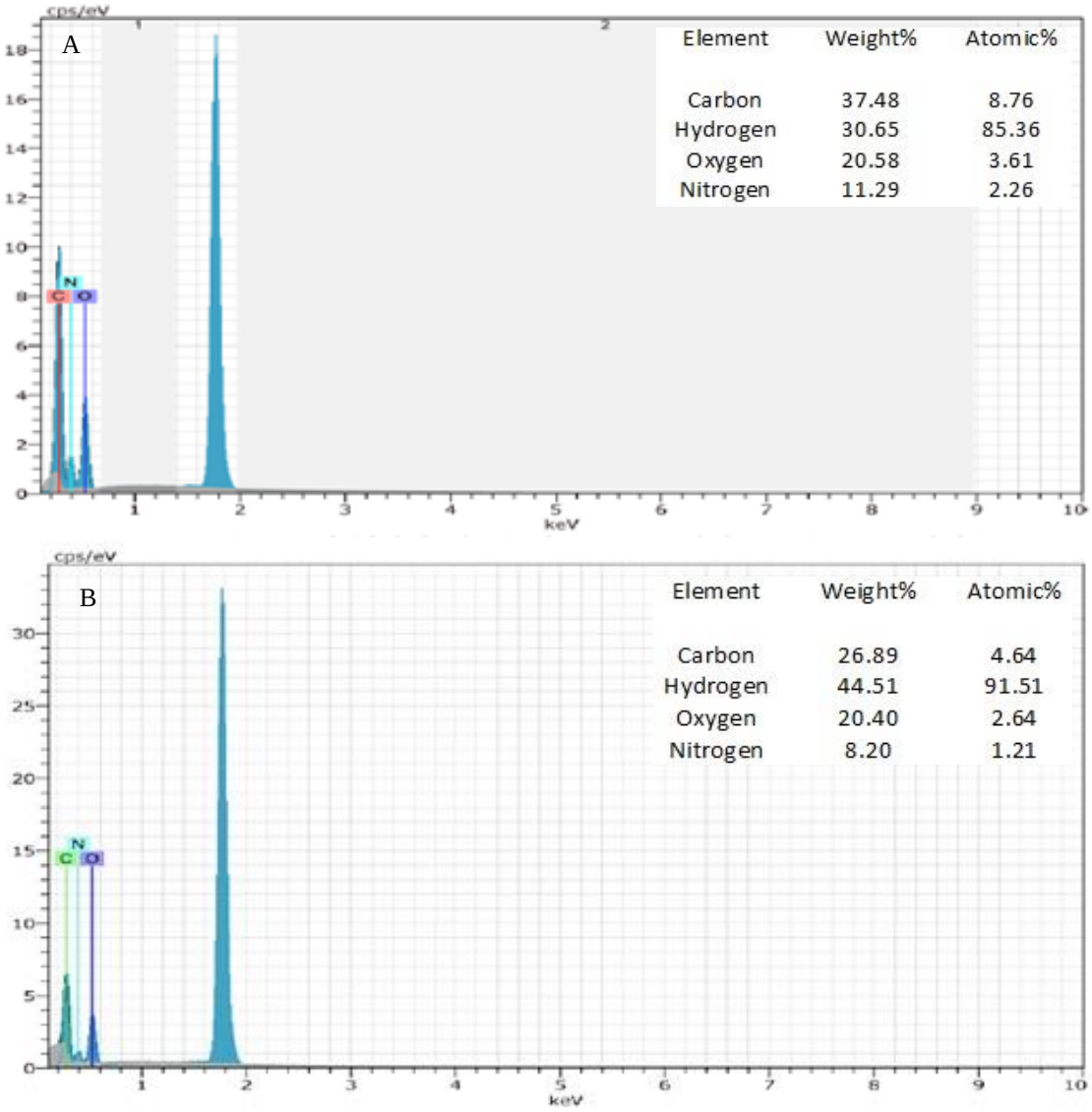

Figure A.S3. EDX Analysis. EDX analysis of E-CNDs (A) and U-CNDs (B) on silicon wafer (inset elemental weight % composition of the constituents).

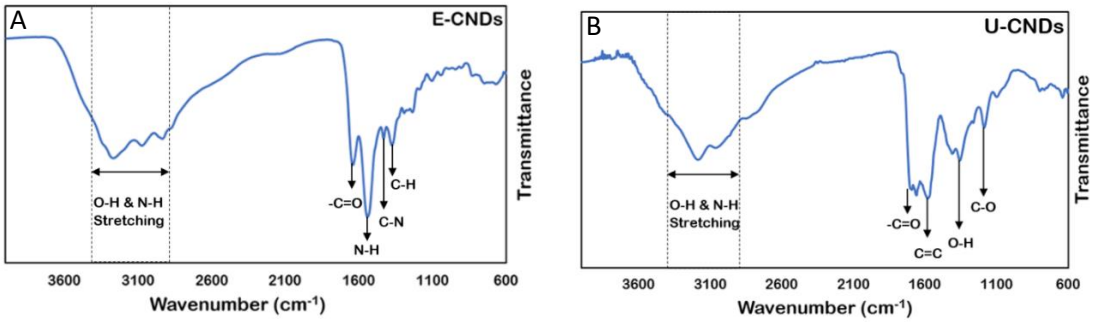

Figure A.S4. FTIR Spectra of CNDs. FTIR spectra of E-CNDs (A) & U-CNDs (B).

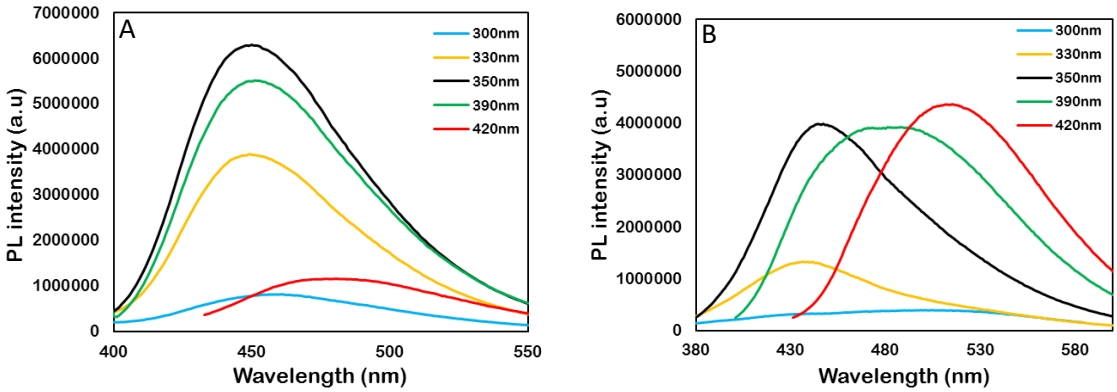

Figure A.S5. Excitation Dependent PL Spectra. Emission spectra of E-CNDs (A) & U-CNDs (B) at different wavelengths.

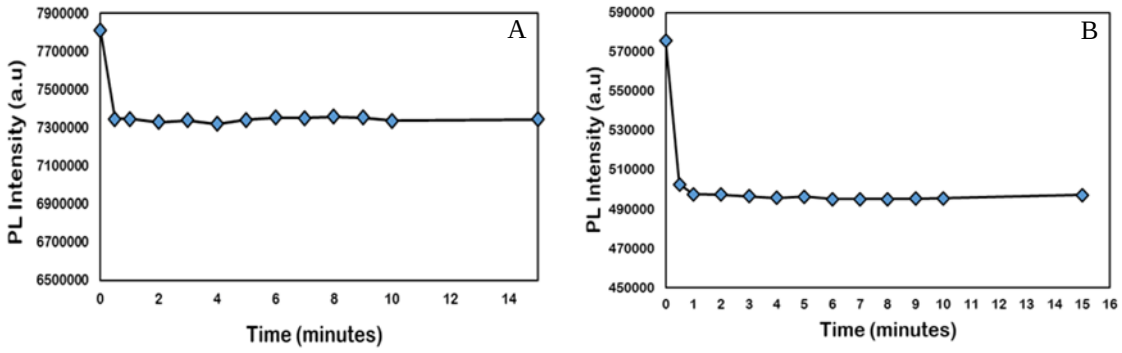

Figure A.S6. Time Course Response. Time course response of fluorescence upon addition of Fe (III) ions to E-CNDs (A) and U-CNDs (B) at an excitation wavelength of 350nm.

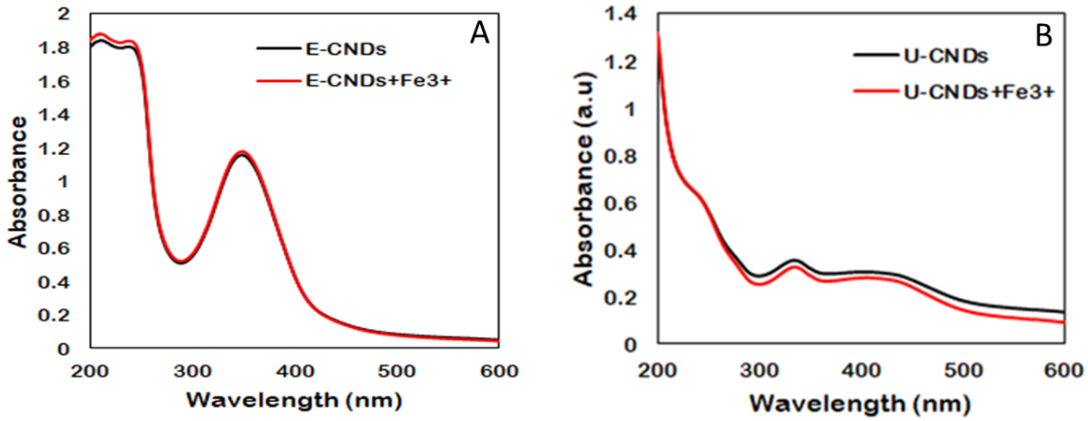

Figure A.S7 Absorption Spectra of CNDs. Absorption spectra of E-CNDs (0.1mg mL^{-1}) (A) and U-CNDs (0.1mg mL^{-1}) (B) upon addition of Fe (III) ions.

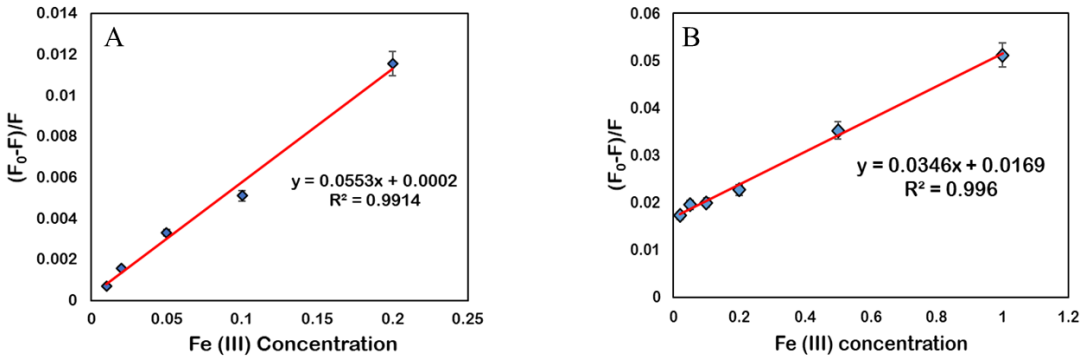

Figure A.S8. Linear Korsmeyer-Peppas Plots. Linear plot of E-CNDs (0.01 mg mL^{-1}) (A) and U-CNDs (0.1 mg mL^{-1}) (B) between $(F_0-F)/F$ and Fe (III) at low concentration range of 0.01 – 0.2 µM for E-CNDs, and 0.01 – 0.5 µM for U-CNDs.

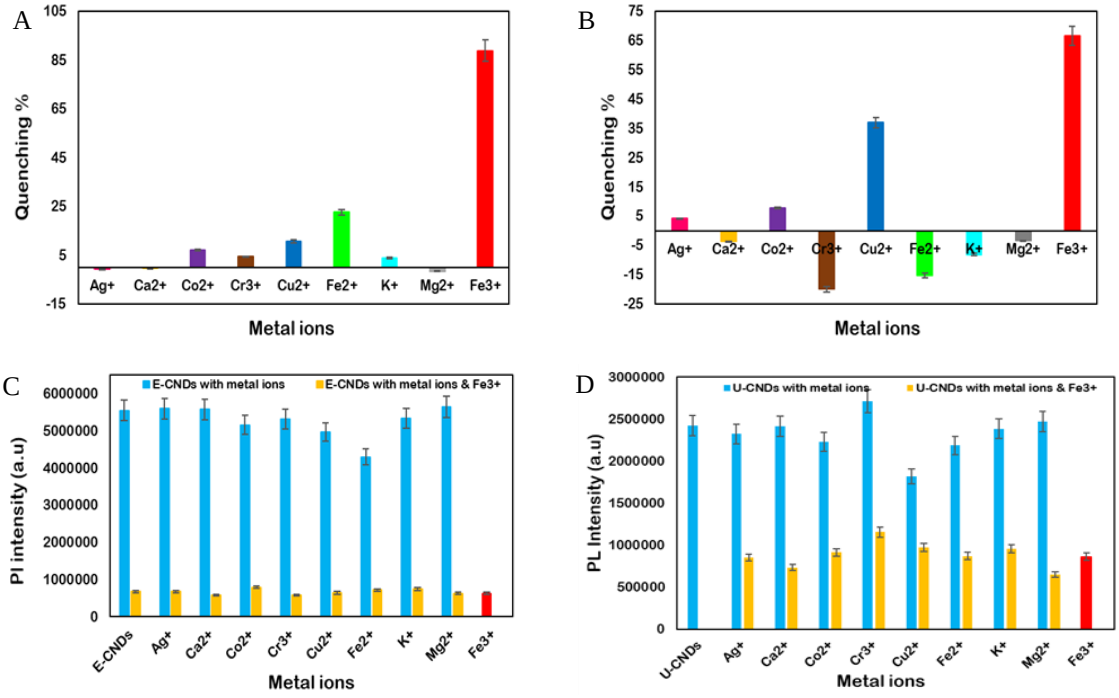

Figure A.S9. Quenching% in Presence of Metal Ions. Quenching% (averaged) of fluorescence of 0.05 mg mL^{-1} E-CNDs (A) and 0.1 mg mL^{-1} U-CNDs (B) in presence of different metal ions (50µM). Interference of E-CNDs (C) and U-CNDs (D) fluorescence intensity with Fe (III) in the presence of competitive metal ions.

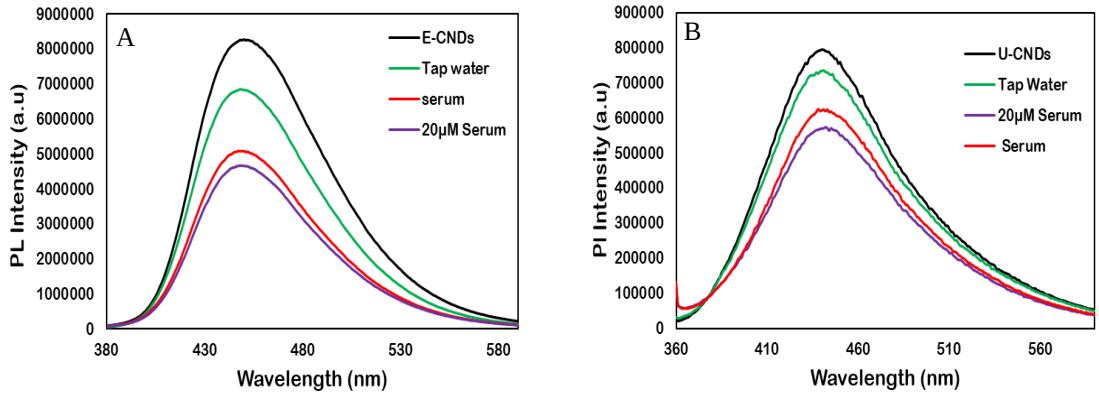

Figure A.S10. Detection of Fe (III) in Real Samples. Detection of Fe (III) in tap water and human serum using E-CNDs (A) and U-CNDs (B) probes.

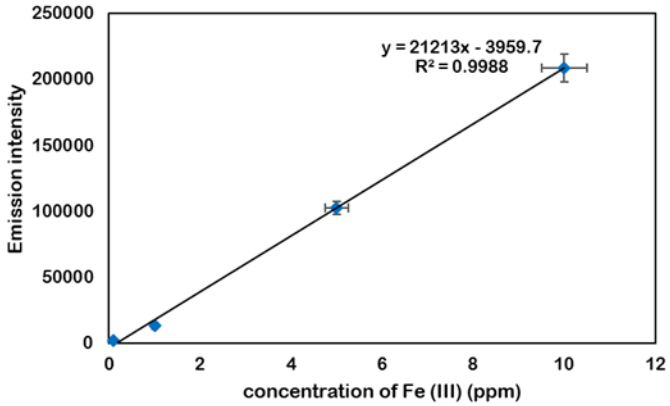

Figure A.S11. ICP Calibration Plot. Fe (III) calibration plot from ICP spectroscopic technique with Fe (III) concentration vs. emission intensity.

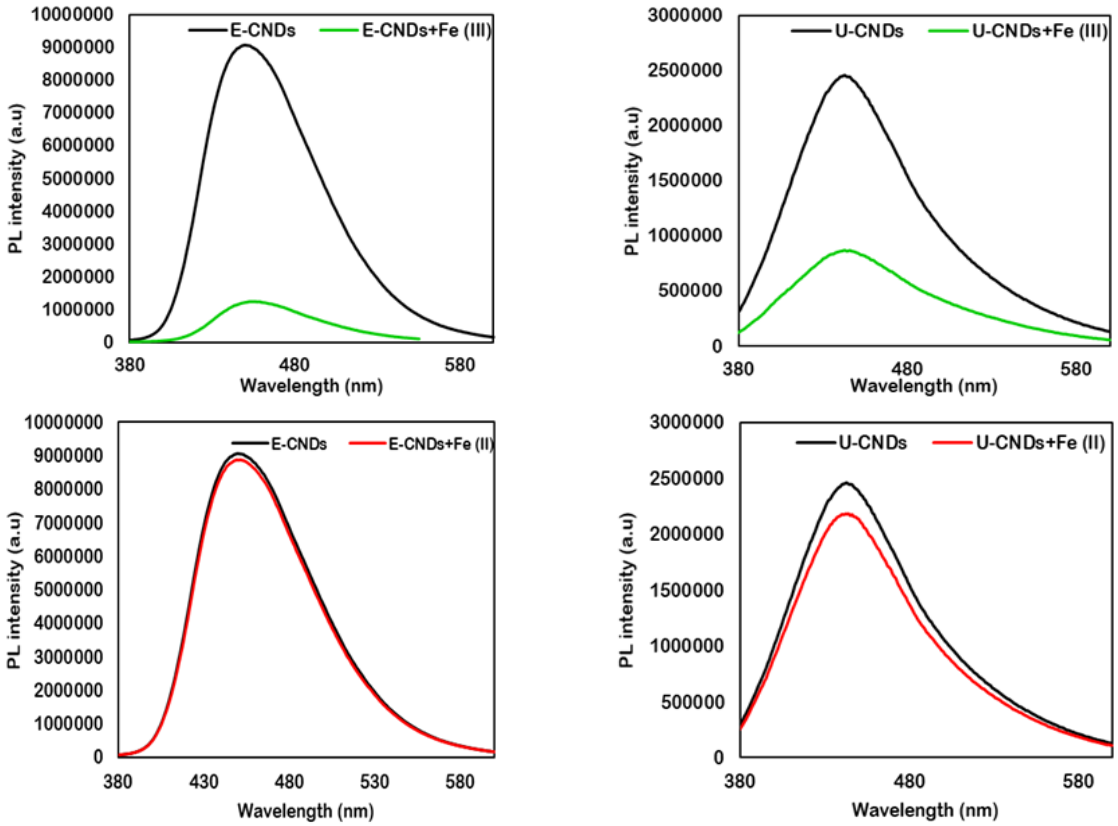

Figure A.S12. Fluorescence Spectra of CNDs. Fluorescence spectra of E-CNDs and U-CNDs with addition of Fe (III) (500 μM, top) and Fe (II) (500 μM, bottom).

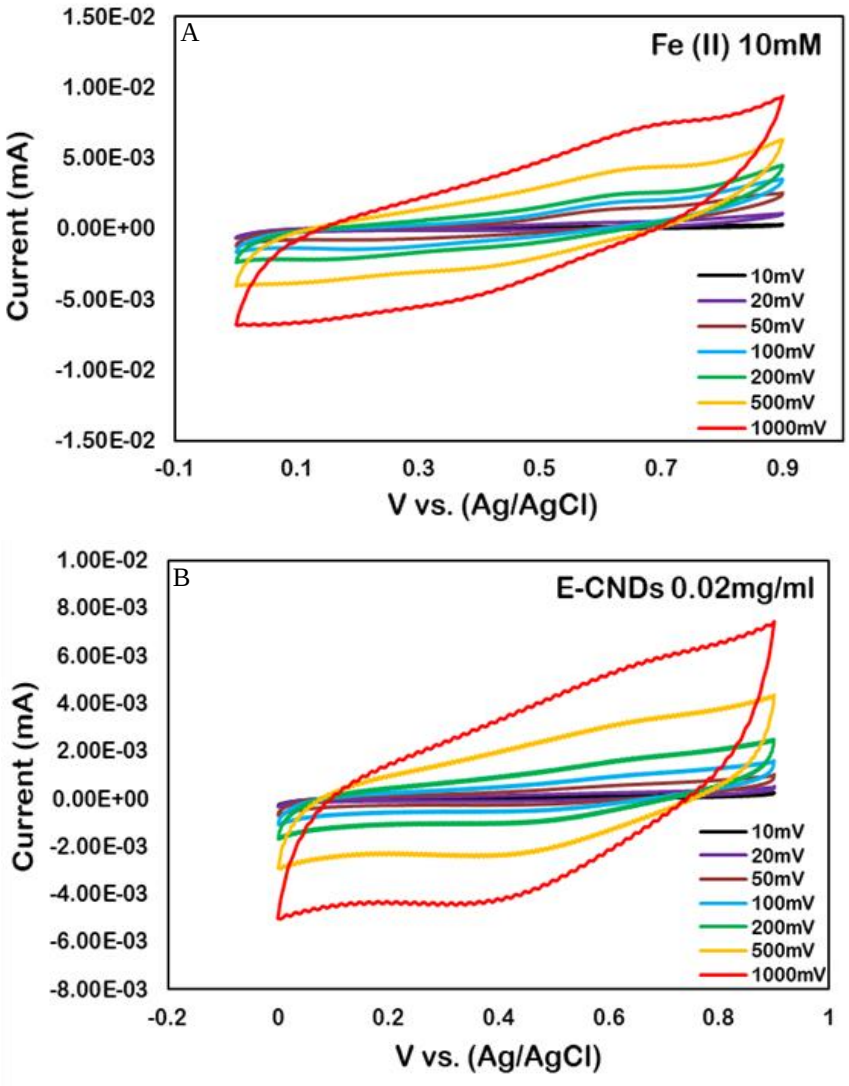

Figure A.S13. Cyclic Voltammograms of Fe (II) Treated with E-CNDs. Cyclic voltammograms of Fe (II) treated with 0.00 (A), 0.02 mg mL^{-1} (B) concentrations of E-CNDs at different scan rates of 10, 20, 50, 100, 200, 500, and 1000 mV s^{-1}.

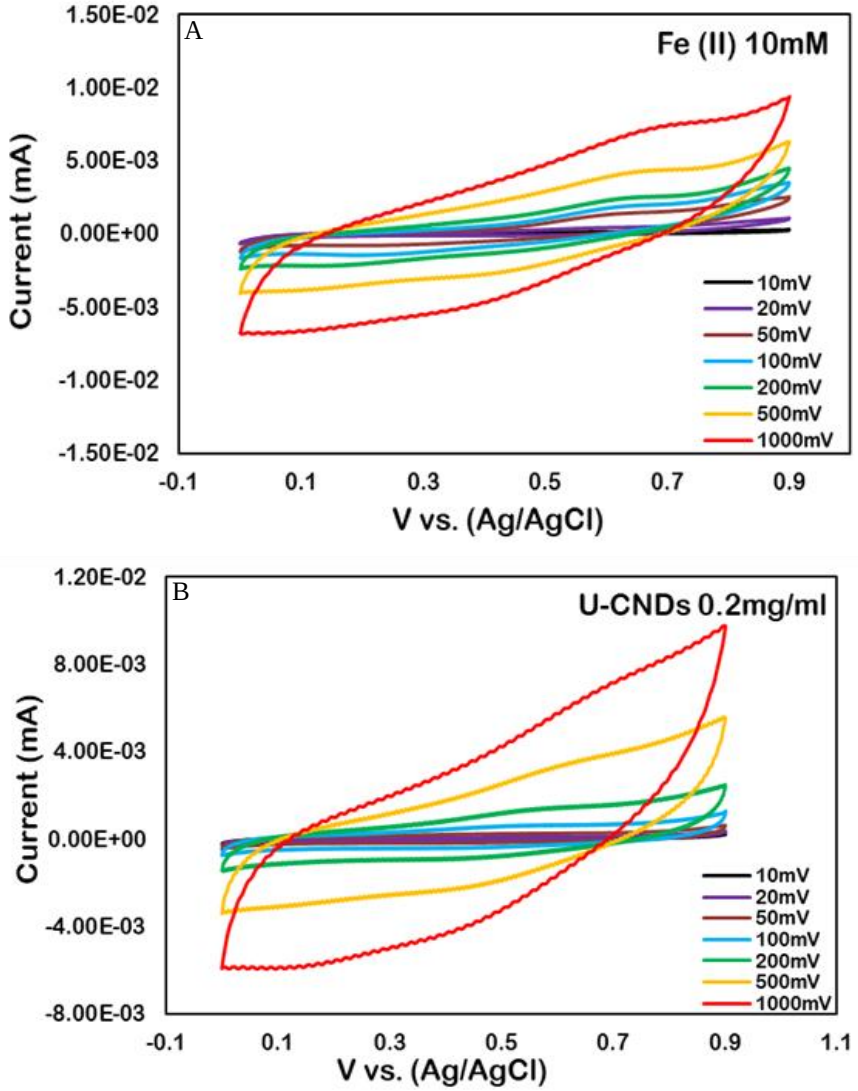

Figure A.S14. Cyclic Voltammograms of Fe (II) Treated with U-CNDs. Cyclic voltammograms of Fe (II) treated with 0.00 (A), 0.2 mg mL^{-1} (B) concentrations of U-CNDs at different scan rates of 10, 20, 50, 100, 200, 500, and 1000 mV s^{-1}.

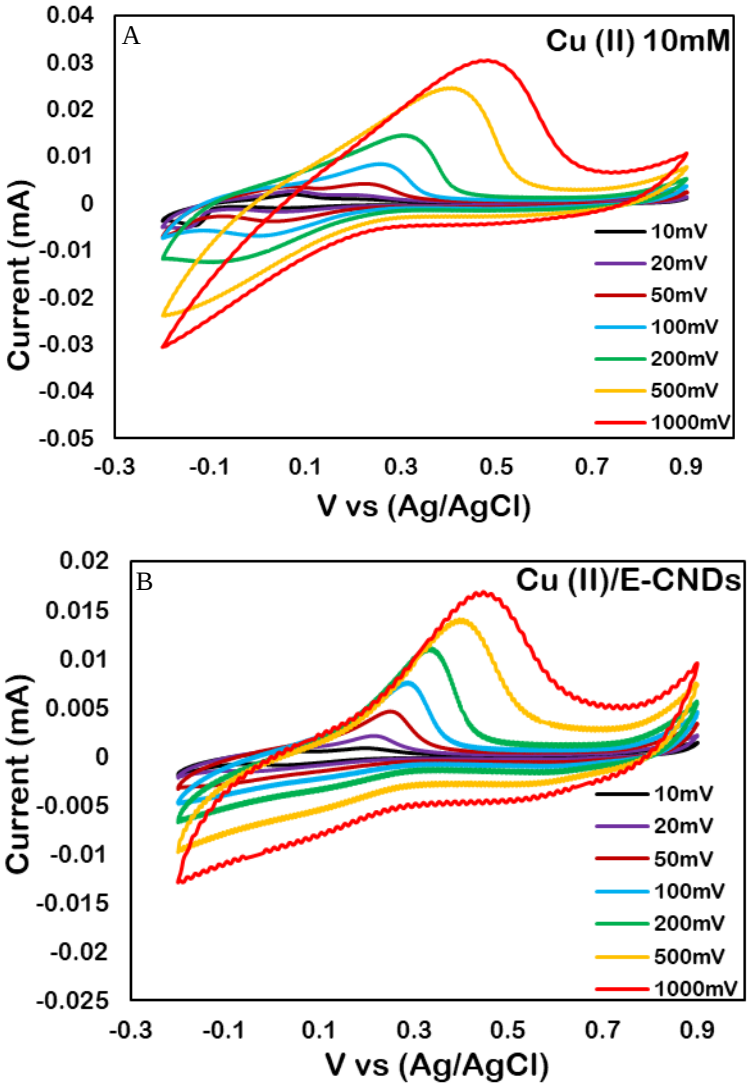

Figure A.S15. Cyclic Voltammograms of Cu (II) Treated with E-CNDs. Cyclic voltammograms of Cu (II) (10 mM) treated with 0.00 (A), 0.1 mg mL^{-1} (B) concentrations of E-CNDs at different scan rates of 10, 20, 50, 100, 200, 500, and 1000 mV s^{-1}.

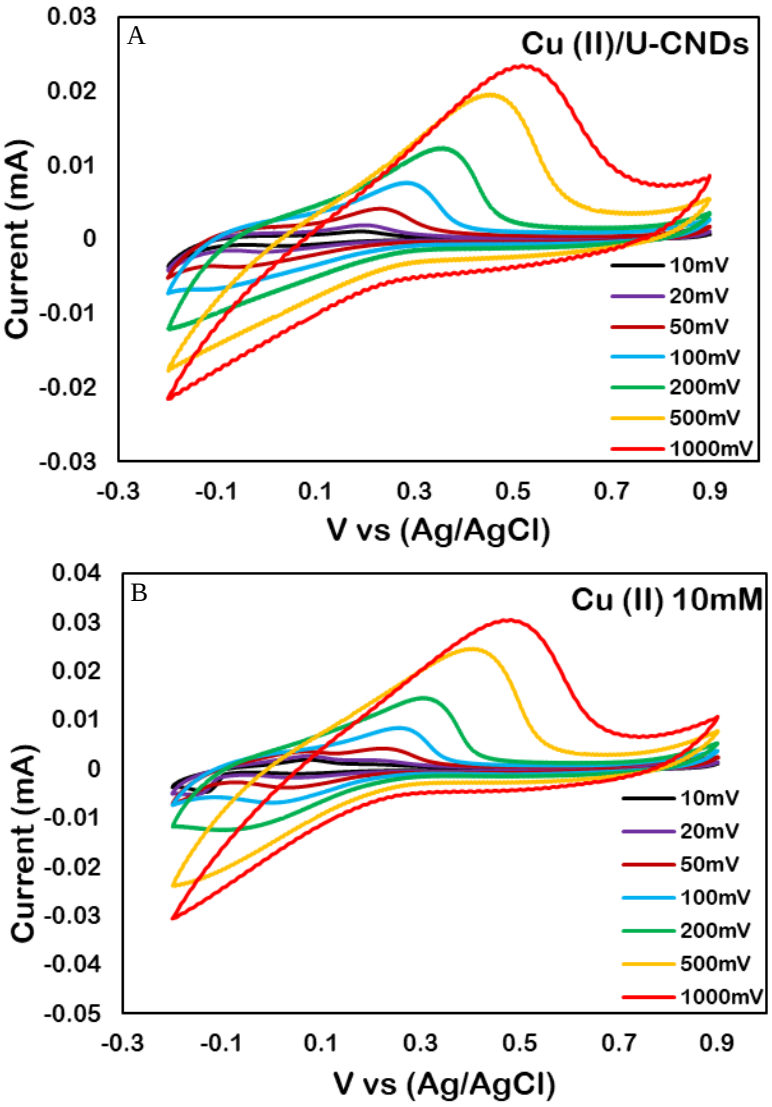

Figure A.S16. Cyclic Voltammograms of Cu (II) Treated with U-CNDs. Cyclic voltammograms of Cu (II) (10mM) treated with 0.00 (A), 0.1 mg mL^{-1} (B) concentrations of U-CNDs at different scan rates of 10, 20, 50, 100, 200, 500, and 1000 mV s^{-1}.

Table A.S1. Comparison of Various Nanoparticles as Sensing Probe for the Detection of Fe (III) Ions

Sensing Probe	**Dynamic Detection Range** (μM)	**LOD (**μM)	**Quantum Yield (%)**	**Reference**
B, N, S Doped Carbon Dots	0.3-546	0.09	5.44	[1]
N-doped Carbon Dots	1-250	0.52	16.4	[2]
N-doped carbon dots	0.01-500	0.0025	31	[3]
N & P co-doped dots	0.005-0.1	0.0018	30	[4]
Sulfur doped graphene dots	0-0.7	0.0042	10.6	[5]
N & S doped carbon dots	40-700	0.03	14.3	[6]
N & Zn doped carbon dots	0.05-125	0.027	63.28	[7]
Green emitting CDs	25-300	19	46.4	[8]
N-CDots	0-50	0.007	34.8	[9]
S-doped C-dots	1-500	0.1	67	[10]
Fluorescent carbon dots	0-185	6.16	80	[11]
N doped carbon dots	0-6	0.034	2.15	[12]
N doped carbon dots	0.05-30	0.013	41	[13]
E-CNDs & U-CNDs	0.02-2000	0.018 & 0.03	64 & 8.4	Present Work

References

1. Liu, Y.; Duan, W.; Song, W.; Liu, J.; Ren, C.; Wu, J.; Liu, D.; Chen, H., Red Emission B, N, S-co-Doped Carbon Dots for Colorimetric and Fluorescent Dual Mode Detection of Fe^{3+} Ions in Complex Biological Fluids and Living Cells. *ACS Appl. Mater. Interfaces* **2017,** *9* (14), 12663-12672.

2. Song, Y.; Zhu, C.; Song, J.; Li, H.; Du, D.; Lin, Y., Drug-Derived Bright and Color-Tunable N-Doped Carbon Dots for Cell Imaging and Sensitive Detection of Fe^{3+} in Living Cells. *ACS Appl. Mater. Interfaces* **2017,** *9* (8), 7399-7405.

3. Zhang, H.; Chen, Y.; Liang, M.; Xu, L.; Qi, S.; Chen, H.; Chen, X., Solid-Phase Synthesis of Highly Fluorescent Nitrogen-Doped Carbon Dots for Sensitive and Selective Probing Ferric Ions in Living Cells. *Anal. Chem.* **2014,** *86* (19), 9846-9852.

4. Shi, B.; Su, Y.; Zhang, L.; Huang, M.; Liu, R.; Zhao, S., Nitrogen and Phosphorus Co-Doped Carbon Nanodots as a Novel Fluorescent Probe for Highly Sensitive Detection of Fe(3+) in Human Serum and Living Cells. *ACS Appl Mater Interfaces* **2016,** *8* (17), 10717-25.

5. Li, S.; Li, Y.; Cao, J.; Zhu, J.; Fan, L.; Li, X., Sulfur-Doped Graphene Quantum Dots as a Novel Fluorescent Probe for Highly Selective and Sensitive Detection of Fe^{3+}. *Anal. Chem.* **2014,** *86* (20), 10201-10207.

6. Cheng, C.; Xing, M.; Wu, Q., A universal facile synthesis of nitrogen and sulfur co-doped carbon dots from cellulose-based biowaste for fluorescent detection of Fe3+ ions and intracellular bioimaging. *Materials Science and Engineering: C* **2019,** *99*, 611-619.

7. Tammina, S. K.; Yang, D.; Li, X.; Koppala, S.; Yang, Y., High photoluminescent nitrogen and zinc doped carbon dots for sensing Fe3+ ions and temperature. *Spectrochimica Acta Part A: Molecular and Biomolecular Spectroscopy* **2019,** *222*, 117141.

8. Khan, W.; Wang, D.; Zheng, W.; Tang, Z.; Ma, X.; Ding, X.; Du, S.; Wang, Y., High Quantum Yield Green-Emitting Carbon Dots for Fe(III) Detection, Biocompatible Fluorescent Ink and Cellular Imaging. *Scientific Reports* **2017,** *7*.

9. Liang, Y.; Liu, Y.; Li, S.; Lu, B.; Liu, C.; Yang, H.; Ren, X.; Hou, Y., Hydrothermal growth of nitrogen-rich carbon dots as a precise multifunctional probe for both Fe3+ detection and cellular bio-imaging. *Optical Materials* **2019,** *89*, 92-99.

10. Xu, Q.; Pu, P.; Zhao, J.; Dong, C.; Gao, C.; Chen, Y.; Chen, J.; Liu, Y.; Zhou, H., Preparation of highly photoluminescent sulfur-doped carbon dots for Fe(iii) detection. *Journal of Materials Chemistry A* **2015,** *3* (2), 542-546.

11. Meng, Q.; Wang, L.; Zhang, J.; Song, Y.; Jin, H.; Zhang, K.; Hongchen, S.; Wang, H.; Yang, B., Highly Photoluminescent Carbon Dots for Multicolor Patterning, Sensors, and Bioimaging. *Angewandte Chemie (International ed. in English)* **2013,** *52*.

12. Cui, F.; Sun, J.; Yang, X.; Ji, J.; Pi, F.; Zhang, Y.; Lei, H.; Sun, X., Ultrasensitive fluorometric determination of iron(iii) and inositol hexaphosphate in cancerous and bacterial cells by using carbon dots with bright yellow fluorescence. *Analyst* **2019,** *144* (16), 5010-5021.

13. Zhou, X.; Zhao, G.; Tan, X.; Qian, X.; Zhang, T.; Gui, J.; Yang, L.; Xie, X., Nitrogen-doped carbon dots with high quantum yield for colorimetric and fluorometric detection of ferric ions and in a fluorescent ink. *Microchimica Acta* **2019,** *186* (2), 67.

APPENDIX B

DESIGN OF CURCUMIN LOADED CARBON NANODOTS DELIVERY SYSTEM: ENHANCED BIOAVAILABILITY, RELEASE KINETICS AND ANTICANCER ACTIVITY

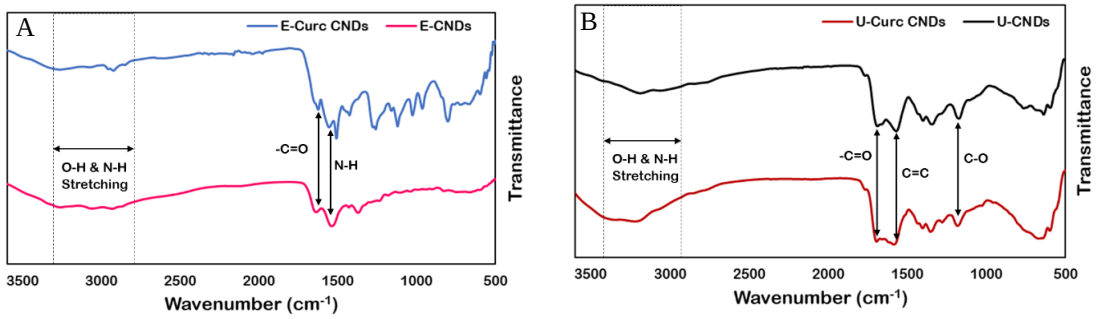

Figure B.S1. FTIR Comparison Spectra. FTIR spectra of Curc-E-CNDs (A) and Curc-U-CNDs (B) with their respective precursor CNDs.

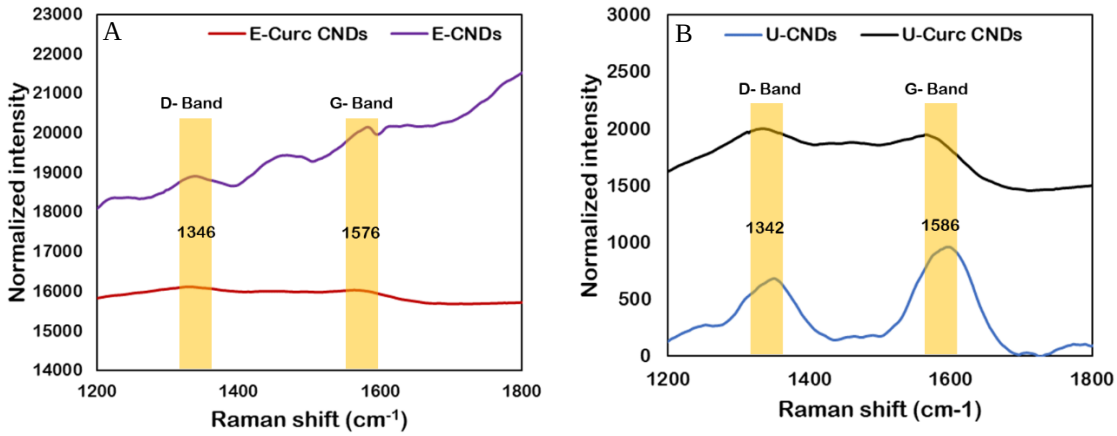

Figure B.S2. Raman Spectra of Curc-CNDs. Raman spectra of Curc-E-CNDs (A) and Curc-U-CNDs (B) respectively.

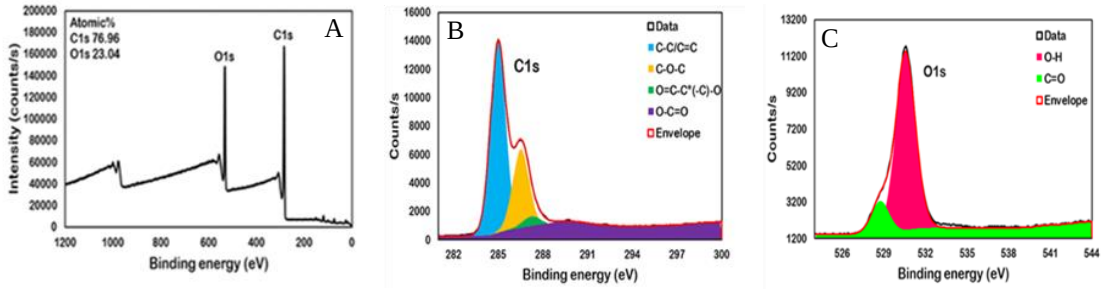

Figure B.S3. XPS Spectra. XPS survey spectrum of curcumin (A) and high resolution C1s (B) and O1s (C) peaks of curcumin respectively.

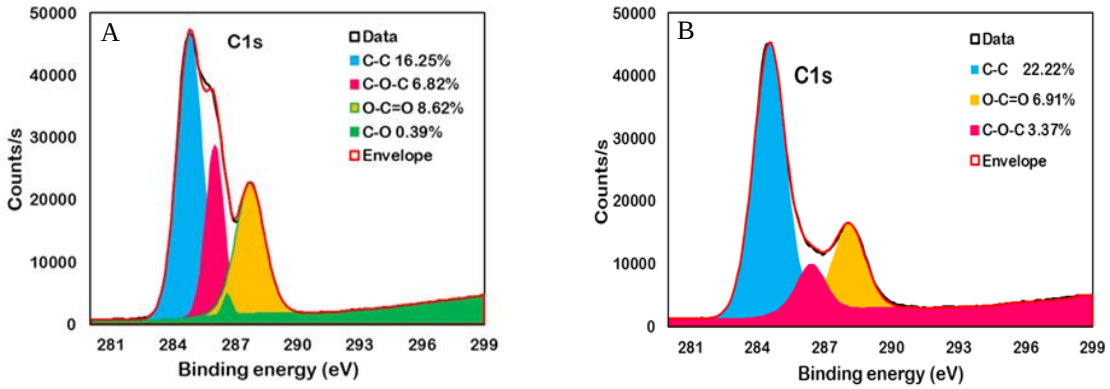

Figure B.S4. High Resolution XPS C1s Spectra of E-CNDs (A) and U-CNDs (B).

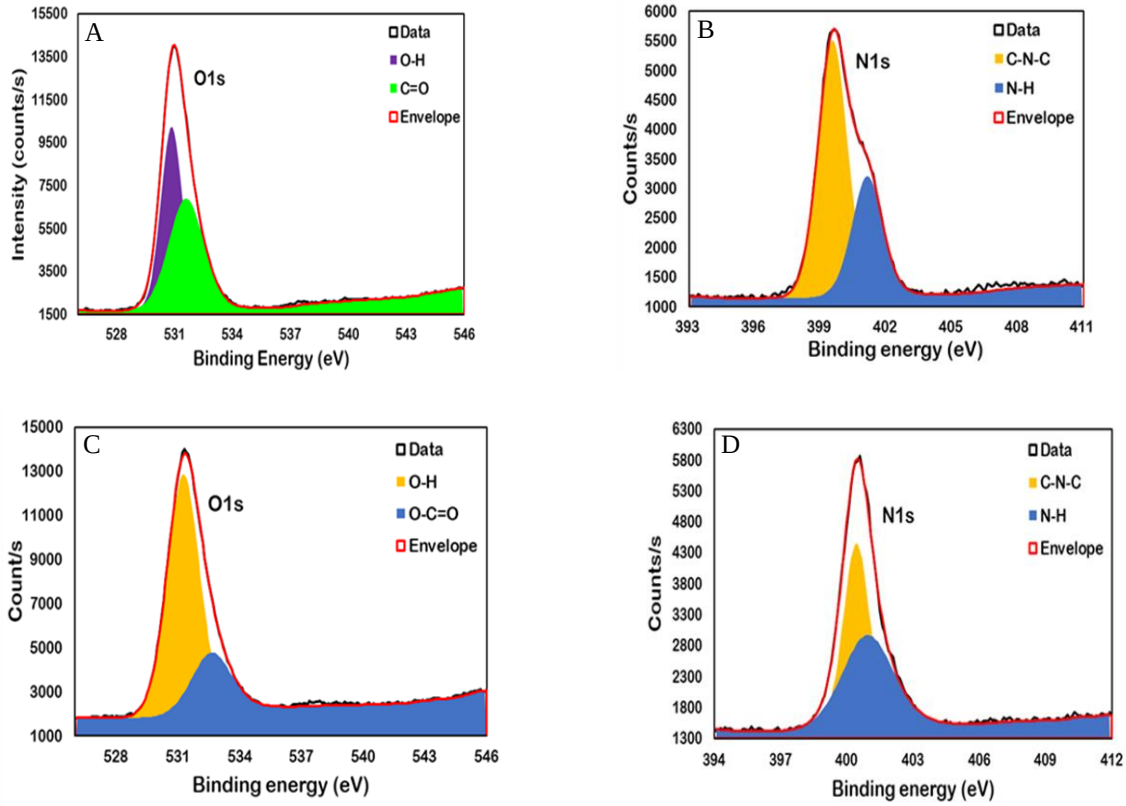

Figure B.S5. XPS Spectra of Curc-CNDs. XPS spectrum of high resolution O1s (A, C) and N1s (B, D) peaks of Curc-E-CNDs and Curc-U-CNDs respectively.

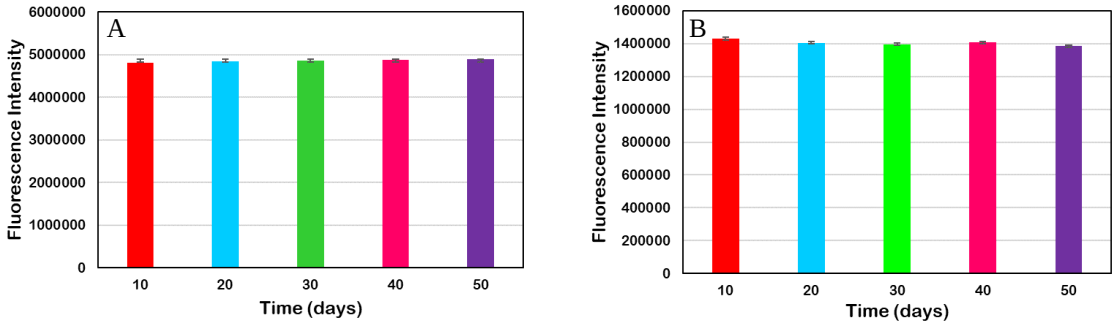

Figure B.S6. Fluorescence Stability. Fluorescence stability of Curc-E-CNDs (A) and Curc-U-CNDs (B) over a time period of 50 days.

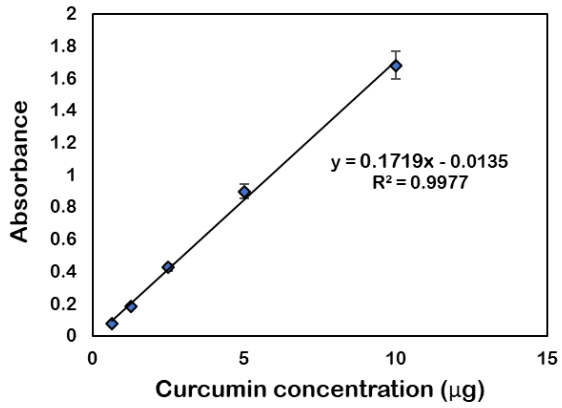

Figure B.S7. Curcumin Standard Curve in Methanol Solvent.

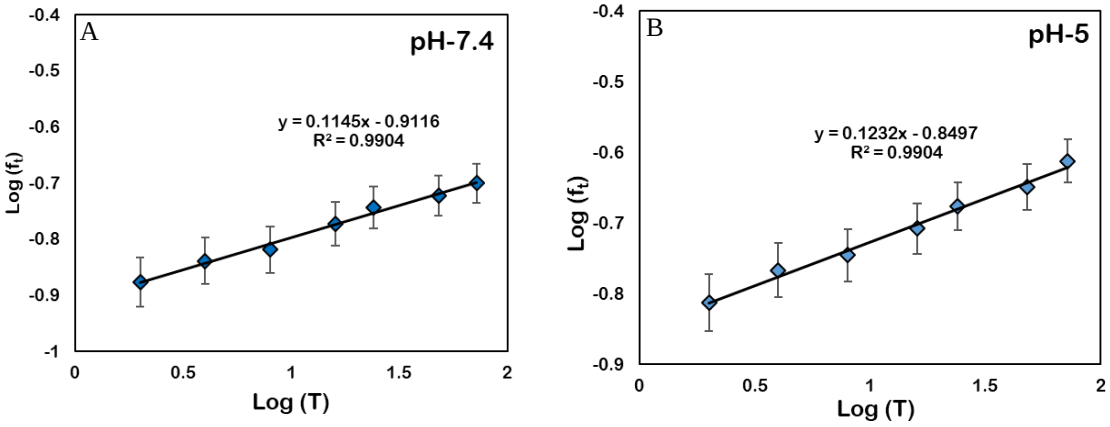

Figure B.S8. Release Model of Curc-E-CNDs. Korsmeyer-Peppas release model of Curcumin from Curc-E-CNDs at pH-7.4 (A) & pH-5 (B) respectively. All the data values were done in triplicates with mean ±SDs.

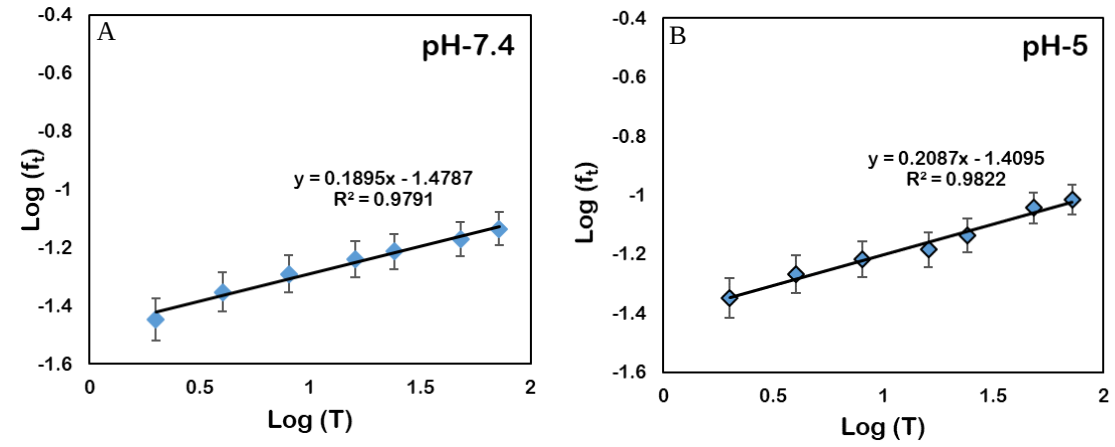

Figure B.S9 Release Model of Curc-U-CNDs Korsmeyer-Peppas release model of Curcumin from Curc U-CNDs at pH-7.4 (A) & pH-5 (B) respectively. All the data values were done in triplicates with mean ±SDs.

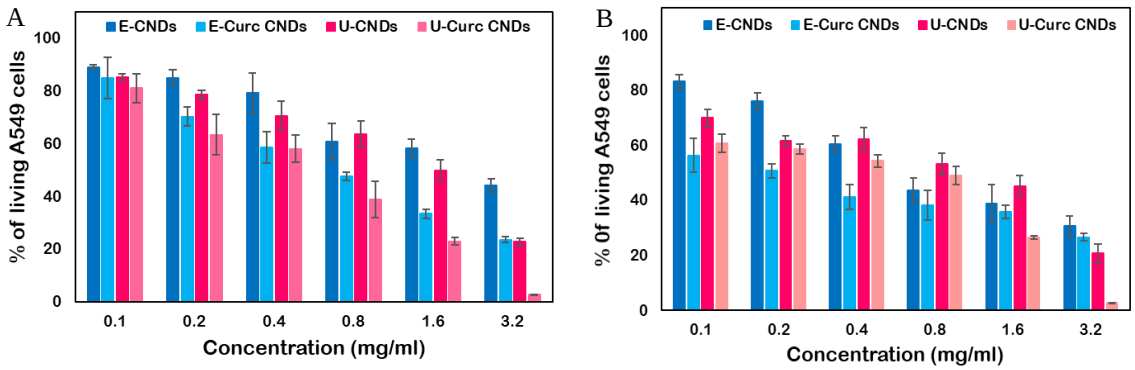

Figure B.S10. Cell Viability Assays. Cell viability of A549 cells treated with different concentrations of E-CNDs & Curc-E-CNDs and U-CNDs & Curc-U-CNDs for 48 (A) & 72 hrs (B).

Table B.S1. Quantum Yields of CNDs Before and After Functionalization with Curcumin with Reference to Quinine Sulfate.

Sample	Quantum Yield
Quinine Sulfate	54%
E-CNDs	64%
E-Curc-CNDs	48.74%
U-CNDs	8.43%
U-Curc-CNDs	6.54%

APPENDIX C

ELUCIDATION OF ANTI-PROLIFERATIVE AND ROS REGULATION ACTIVITY OF PHOTOLUMINESCENT CURCUMIN NANOPARTICLES

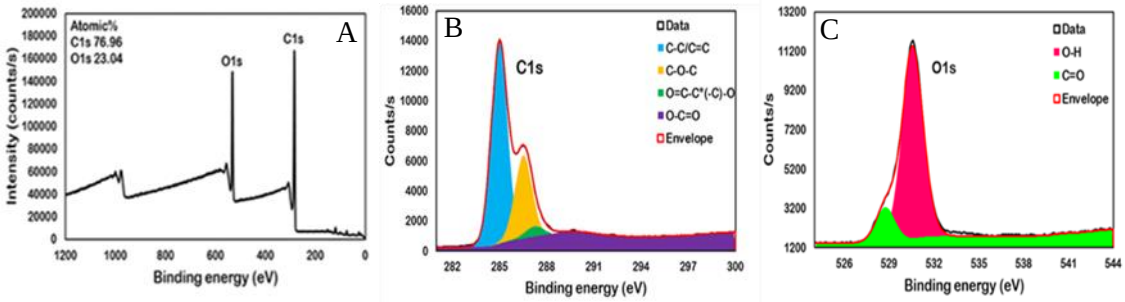

Figure C.S1. XPS Spectra. XPS survey spectra (A) and high resolution C1s (B) and O1s (C) peaks of curcumin respectively.

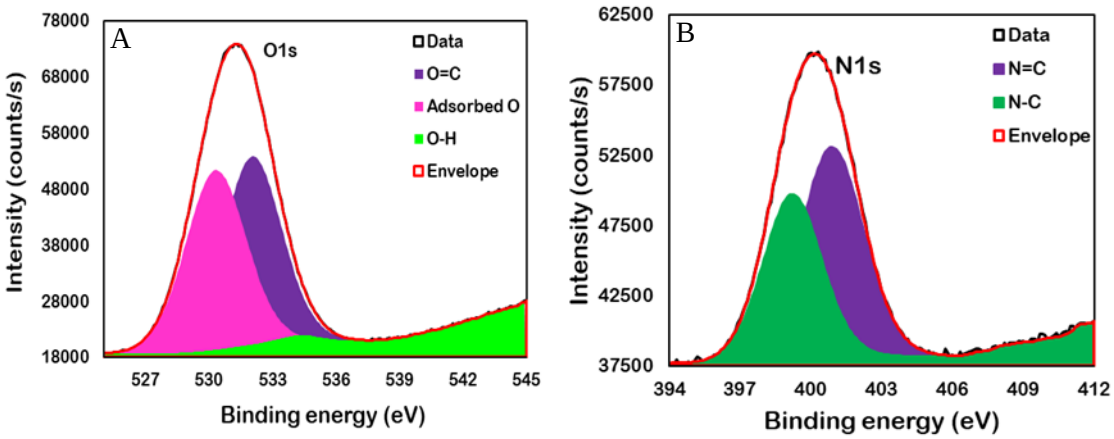

Figure C.S2. XPS Spectra of O1s (A), N1s (B) of E-Curc Dots.

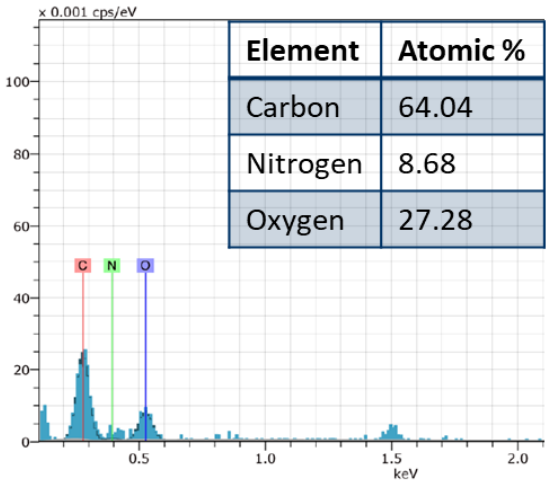

Element	Atomic %
Carbon	64.04
Nitrogen	8.68
Oxygen	27.28

Figure C.S3. XRD Pattern of E-Curc Dots.

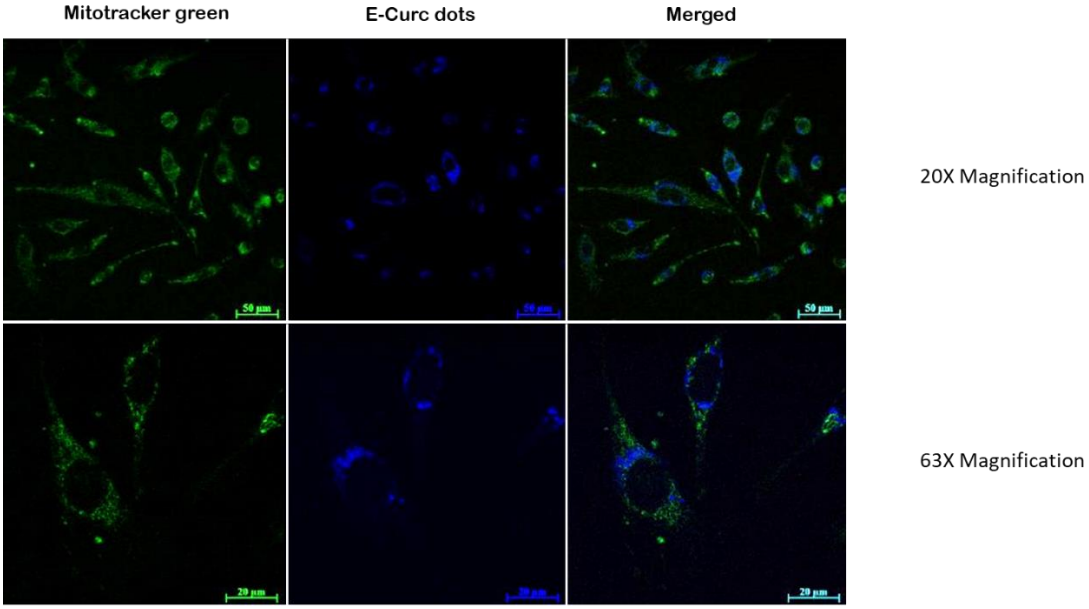

Figure C.S4. Subcellular Localization of E-Curc Dots. Subcellular localization of E-Curc dots (0.8 mg/mL) inside EA. hy926 cells at different magnifications.

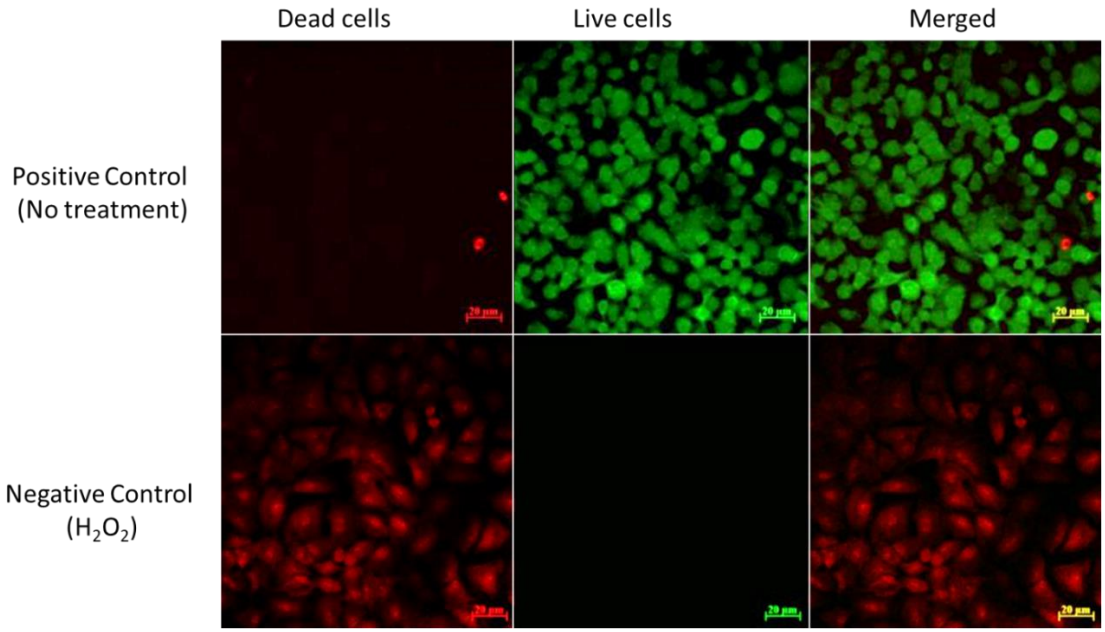

Figure C.S5. Controls of Live/Dead Assay for A549 Cells.